

2014

GROUND MAGNETOMETER SURVEY IN THE VALLEY OF
TEN THOUSAND SMOKES, ALASKA

A
THESIS

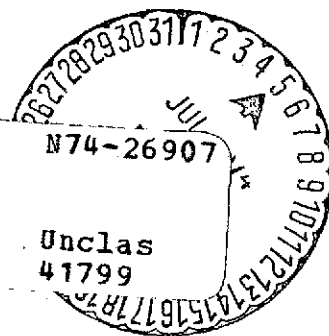
Presented to the Faculty of the
University of Alaska in Partial Fulfillment
of the Requirements
for the Degree of
MASTER OF SCIENCE

(NASA-CR-138779) GROUND MAGNETOMETER
SURVEY IN THE VALLEY OF TEN THOUSAND
SMOKES, ALASKA M.S. Thesis (Alaska
Univ., College.) 210 p HC \$13.50

208

G3/13

Unclas
41799



by

Marla Cave Tribble, B.S.

College, Alaska

May, 1972

ABSTRACT

During July 1969 a reconnaissance magnetometer survey was conducted in the Valley of Ten Thousand Smokes with both total- and vertical-field magnetometers.

The large, sharp, narrow total magnetic anomalies observed over a zone of relict fumaroles in Broken Mountain Valley showed spectacular agreement with the surficial geology. Such a correlation is a strong indication that accumulations of magnetic minerals have been preserved along these fissure vents at shallow depths. Since large magnetic anomalies were measured near fumarolic markings along all of the traverses, it is proposed that the retention of sublimates along fumarolic vents is common throughout the Valley.

The generally concentric contours of the vertical magnetic anomaly at the head of the Valley suggest that the dome of Novarupta is merely the surficial expression of a very massive conical-shaped intrusive centered just northeast of the dome. Corresponding offsets in the anomalies along adjacent radial traverses, however, imply the presence of concentric faulting around the dome, probably in the bedrock as well as in the pyroclastic flow.

Profiles across the various branches of the Valley indicate that the flow is very heterogeneous. The variations in thickness and susceptibility implied by the total magnetic anomalies are consistent with the hypothesis of fissure-feeders for the flow.

The magnetometer survey indicates that the pyroclastics in the Valley may be over 150 meters thick. Such an estimate is compatible with the volume of eruptive material needed to compensate for the subsidence surrounding Novarupta as well as a sizable amount of other regional subsidence.

PRECEDING PAGE BLANK NOT FILMED

ACKNOWLEDGEMENTS

Special thanks are due my Committee Chairman, Dr. D. B. Stone, for suggesting this project, and for his supervision, assistance, and patience during the field operations and throughout the preparation of my thesis. I am particularly indebted to Dr. R. B. Forbes for affording me the opportunity of participating in the Katmai research project, and for our many stimulating discussions. I am also especially grateful to Dr. J. Kienle for his continued encouragement, for our many enlightening discussions, and for permitting the inclusion of his unpublished density and seismic refraction data. Thanks are also due each of the above as well as Dr. F. F. Wright and Dr. H. Pulpan for their constructive criticism in preparing the final manuscript.

I want to thank Dr. D. K. Bingham, who along with Drs. Stone and Forbes, assisted in conducting most of the magnetometer traverses; L. Gedney, Dr. G. Lofgren, and C. Matteson also helped during the survey over the relict fumaroles. Dr. D. R. Packer was kind to permit the inclusion of his unpublished magnetic susceptibility data.

I am very appreciative of the time and talents spent on preparing the final manuscript by G. Edsall, and on the drafting by S. Wilson. The assistance offered during the computer programming aspects of this work by S. Dean, S. Geller, and J. Murray is gratefully acknowledged.

I am also grateful for the loan of the Elsec magnetometer by the Anchorage, Alaska office of the Coast and Geodetic Survey, and for the logistic support of the United States Air Force.

Most of all, I want to thank Tom, my husband, and my parents for their endless encouragement throughout my graduate endeavors.

This research has been supported by NASA grant NGL-02-001-063.

TABLE OF CONTENTS

	Page
ABSTRACT	3
ACKNOWLEDGEMENTS	4
TABLE OF CONTENTS	5
LIST OF ILLUSTRATIONS	8
LIST OF TABLES	11
LIST OF PLATES	12
CHAPTER I - THE VALLEY OF TEN THOUSAND SMOKES	13
1.1 Foreward	13
1.2 Description of the Valley	13
1.3 History of Investigations Within the Valley	18
1.4 Areas of Controversy	23
a) The Source of the 1912 Pyroclastic Flow	23
b) The Banded Ejecta of Novarupta	29
c) Nature of the Fissure Fumaroles	30
d) Possible Concentrations of Magnetic Minerals	34
e) The Cause of the Marginal Terrace	39
f) The Age of the Lower Tuff Unit	40
g) Thickness of the Flow	41
1.5 Field Procedure for the Ground Magnetometer Survey	44
CHAPTER II - MAGNETIC SUSCEPTIBILITIES FOR ROCKS FROM THE KATMAI AREA	49
2.1 Purpose of Magnetic Susceptibility Determination	49
2.2 Determination of Susceptibility	51

	Page
2.3 Discussion of Results	52
a) Naknek Sediments	52
b) Lavas	57
c) Glacial Deposits	60
d) Pyroclastic Flow	62
e) Air-Fall Pyroclastics	65
f) Fumarolic-Altered Pyroclastics	70
2.4 Conclusions	72
CHAPTER III - SMALL SCALE MAGNETOMETER SURVEY OVER A ZONE OF RELICT FUMAROLES	76
3.1 Small-Scale Magnetometer Survey	76
3.2 Analysis of Magnetometer Data	79
3.3 Implied Source for the Anomalies	82
3.4 Conclusions	85
CHAPTER IV - CROSS-VALLEY MAGNETIC PROFILES IN THE VALLEY OF TEN THOUSAND SMOKES	86
4.1 Magnetometer Survey in the Valley Region	86
4.2 The Character of the Flow	98
4.3 Magnetic Models of the Flow	114
4.4 Conclusions	130
CHAPTER V - RECONNAISSANCE MAGNETOMETER SURVEY IN THE VICINITY OF NOVARUPTA VOLCANO	133
5.1 Description of Novarupta	133
5.2 Patterns of Subsidence Around Novarupta	134
5.3 Magnetometer Survey Around Novarupta	140

	Page
5.4 Anomalous Geophysical Parameters in Novarupta Basin	145
5.5 Conclusions	151
CHAPTER VI - SUMMARY OF THE GROUND MAGNETOMETER SURVEY	154
APPENDICES	158
BIBLIOGRAPHY	206

LIST OF ILLUSTRATIONS

	Page
Figure 1.1. Generalized geologic map of the Katmai area.	14
Figure 1.2. The various historical and newly designated nomenclature for the Valley of Ten Thousand Smokes.	17
Figure 1.3. Locations of other geophysical investigations in the Valley of Ten Thousand Smokes.	22
Figure 1.4. Variation of ferrous, ferric and total iron in alteration zones around fumarole No. 1 (Zies, 1929) in the Valley of Ten Thousand Smokes in 1952.	38
Figure 2.1. Location of magnetic susceptibility sampling sites I through X.	50
Figure 2.2. Comparative tephra sections based on Curtis (1968) and the section exposed at sampling site III.	68
Figure 2.3. Susceptibility of individual measuring discs as a function of rock type and sampling site.	73
Figure 3.1a. Surficial geology of the fumarole study area.	78
Figure 3.1b. Total field magnetic anomaly map over the fumarole study area.	78
Figure 3.2. Computer drawn perspective magnetic anomaly map of the fumarole study area.	80
Figure 4.1. Magnetometer traverses in the Valley of Ten Thousand Smokes, Katmai National Monument, Alaska.	87
Figure 4.2a. Reduced magnetic profile data for traverse A-A'.	88
Figure 4.2b. Reduced magnetic profile data for traverse B-B'.	88
Figure 4.3a. Reduced magnetic profile data for traverse B-B''.	89
Figure 4.3b. Reduced magnetic profile data for traverse b-b'.	89
Figure 4.3c. Reduced magnetic profile data for traverse B''-b''.	89
Figure 4.3d. Reduced magnetic profile data for traverse B-B'''.	89
Figure 4.4a. Reduced magnetic profile data for traverse C-C'.	90
Figure 4.4b. Reduced magnetic profile data for traverse D-D'.	90

	Page
Figure 4.5. Reduced magnetic profile data for traverse E-E'.	91
Figure 4.6a. Total magnetic intensity profile along Anna's (1972) flight line 31NW in the lower Valley near Tribble's profile A-A'.	92
Figure 4.6b. Total magnetic intensity profile along Anna's (1972) flight line 15E in the southern branch near Tribble's profile C-C'.	92
Figure 4.7. Comparison of smoothed magnetic anomaly profiles along adjacent traverses in the southern branch of the Valley.	95
Figure 4.8. Comparison of smoothed magnetic anomaly profiles along adjacent traverses in Novarupta Basin.	96
Figure 4.9a. Location of magnetometer traverses in Broken Mountain Valley.	97
Figure 4.9b. Magnetic anomaly map of a part of Broken Mountain Valley	97
Figure 4.10. Correlation of adjacent geophysical profiles in the southern branch of the Valley.	109
Figure 4.11a. Correlation of adjacent geophysical profiles in the lower Valley.	110
Figure 4.11b. Correlation of adjacent geophysical profiles in Broken Mountain and Knife Creek Valleys.	110
Figure 4.12a. Correlation of adjacent geophysical profiles in Novarupta Basin.	111
Figure 4.12b. Correlation of adjacent geophysical profiles in Broken Mountain Valley.	111
Figure 4.13. Summary of Kienle's (1969) structure sections derived from gravity data.	113
Figure 4.14. Smoothed residual magnetic anomalies and their corresponding simple and local anomalies along the Valley traverses.	119
Figure 5.1. Map of structural features in the vicinity of Novarupta Volcano.	136
Figure 5.2. Isopachs of tephra layers C, D, F and G.	139

	Page
Figure 5.3a. Location of magnetometer traverses and isolated readings in the vicinity of Novarupta dome.	142
Figure 5.3b. Anomalous vertical magnetic field near Novarupta dome.	142
Figure 5.4. Vertical magnetic anomaly profiles radial to Novarupta dome.	146
Figure 5.5a. Location of fumaroles studied by Allen and Zies in 1919.	148
Figure 5.5b. Isothermal map of fumarole vapor temperatures as measured by Allen and Zies in 1919.	148
Figure A.1. The diurnal correction 'B' as a function of local time.	161
Figure E.1. Mathematical relations used in the computation of magnetic models.	195

LIST OF TABLES

	Page
Table 1.1. Variation (weight percent) of ferrous- and ferric-oxide in samples from alteration zones about fumarole No. 1, from Lovering (1957, Table 1, p. 1593).	37
Table 1.2. Variation of ferrous- and ferric-oxide in the Bishop tuff, after Sheridan (1970, Table 1, p. 864).	37
Table 1.3. Previously suggested maximum tuff thickness (meters).	42
Table 2.1. Susceptibility studies of rocks from the Valley of Ten Thousand Smokes.	53
Table 2.2. Additional susceptibility data for rocks in the Katmai region.	55
Table 2.3. Bimodal susceptibility of Novarupta Volcanics.	59
Table 2.4. Susceptibility studies of Lethe indurated ash.	63
Table 2.5. Magnetic susceptibilities of some common constituents of fumarolic alterations reported by Shipley (1920), Zies (1929) and Lovering (1957).	71
Table 2.6. Summary of susceptibility data.	74
Table 4.1. Summary of density data.	99
Table 4.2. Summary of seismic parameters.	101
Table 4.3. Rock types in the Valley of Ten Thousand Smokes, their modeling susceptibilities and conversion factors.	116
Table 4.4. Summary of central total anomalies (in gammas) for computerized magnetic bodies of susceptibility = 1250×10^{-6} emu/cc at a depth of 2 meters.	117
Table 4.5. Simple magnetic anomalies and three computer models.	121
Table 4.6. Multiple local anomalies and three computer models.	123
Table 4.7. Correlation of four computerized magnetic models with observed local magnetic anomalies and nearby seismic refraction profiles.	124
Table A.1. Simultaneous magnetometer readings at the magnetometer base station.	162

LIST OF PLATES

	Page
Plate I. Air-fall sequence exposed along Knife Creek in the southeast branch of the Valley at sampling site III (refer to Figures 2.1 and 2.2 and Table 2.1).	67
Plate II. The zone of relict fumaroles in Broken Mountain Valley which was included in the small scale magnetometer survey (refer to Figures 4.1, 3.1 and 3.2).	77

CHAPTER 1

THE VALLEY OF TEN THOUSAND SMOKES

1.1 Foreward

On June 1, 1912, the pyroclastic flow of the Valley of Ten Thousand Smokes and its many fumaroles, the collapse caldera of Katmai Volcano, and the plug dome of Novarupta volcano were formed by one of the world's largest recorded volcanic eruptions.

After sixty years, many of the facts of this eruption are subject to controversy; chief among these are: the origin and mode of emplacement of the flow, as well as its thickness and internal composition and structure; the source of the fumarolic emanations and the chance that some of the fumarolic sublimates have been preserved; the cause of the banded ejecta which characterizes Novarupta and some portions of the flow; the events leading to the collapse of Katmai caldera; and the cause of the marginal terrace throughout the Valley.

1.2 Description of the Valley

The Valley of Ten Thousand Smokes is situated about half-way down the Alaska Peninsula, within Katmai National Monument. It is bounded on the south by the volcanic peaks of Mounts Katmai, Trident and Mageik; on the west by the sedimentary Buttress Range; on the east by the volcanics of Mount Griggs (formerly Knife Peak) and sedimentary mountains; and on the south by the Ukak River which runs along the base of sedimentary Mount Katolinat.

Three formational units are exposed in the vicinity of the Valley

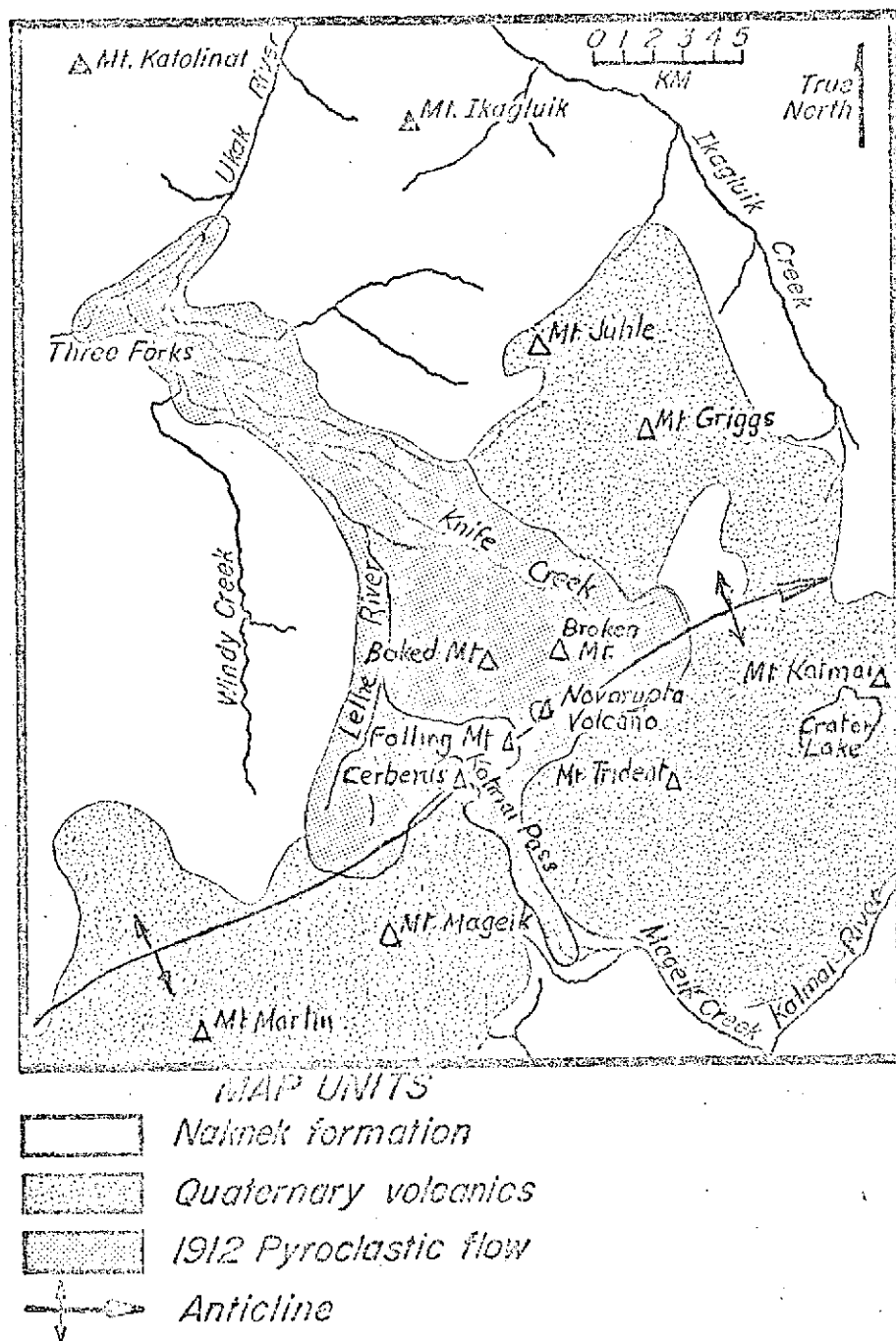


Figure 1.1. Generalized geologic map of the Katmai area based on Keller and Reiser (1959, Plate 29) and Curtis (1968, Figure 1). Three major formational units are exposed in the Valley of Ten Thousand Smokes: the Naknek sedimentary formation, Quaternary Volcanics, and the 1912 Pyroclastic Flow.

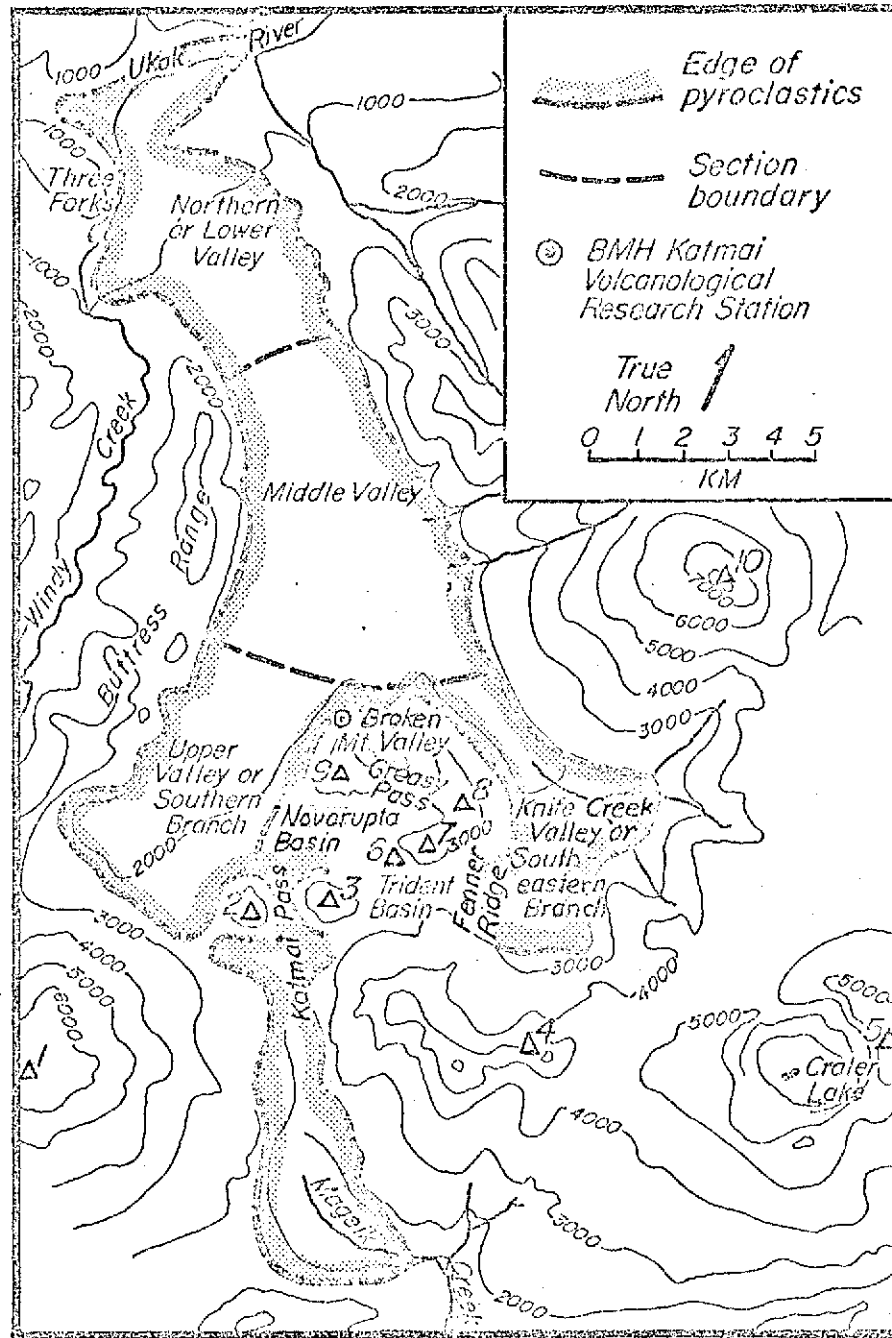
(capitalized Valley refers to entire Valley of Ten Thousand Smokes): Naknek sediments, quaternary volcanics, and the 1912 ash flow. Figure 1.1 is a generalized geologic map of the Valley region. The dominant formation of Upper Jurassic Naknek sediments is over 3000 meters thick and includes stratified, highly fossiliferous sandstones, siltstones, and shales with a basal conglomerate member (Keller and Reiser, 1959, p. 261). Its strata are gently arched along the axis of the peninsula. This trend parallels the Bruin Bay fault to the north. The region also lines on the north-west margin of the area which was tectonically deformed during the 1964 Alaska Earthquake (Ward and Matumoto, 1967, p. 107). The next most prominent formation is the Quaternary volcanoes which are located along the major volcanic arc extending from the Kamchatka Peninsula to the Alaska Range. The third formational unit is the recent pyroclastic deposits which fill the Valley. It consists of a covering of air-fall pyroclastics overlying a very lightly welded tuff. The thickness of deposits of air-fall pumice, ash and lapilli vary from a trace at the terminus of the Valley to several meters at the head of the Valley. Individual layers within the tephra have been studied in detail by Fenner (1923; 1950) and Curtis (1968). Near the terminus of the Valley where the deposits are indurated and show prominent columnar jointing along the river gorges, the flow is quite homogeneous and possesses a pinkish cast. Up-valley the deposits take on a grayish hue, distinct layers of tephra are exposed along stream cuts, and a vitric tuff is exposed at several locations: Novarupta Basin, Knife Creek Valley, and along the River Lethe. The maximum thickness of these deposits has not been measured directly at the head of the Valley, but recent geophysical investigations suggest an

average thickness of at least 45 meters. The volume of these deposits has been estimated to be no less than 3.8 cubic kilometers (Kienle, 1970, p. 6641).

The Valley is Y-shaped, being 17 km long and from 4 km to 12 km wide. Figure 1.2 presents much of the nomenclature for the Valley. For ease in reference, the various branches of the Valley have been distinguished as the lower valley, middle valley, southern branch and southeastern branch. Between the southern and southeast branches are Novarupta Volcano and sedimentary Baked and Broken Mountains. Broken Mountain Valley lies between the latter two mountains, and heads at Greasy Pass (Griggs called this "Greased Hill", 1922, p. 241) which connects these mountains just north of Novarupta. The Valley extending west of Novarupta is known as Novarupta Basin (Allen and Zies, 1923). Mageik Basin (Fenner, 1925) and Trident Basin refer to the minor depressions just north of each peak, respectively. The ridge separating Knife Creek Valley from Trident Basin was first referred to by Fenner (1923, pp. 34-35), who considered it to be the remains of a terminal moraine; it will be called Fenner Ridge. The southern peak of Broken Mountain which rises adjacent to Novarupta has been designated as Stumbling Mountain.

The Katmai Trail traverses the Valley from the village of Savonoski, to Katmai Village via Katmai Pass. The pass lies between two old volcanic domes: Falling Mountain and Mount Cerberus. Both of these mountains are surrounded by the Valley of Ten Thousand Smokes pyroclastic flow which extends southward through the Pass into the valley of Mageik Creek.

In the southeastern branch, Knife Creek heads at the base of Mount



LEGEND

- | | |
|---------------------|--|
| 1. Mount Mageik | 6. Novarupta Volcano |
| 2. Mount Cerberus | 7. Stumbling Mountain |
| 3. Falling Mountain | 8. Broken Mountain |
| 4. Mount Trident | 9. Baked Mountain |
| 5. Mount Katmai | 10. Mount Griggs (formerly Knife Peak) |

Figure 1.2. The various historical and newly designated nomenclature for the Valley of Ten Thousand Smokes. Refer to text for explanations.

Katmai where it issues from the Knife Creek Glaciers. The glaciers of Mount Mageik are the main source of the River Lethe in the southern branch of the Valley. The River Lethe has cut a deep gorge in the Upper Valley. Below Baked and Broken Mountains, both rivers have cut impressive narrow courses over 30 meters in depth. Except for the stream cuts and a marginal terrace called either the strand line or "high water mark", the general profile of the Valley floor is flat.

The present volcanic activity in the immediate vicinity of the Valley is restricted to a few fumaroles. In 1969, steam was issuing from near the summits of Mounts Griggs, Trident, Martin and Mageik, two pits at the margin of the Valley at the south-western edge of Baked Mountain, along the crater rim of Novarupta, and the fractures on the southern slopes of Broken Mountain. The ground was perceptibly warm at the vent of a small aromatic fumarole on the ridge line of Baked Mountain as well as at some of the fumaroles at the terminus of Broken Mountain Valley.

1.3 History of Investigations within the Valley

In October 1898, Spurr visited this region during a reconnaissance study for the U. S. Geological Survey. The account (Spurr, 1900) of his party's journey from Savonoski on the Savonoski River to Katmai Village on the Shelikof Strait via Katmai Pass yields the only geologic commentary on this area prior to the 1912 volcanic holocaust. It is most difficult to reconcile the present topography with the Katmai region prior to 1912 as shown on Spurr's reconnaissance map (Spurr, 1900, Map No. 11). The agreement of the map south of the Aleutian range is excellent, but just to the north of the range correlation is practically impossible until one reaches Naknek Lake. There has been some speculation

that Spurr did not traverse the Valley of Ten Thousand Smokes, but rather the valley of Windy Creek. This supposition is based on the angle at which the Katmai Trail continues north of the Pass on his map. Of particular interest is the fact that the angle between the true strike of the Aleutian Mountains and that depicted on Spurr's map is approximately the magnetic declination. It is known that Spurr's journey through the pass was hurried and such an error is understandable. His party was delayed in Katmai Village, thus allowing time for better mapping south of the range. After studying Spurr's original field notes, Forbes concluded that Spurr did travel up the valley which was to become the Valley of Ten Thousand Smokes, though none of the evidence either way is conclusive (Forbes, personal communication, 1971). The following conclusions are based on the supposition that Spurr did indeed map the Valley of Ten Thousand Smokes.

The topography of the head of the Valley in 1898 was much different than today. Most obvious differences were the presence of a half-mile long lake on the northwestern side of the pass near the summit, which was dammed by the debris of three volcanoes rising above it, and a cone-shaped mountain adjacent to the lake on the west. Both of these features would have been located at the head of the present valley. One can assume that this mountain, which Spurr describes as "having a cone scarcely modified by erosion" (Spurr, 1900, p. 146), was the ancestral Novarupta. It stood at least 1070 meters high (Spurr, 1960, Map. No. 11). Originally it would have encompassed, or at least overshadowed, Baked and Broken Mountains.

Spurr remarks that the only instance in which the otherwise

horizontal green sedimentary strata forming the mountains bordering the valley showed any folding was adjacent to one of the volcanoes. In the Valley of Ten Thousand Smokes, the Naknek strata are folded where the southern end of the Buttress Range abuts Mount Mageik.

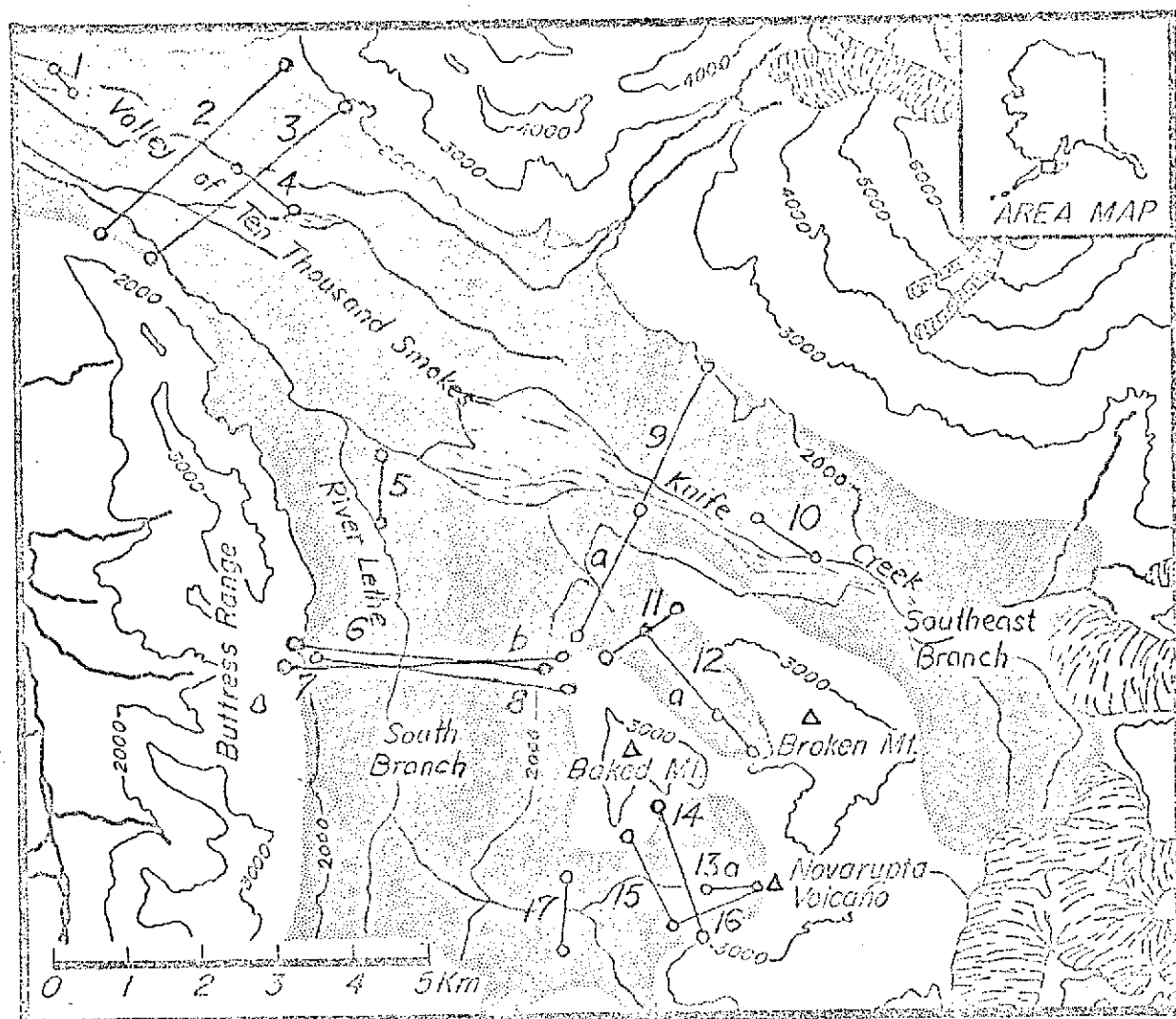
Spurr describes the valley floor as relatively flat except for marginal terraces at 305 meters and 30 meters deep river gorges. The valleys were filled with glacial drift composed of stratified sands, gravels and even boulders near the pass, as well as some sedimentary rock fragments containing Jurassic fossils. Nearer the pass the surface was strewn with boulders, some forming sharp hillocks. The only unmodified drift was that in recently abandoned moraines. Several such moraines were damming mountain gorges.

The National Geographic Society was responsible for the earliest investigations to the Katmai region following the 1912 eruption. In the summer of 1912, Martin (1913) visited Kodiak and Katmai Village. In 1916, Griggs (1922) led a scientific party to the area, but not until the end of the field season did they venture north of Katmai Pass and discover the Valley of Ten Thousand Smokes. Griggs returned in the following years to head the investigations in the Valley. In 1917, Shipley (1920) took gas samples and measured the temperature of several fumaroles, studied the encrustations near some of the vents, and made a ground temperature profile across the terminus of Novarupta Basin. In 1918, Sayre and Hagelbarger (1919) continued the study of the temperatures of the fumarolic emanations. In 1919, Zies and Allen conducted even more extensive investigations of the fumaroles and their gasses and sublimates. Their reports have become classics (Allen and Zies, 1923; Zies, 1924a; Zies,

1924b; Zies, 1929). In 1919, Fenner accompanied Griggs' expedition. Fenner returned to the Valley in 1923 to complete his studies. His geologic research resulted in a series of papers published over a span of 30 years from 1920 to 1950. (Most of these are listed in the bibliography.)

For many years no scientific parties visited the area; then a new round of studies began in the 1950's and is still continuing. In 1952, Wilcox of the U. S. G. S. collected a suite of specimens from alteration zones adjacent to a fumarole at the terminus of the Valley. Lovering analyzed these samples for major and minor constituents (Lovering, 1957). In 1953, the National Park Service promoted geological surveys within the Katmai region. Curtis, Juhle and Williams took part in this re-examination of the Valley (Williams, 1954). Curtis conducted a detailed study of the distribution of several distinct layers of tephra (Curtis, 1968). Then, in the early 1960's, a group of European investigators visited the Valley. Their views are presented in an article by Bordet et al. (1963).

With the construction of the Baked Mountain volcanological research station (BHM) a new series of investigations began. From this base, Kubota and Berg (1967) used seismic techniques to locate magma chambers in the area. Ward and Matumoto (1967) studied the seismicity of the region and conducted a limited seismic refraction profile near the terminus of the Valley to test the applicability of hammer seismology in determination of the thickness of the pyroclastic deposits. Sbar and Matumoto (1971) conducted several such seismic refraction profiles across major branches of the Valley. Kienle (1969, 1970) surveyed four



LEGEND

- | | |
|---|--|
| 1. Ward and Matumoto's seismic profile | 12. Anna's surface magnetic profile M-M' |
| 2. Anna's aeromagnetic profile 31 | 12a. Kienle and Bingham's seismic profile C-C' |
| 3. Kienle's gravity profile KV-4 | 13. Anna's ground magnetic profile H-N'' |
| 4. Kienle's seismic profile E-E' | 13a. Kienle and Bingham's seismic profile D-D' |
| 5. Kienle's seismic profile H-H' | 14. Kienle's gravity profile KV-3 |
| 6. Gedney et al.'s seismic profile A-A' | 14. Sbar and Matumoto's seismic profile 3 |
| 7. Kienle's gravity profile KV-1 | 15. Anna's surface magnetic profile N'-N''' |
| 7b. Sbar and Matumoto's seismic profile 2 | 16. Anna's surface magnetic profile N'''-n |
| 8. Anna's aeromagnetic profile 15 | 17. Shipley's surface temperature profile |
| 9. Kienle's gravity profile KV-2 | |
| 9a. Sbar and Matumoto's seismic profile 1 | |
| 10. Kienle's seismic profile F-F' | |
| 11. Gedney et al.'s seismic profile B-B' | |

Figure 1.3. Locations of other geophysical investigations in the Valley of Ten Thousand Smokes.

gravity traverses across the main arms of the Valley. In 1969, Gedney et al. (1970) made two explosion seismic refraction profiles near Baked Mountain. This seismic work was continued in 1970 by Kienle and Bingham, who conducted two more profiles and in 1971, Kienle added 5 more short profiles. The ground magnetometer survey treated in this report was conducted in 1969. In 1970 and 1971, Anna and Stone continued the magnetometer survey, primarily from helicopter.

1.4 Areas of Controversy

a) The Source of the 1912 Pyroclastic Flow

Immediately following the ash-falls of 1912 and the concurrent disappearance of the top of Mount Katmai, it was mistakenly assumed that Katmai was the sole source of the eruption. Later it became apparent that Novarupta had also contributed to the pyroclastic deposits in the Valley.

At first, the early travelers to the Valley of Ten Thousand Smokes thought the pyroclastic fill had been emplaced by a mudflow. Shipley (1920) proposed this sequence of events to account for the Valley fill: first, Novarupta exploded throwing out vast amounts of material; this ejecta fell on the snow-covered northern slopes causing much melt; heavy rain accompanied the eruption and aided this hot slush to slide into the valley forming a gigantic mudflow. The eruption of Mount Katmai followed the emplacement of the mudflow (Shipley, 1920, p. 141). The mudflow hypothesis was quickly abandoned once its obvious inadequacies were exposed. The arguments against a mudflow are presented by Fenner (1920, pp. 577-578). Basically, the existence of liquid water

at eruptive temperatures near incandescence would be incredible.

Griggs (1922) postulated that a granitic batholith was approaching the surface over a wide area encompassing the volcanic range and the Valley. He believed that this mechanism could account for eruptions from Katmai and Novarupta, as well as from fissures throughout the Valley. A batholith would also result in continued fumarolic activity. Griggs interpreted the eruptive events as beginning with the opening of many vents in the Valley floor and the release of lava through these. He supposed that the lava gave off so much gas following its release, that it became a fiery suspension of incandescent fragments buoyed up by the gasses they themselves were evolving. The masses accumulating about individual vents ran together until they covered the entire valley floor and then, under the influence of gravity, the entire mass poured down the Valley much like a flooding river. Next, Novarupta went into typical explosive eruption, followed closely by violent explosions from Mount Katmai. Meanwhile, the craters of Mounts Mageik and Martin supposedly opened too.

The relatively undisturbed, horizontal Naknek sedimentary strata of the Valley walls led Fenner (1925b) to propose that the source of the pyroclastic flow was a sill intruded at shallow depths. The diminution of fumarolic activity by 1923 (estimated to be 1/3 of that in 1912) further indicated that the mass of hot material was not great. Fenner deduced that the source of the sill was a magma reservoir situated beneath the volcanic zone of Mounts Katmai, Trident, Mageik and Martin. As the magma rose from this reservoir, a portion found release northward

shattering the lower slopes of Mount Trident and fracturing the valley areas as they were raised relative to the surrounding more massive mountains. These fractures served as vents for the magma. Fenner (1920, p. 589; 1925b, p. 202) felt that Novarupta was similar to the other feeders for the tuff flow, although it was unique in that it broke out on a slope rather than along the Valley floor. Chance conditions were such that later this vent became enlarged and erupted great quantities of pumice and ash and extruded a lava dome.

According to Fenner, much ejecta was also thrown out from Mount Katmai following the flow. At first Fenner (1925b, p. 201) believed the channel supplying magma to the Valley region from the chamber underlying the volcanic chain was not necessarily the same conduit supplying material to the Katmai crater; but in his last paper Fenner (1950b, pp. 707-708) acknowledged the interconnection of the vents and assumed that the Valley sill escaped from the Katmai conduit before the magma reached an explosive stage in the crater. Fenner (1920, p. 606) attributed the formation of the Katmai crater to collapse of the crater walls and incorporation of this material in the new magma.

Fenner was the first to point out that the topographic regime of the Valley region would have prevented the present distribution of pyroclastics had Katmai been the primary source. Indeed, Fenner proved that "from no single source...could the material well have reached all the areas where it is to be found" (Fenner, 1923, p. 17). Fenner (1950b, pp. 707-708) recognized Novarupta as a major source, but he believed

that much of the tuff flow erupted from fissures throughout the Valley. He did not appreciate the amount of subsidence around Novarupta although he did realize that the settling around the dome did seem referable to a collapse of the roof over the body of magma (Fenner, 1925b, p. 219).

Williams (1954, pp. 58-59) was convinced that no sill was injected beneath the Valley and that the fumarolic gasses and associated sublimates were derived from the fragmental ejecta itself. He attributes the pyroclastic eruptions to "glowing avalanches" issuing from swarms of fissures at the head of the Valley. These fissures were supposedly aligned along a zone essentially paralleling the volcanic axis, although offset to the north. He also concluded that voluminous amounts of the two magmas were erupted from Mount Katmai, leading to the wholesale collapse of the summit to form the huge caldera. According to Smith (1960, pp. 809-810) the pyroclastic fill of the Valley was erupted from fissures at the head of the Valley and emplaced by flowage of fragmental material which was itself continuously emitting hot gasses. Similarly, Bordet, Marinelli, Mittenpergher and Tazieff believe that the ignimbritic deposits had been poured out through a swarm of fissures as an "overflowing glowing cloud" consisting of an emulsion of gas, glass splinters, hard particles of pumice, and intratelluric phenocrists. They were impressed by the apparent interconnections underlying the Katmai district volcanoes. They assume that these interconnections probably correspond to regional tectonic faults (Bordet et al., 1963, pp. 7-8). Ward and Matumoto (1967) also attributed the main ash flow to Novarupta or fissures near the head

of the Valley.

Finally, Curtis's (1968) tephra studies prove that Novarupta was the main source of eruptive material in 1912. Curtis distinguished 9 layers of tephra overlying the tuff flow. For 4 of these he was able to measure sufficient sections to prepare isopachous maps (a composite of these is presented in Figure 5.2). The contours of these maps close about Novarupta, and the general trend of most of the other layers also attests that the dome was their source. Apparently, only the last thin layers were erupted from Mount Katmai.

Curtis thought that the layering of the tephra reflected individual eruptive events. He recognized the possibility that orientation of the conduit may have been partially responsible for the differing distribution patterns exhibited by successive tephra layers. However, he thought that the low correlative value of the stratification among various outcrops was due to variations in wind direction, speed and turbulence, and the eruptive stage. Since one of the first layers shows evidence of having been deposited by running water, Curtis concludes that temperatures during this part of the eruptions were sufficiently high to promote rapid melting of glaciers and snowfields adjacent to the Valley.

Sbar and Matumoto's (1971) seismic refraction profile in Novarupta Basin shows a general thickening and greater complexity for the flow here than in the other branches of the Valley. This evidence also supports the assumption that Novarupta was a major source of the flow.

Curtis (1968) deduced that two magma chambers took part in the 1912 eruptions. He believes that the rhyolitic chamber underlies

Novarupta, while the andesitic chamber underlies the arcuate chain of four volcanoes: Katmai through Martin. It appears then that the conduits of the two chambers were connected throughout most of the 1912 eruptions. Supposedly a column of magma supported the summit of Katmai during most of the eruption, allowing the summit to slowly collapse as the magma found release at Novarupta. When all activity had ceased at Novarupta and the two chambers were again distinct, a small amount of ash was erupted from Mount Katmai. In the waning eruptive stages of Novarupta, subsidence of the surrounding area began. The total subsidence seems to have amounted to over 250 meters. At the time of eruption therefore, Novarupta's vent would have been at a sufficient elevation to supply tuff to all areas where it is found. Curtis (1968, p. 192) concluded that "Novarupta and its radial and, possibly also, concentric fissure systems were the source vents for the great tuff flow." Curtis (1968, p. 194) believes that the continued activity of fissure fumaroles within a mile radius of the dome strongly attests to the existence of conduits leading to a magmatic source at depth, although no feeder dikes of any kind have been discovered in this area of disturbance.

If it had had an elevation some 250 meters (800 feet) higher than today, Novarupta is the one location in all of the Valley of Ten Thousand Smokes from which the tuff flow could have reached all the places where it is found (Curtis, 1968, p. 192). Eruptions from this higher vent could easily have moved into all branches of the Valley and down the valley of Mageik Creek, too. Spurr's map of the Katmai region in 1898 substantiates the notion of a higher ancestral Novarupta.

b) The Banded Ejecta of Novarupta

The banded structure of some Novarupta lava and pumice has been the subject of much debate. According to Griggs (1922, p. 297) the new eruptive magma (rhyolite) dissolved the old rock (andesite) from the summit of Mount Katmai by the process of "overhead-stopping". Fragments of the old rock in the process of sinking contaminated the newly extruded lava, resulting in the andesitic bands in the rhyolitic extrusives. Fenner (1950b, pp. 708-710) also believed that the primary eruptive magma was the rhyolite, but that the andesitic streaks are fragments of volcanic glacial debris and Naknek sediments which were attacked by the rhyolites as it was erupted from fissures in the valley floor, and through the detrital material covering the valley floor. While the magma was at first quiescent in the vents, it would have assimilated the wall rocks of Naknek sediments and the overlying volcanic glacial drift. This contaminated lava would next have mingled with the eruptive rhyolite. Fenner therefore considered that the dark scoria and inclusions represented partially digested rocks from the conduit walls. He was able to correlate spatial differences in the pyroclastic flow with the probable composition of the glacial drift at each location (Fenner, 1950b, pp. 707-710).

Others attributed the andesitic inclusions to processes of magmatic differentiation. Fenner (1926, p. 772) thought that the crystallization process was incompetent to explain the form of variation of Katmai rocks. But, Forbes' (personal communication, 1968) studies suggest that the 1912 pyroclastics are differentiates of an andesitic magma which was subjected to a period of stillstand and subsequent fractionation by gravity settling

of mafics. The basic bands may be due to flow differentiation of mafic cumulates dragged up along the vent contacts during the terminal movement of magma along the conduit system (see also sections 2.3b and 5.3).

Another view was proposed by Williams (1954, p. 58), who considered that the intermingled rhyolitic and andesitic ejecta were formed by simultaneous discharge of the two magmas from the same or closely adjacent fissures at the head of the Valley. On the other hand, Curtis (1968, pp. 194 and 207) proposed that a rhyolitic magma chamber underlying Novarupta was contaminated by andesitic lava from beneath Mount Katmai and its probable interconnections with other recently active volcanoes in the area. Under this regime, the andesitic lava would have reached Novarupta via a conduit which became closed in the later stages of eruption. The distribution of dark bands in Novarupta dome suggests that the conduit supplying andesitic magma to the rhyolite was sheet-like in cross section.

c) Nature of the Fissure Fumaroles

The presence of numerous high temperature fumaroles for several years after the eruption was interpreted by Griggs (1922) as support for his hypothesis that a batholith was approaching the surface beneath the valley region. Similarly, the distribution of fumarolic activity led Shipley (1920, p. 149) to conclude that "the mudflow is either in intimate contact with a heated mass of the earth's crust or the outlets for the gaseous emanations from the magma are well distributed beneath the flow". Shipley (1920, p. 142) proposed that fumaroles are principally located along cracks in the mudflow which had been formed as the mudflow

dried and contracted over an uneven bedrock topography.

Allen and Zies also believed that certain features of the fumaroles indicated the presence of a lava body beneath the old valley floor. They attributed the rectilinear alignment of the fumarolic cracks to their deep-seated fissure origin. They could not believe that a reasonable (about 60 meters) thickness of pumiceous material would be able to account for the high temperatures persisting in many fumaroles throughout the Valley in 1919, and since the structure of the pumice showed that it had lost most of its gasses during eruption, it could not be the source of the amounts of gasses still being exhaled in 1919 (Allen and Zies, 1923, p. 95). Furthermore, analysis of the metallic sublimates from some of the fumaroles as contrasted to the unaffected ash evidenced that the prevalent magnetite could not have been derived from the surrounding pumice (Zies, 1924a, p. 166).

Fenner (1925b) interpreted the diminuation of fumarolic activity by 1923 as support for his hypothesis that a sill, not a batholith, had been intruded beneath the Valley in 1912. According to Fenner, bedrock fissures served as feeders for the tuff flow. The distribution of the fumaroles was similarly controlled. Such a deep-seated fissure origin of fumaroles was challenged by Williams (1954, p. 58) who observed that the fumarole cracks gradually disappear downward within the avalanche deposits. In concordance with Williams, Curtis (1968, p. 186) reports that his examination of all the bedrock exposed below the ash revealed no feeders for either the tuff flow or the fumaroles. The old fumarole conduits and their surrounding alterations fade rapidly with depth; none

were observed to extend more than 12 meters into the tuff flow.

In a recent seismic survey by Sbar and Matumoto (1969, p. 340), however, it was noted that in a number of places where the refraction profiles crossed fumarole lines, a discontinuity in the deeper horizons was observed. To them, this correspondence suggested that the vents penetrated to the old valley floor. Gedney et al. (1970, p. 2623) suggest that the correspondence of fissure fumarole lines with a fault in the lower seismic horizon shows that some fumarolic activity did originate through bedrock faults, probably from the degassing of residual magma in a subsurface reservoir.

Correlation of the seismic, gravimetric and magnetic data across the mouth of the southern branch of the Valley (see Figure 4.10) suggests an undulating, if not faulted, surface for the bedrock. Since the exposed Naknek strata are nearly horizontal in this region, and Spurr (1900) reported the 1898 valley as generally level, one must conclude that the floor was subsequently faulted; perhaps in connection with the 1912 eruption as suggested by Fenner (1925b, pp. 204-206). The positioning of the fumaroles above steep bedrock slopes in no means proves that the vents have their "roots" in the bedrock, or below. Rather, it may only suggest that the bedrock relief controlled the establishment of fumaroles by influencing the location of faulting within the flow, by guiding the rising vapors, and by concentrating the ground water.

The general consensus (Lovering, 1957; Smith, 1960; Ward and Matumoto, 1967) is that the majority of the valley fumaroles were generated by degassing of the pyroclastics and the vaporizing of ground water.

This process could account for the waning of fumarolic activity as the deposits cooled.

A deep-seated origin, however, is suggested for some of the fumaroles at the head of the Valley. Griggs (1922, pp. 238-239) describes several locations at the head of the valley where the fumaroles were observed to extend into undisturbed sandstone strata. Ward and Matumoto (1967) contend that the prominence and persistence of fumaroles along the bench (strand line) on the western side of Baked Mountain require more explanation than merely sweating out of the flow, which would necessarily thin near the edge of the Valley. According to Forbes (personal communication, 1968), the fumaroles which are now active along linear trends on Broken Mountain, the summit ridge of Baked Mountain and the solfatara field adjacent to Novarupta are degassing through fissures which cut the underlying sediments. The persistence of the fumaroles at the head of the Valley have been attributed to the presence of magma in the subsurface in this area (Lovering, 1957; Smith, 1960; Forbes, personal communication, 1968).

Allen and Zies (1923, p. 152) report that the highest fumarolic temperatures in 1919 followed a discontinuous zone about Baked and Broken Mountains with an extension out into the middle valley (refer to Figure 5.4). This zone is also marked by faulting, perhaps related to the subsidence of Novarupta in the waning eruptive stage. Lovering (1957, pp. 1586, 1588) also remarks that the areas richest CO_2 and the sulfur acid gasses in 1919 surround Baked Mountain and Broken Mountain near Novarupta. Sulfur enrichment is characteristic of active volcanism,

not later degassing of effusives. Drainage of a magma chamber underlying the head of the Valley through the major vent at Novarupta could have led to settling of the Baked-Broken Mountain complex, as well as to the obvious subsidence in the immediate vicinity of Novarupta. Such collapse has been postulated by Fenner (1925b, p. 210). Escape of magmatic gasses along such an encircling zone of bedrock faulting could be responsible for the elevated temperatures and sulfur content peculiar to this area in the early years after the 1912 eruption.

The seismic recordings of Kubota and Berg (1967) suggest the presence of several magma chambers in the neighborhood of the Valley. Magma chambers were located at intersections of ray paths (epicenter to recording station) which show no S-phase, indicating transmission through a medium of low rigidity. Magma chambers were found beneath Mounts Katmai and Trident, Mount Griggs, and Mounts Mageik and Martin. None of the data collected indicate the presence of magma beneath the Novarupta area; however, one of the inadequacies of the mode of location is that it cannot detect small pockets near or beneath the recording stations and one of their stations was operated from the Baked Mountain Research Station.

d) Possible Concentrations of Magnetic Minerals

It has been much debated whether or not any of the abundant accumulations of magnetite observed throughout the Valley in the first few years of intense fumarolic activity could have been preserved. For example, only one magnetite accumulation has been described in the literature. In 1919, Zies (1924a, p. 166) observed "loosely coherent

octahedra of almost pure magnetite" forming the lining of the roof of a series of fissure vents occupying an area approximately 100 ft by 100 ft (30.5 m x 30.5 m) at fumarole 148 in the middle Valley. The deposit was concentrated along ten parallel fissures. "The depth of the deposit varied from four to nine inches...the width varied from twelve to fifteen inches" (Zies, 1929, p. 16), and "in places the deposit was four inches thick" (Zies, 1924a, p. 166). Fenner revisited this site in 1923 and reported the absence of visible magnetite (Zies, 1929, p. 16).

Both Shipley (1920) and Zies (1924a) recognized that although exposure to high temperature emanations could increase the iron content of the ash nearby, prolonged exposure tended to decrease the iron-content. Zies (1929) offered this explanation: rising hot acid gasses may have extracted metallic constituents from their source areas, and also along their routes. As these emanations cooled, metallic sublimates would form a lining in the conduits, many encrustations would be built up around the vents, and the nearby ash would be altered. Fumarolic magnetite and hematite, formed by the hydrolysis of iron transported as a halide in the vapor phase, would thus be concentrated in the upper portions of high temperature vents and under proper pressure conditions, as the temperature of the emanations dropped, magnetite might even have been deposited along the vents at considerable depths. When the temperature of these fumaroles fell to a point where active condensation of the acid steam could take place in or near the vent, however, the acid gases would go into solution and leach the surrounding area, decomposing the magnetite and releasing the iron unless the conduit had developed some form of

protective cover. Certainly many sublimates were leached by the acid solutions or removed by runoff over the years.

If the vents had become blocked off early in their history, and thus protected from the ready access of surface waters, a deposit resembling a mineral vein might result (Zies, 1929, p. 60; Fenner, 1923, p. 51). Early investigators in the Valley report instances in which vents were blanketed by deposits from heavily laden waters (Griggs, 1922, p. 245), or filled in by the constantly shifting surficial ash (Fenner, 1925b, pp. 206-207). In other instances, surficial accumulations of fumarolic clays could certainly have formed an effective seal over some of the vents.

In a recent study of the alteration zones around fumarole No. 1, Lovering (1957, p. 1596) discovered that the iron content was high just outside the inner lining of the vent. His findings are presented in Table 1.1 and Figure 1.4. Apparently here the magnetite and hematite, which had been precipitated by hydrolysis early in the life of the fumarole, were protected from the leaching acids as the temperature of the emanations dropped.

Accumulations of iron have been observed in other ash flow deposits. Mackin (1952, p. 1338) discovered veinlets of crystalline hematite occurring in joints and minor breccia zones in the upper lithoidal unit in the ignimbritic deposits of the Iron Springs District of Utah. Gilbert (1938, p. 1851) identified the grains of magnetite and hematite at the top of a welded tuff in eastern California as products of sublimation of gasses. In extensive studies of the Bishop Tuff, a region apparently similar to

Table 1.1

Variation (Weight Percent) of Ferrous- and Ferric-oxide
in Samples from Alteration Zones about
Fumarole No. 1, from Lovering (1957, Table 1, p. 1593).
Refer to Figure 1.4 for explanation of zones.

Zone	1	2	3	4	5	6	7
% Fe_2O_3	1.22	4.59	3.11	3.20	1.15	1.99	1.33
% FeO	.58	.74	1.41	.99	.59	.90	1.38

Table 1.2

Variation of Ferrous- and Ferric-oxide in the
Bishop Tuff, after Sheridan (1970, Table 1, p. 864).

	Average for unaltered tuff	Average for unaltered fumaroles	Average for rare intensely altered inner zone of some fumaroles
% Fe_2O_3	0.43	0.93	4.6
% FeO	0.19	0.24	1.53

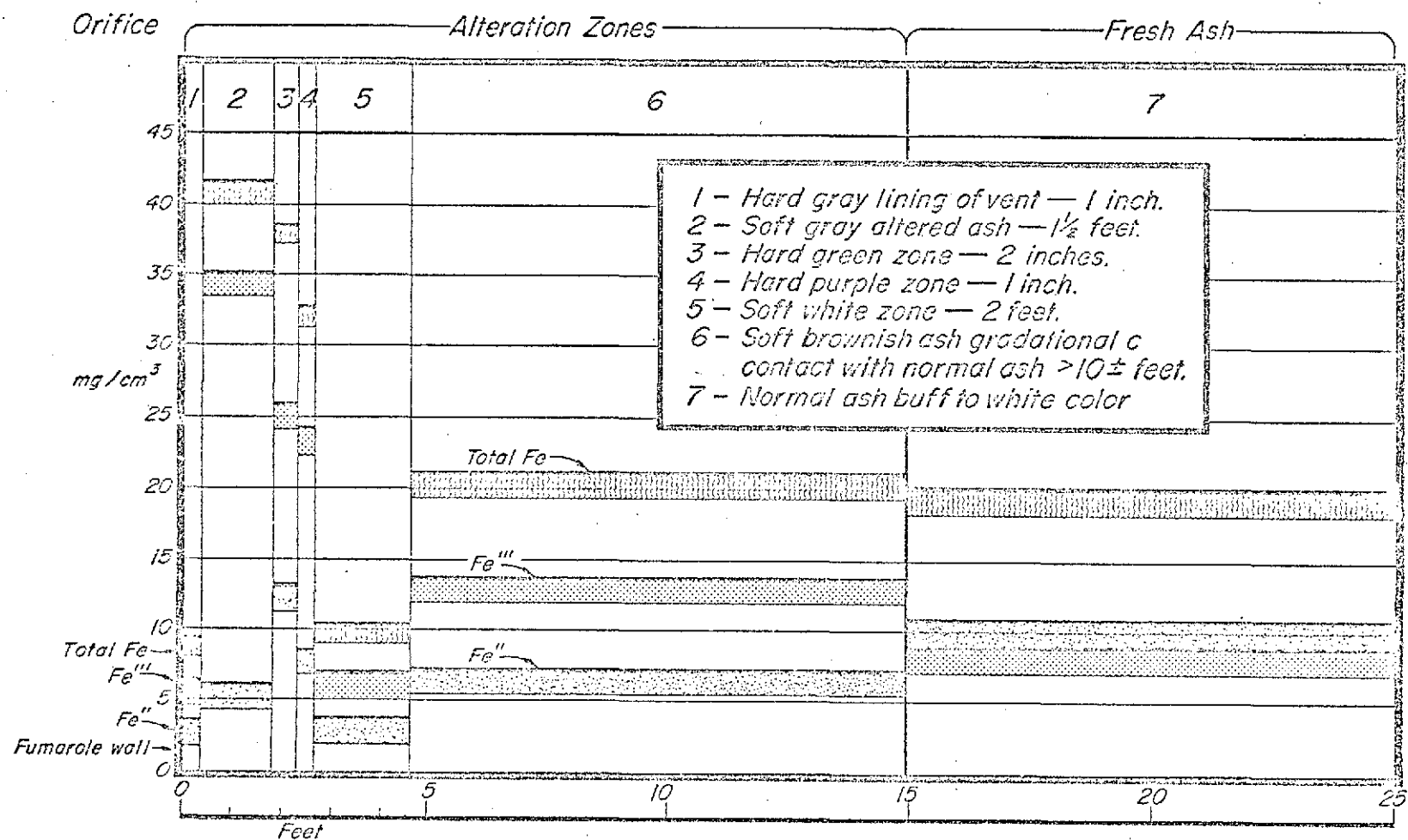


Figure 1.4. Variation of ferrous, ferric and total iron in alteration zones around fumarole No. 1 (Zies, 1929) in the Valley of Ten Thousand Smokes in 1952 (After Lovering, 1957, Figures 3 and 5). Refer to Table 1.1.

the Valley of Ten Thousand Smokes, Sheridan (1970, pp. 860 and 864) discovered that the great majority of fumarolic mounds have no significant overall chemical difference from the surrounding tuff, although their iron content is increased. A few fumaroles showed an inner zone of extreme black and red discoloration about their central joints. The average iron content was found to vary among unaltered tuff, fumarolic tuff, and the rare inner zone altered tuff. These variations are given in Table 1.2. Sheridan also noted that although some fumarolic fractures are coated with hematite and opal, minerals that might have formed during the early fumarolic stage are now missing from most fumaroles. He attributes this absence to probable attack by acidic fluids in the latter part of fumarolic activity.

There may also be some secondary concentrations of magnetite. Kienle discovered several small accumulations of magnetite grains in depressions near streams where they were apparently deposited during periods of large runoff (Kienle, personal communication, 1970).

e) The Cause of the Marginal Terrace

Almost throughout the Valley is a marginal terrace about 100 meters above the valley floor. The cause of this terrace has been much debated. According to Shipley (1920), the terrace marks the highest level of the flow; thus the synonym "high water mark". Others thought that the terrace was formed as the center of the flow compacted after coming to rest. Fenner (1925b, pp. 204-206) did not believe there was a sufficient volume of pyroclastic fill to account for the strand line by mere compaction, besides, he believed there was evidence that the flow was indurated

prior to any downward movement of the valley floors. Fenner proposed that as the magma was drained through the sill into the valley regions, the area readjusted. The terrace, or strand line, was formed along the valley walls as the bedrock settled over the body of the intruded magma.

Curtis (1968, p. 186) attributed the strand line or "high water mark" around much of the margin of the Valley to gradual compaction of the tuff flow after the emplacement. He concluded that probably the compaction was proportional to thickness and thus would have been greatest over the old stream channels; consequently, the location of present streams would be over the old channels. Partial welding within the flow (Smith, 1960), subsequent melting of an ice lens buried during the eruption (Hamilton, personal communication, 1971), or the existence of buried glacial terrace (as described by Spurr, 1900) are other explanations for the configuration of the cross-valley profile.

f) The Age of the Lower Tuff Unit

There has been some speculation that some of the tuff in the Valley of Ten Thousand Smokes originated prior to the 1912 pyroclastic flow.

Fenner (1923) concluded that some of the tuffs which had been thrown out by explosion craters at the base of Mt. Griggs represented a pre-1912 tuff. These particular tuffs, although similar in appearance to the recent tuffs, are much more indurated and their inclusions are much more decomposed. Fenner regarded these as representative of "a hardened tuff of considerable age that formed a layer at or near the old surface along a stream or wet piece of ground at the time when the sandflow spread over it" and he supposed that "the ensuing explosions broke it up and

threw it broadcast" (Fenner, 1923, p. 23).

Curtis (1968, p. 204) describes two sections of tuff within Katmai caldera which are evidently of pre-1912 origin. Forbes (personal communication, 1971) also suggests that the lower tuff unit exposed at several locations in the upper Valley, in particular at Fissure Lake, may well be of pre-1912 origin.

g) Thickness of the Flow

The objective of most of the investigations in the Valley of Ten Thousand Smokes has been estimating the total volume of the pyroclastics erupted in 1912. The primary unknown factor in such a determination is the thickness of the flow. The several estimates for the thickness of the tuff are given in Table 1.3. As more geophysical evidence is gathered, the more conservative become the initial predictions of Fenner (1923, p. 67); but besides the geophysical evidence there is another, to date apparently ignored, indication of the thickness of the deposits. Spurr (1900, p. 146) describes the pre-1912 Valley as generally level except for river gorges and a distinct horizontal terrace about 305 meters above the floor. If one assumes that the so-called "strand line" is indeed an expression of this terrace since buried beneath the pyroclastic material, it is possible to deduce a minimum thickness for the flow. Today the terrace along the western flank of Baked Mountain is approximately 100 meters above the level of the present floor. It is clear therefore that the pyroclastic deposits in this branch of the Valley are at least 200 meters thick. Since the terrace also is covered by a mantle of ash, the flow in the valley must be thicker by this amount of ash. Also, any

Table 1.3

Previously Suggested Maximum Tuff Thickness (meters)

Investigator	Method	Lower Valley	Middle Valley	Southern Branch	Southeast Branch	Broken Mtn. Valley	Novarupta Basin
Fenner	induction	---	30	60	60	---	---
Curtis	geomorphology	120	200	225	150	50	---
Kienle	gravimetrics (Model P)	65	---	70	69	25	25*
Kienle	gravimetrics (Model F)	140	---	150	170	60	50*
Matumoto and Ward	seismic refraction	46	---	---	---	---	---
Gedney et al.	seismic refraction	---	---	72	---	36	---
Sbar and Matumoto	seismic refraction	---	---	92	22	27	80
Kienle	seismic refraction	>46	>63	---	>100	104	>94

*value queried since no bedrock reference data for these calculations.

subsidence of the valley floor during the eruption would have the effect of increasing the thickness of the flow above the 200 meter estimate.

By imposing the gradients of adjacent valleys to the Valley of Ten Thousand Smokes according to the elevation of the base of the flow at the end of the valley, Curtis (1968, p. 187) reconstructed probable pre-1912 Valley profiles. Based on this reconstructed profile, the pyroclastic fill is probably between 700 and 900 feet thick and would amount to some 2.63 cubic miles (11 km^3).

In 1966, Kienle (1969) completed four gravity traverses across the main branches of the Valley. He determined that the minimum average thickness of the pyroclastic deposits is fairly uniform and ranges from 35 to 40 meters. His estimates show minimum ash thickness of 6 to 8 meters over the ridges of Baked and Broken Mountains, respectively (Kienle, 1969, p. 138), and maximum thickness of 70 meters over the buried river channels (Kienle, 1970, p. 6647). Kienle (1970, p. 6659) estimates the volume of the flow to be between 3.8 and 4.7 km^3 , depending upon the assumed density contrast.

Various thicknesses have been suggested from seismic refraction surveys. Sbar and Matumoto (1971) determined that the main body of the tuff varies in thickness from 20 to over 70 meters. Gedney et al. (1970) found a maximum thickness of 50 meters for the pyroclastics in the southern arm of the Valley, and of 25 meters in Broken Mountain Valley. Kienle's (personal communication, 1971) profiles imply tuff thicknesses varying from 50 meters in the lower valley to over 100 meters in Broken Mountain Valley.

The reduced data from all available seismic refraction profiles is presented in Appendix D. The implications of these data are further discussed in Chapters IV and V.

1.5 Field Procedure for the Ground Magnetometer Survey

In the hope of answering some of the many questions about the pyroclastic flow in the Valley of Ten Thousand Smokes, a ground magnetometer survey of the region was undertaken in 1969.

The purpose of magnetometer surveying is to ascertain local spatial variations in the magnetic field which can be related to local geologic structure. It is required, then, to remove the gross effects of the geomagnetic field and its diurnal variations from all survey data. Since the temporal changes in the Earth's field can be considered constant within an area the size of the Valley of Ten Thousand Smokes (Grant and West, 1965, p. 207), it is possible to use the record of the daily fluctuations in the field taken at a local base station to apply a diurnal correction to all magnetometer survey data. Such a magnetometer base station was established at the Katmai Volcanological Research Station on Baked Mountain. It is marked by a wooden post upslope and to the west of the Baked Mountain Hut. Diurnal fluctuations in the geomagnetic field were monitored at this station with a Varian Model V-4938 Rubidium Vapor Magnetometer. The sensing head of the magnetometer was buried adjacent to the post designating the magnetometer base. The Lamor frequency output of this instrument was monitored from within the camp. Due to malfunction of the recorder, the Lamor frequency display had to be manually recorded, usually at half-hour intervals during field survey. The Lamor

frequency can be converted to magnetic intensity to a precision of 0.01 gammas.

The magnetometer base station also served as a check point for all the field survey instruments. In order to be able to compensate for possible instrumental drift, the various instruments were read at the base prior to and following each day of surveying.

Relative spatial variations in the vertical magnetic field were measured with a Cisco-Sharpe Model MF1-100 fluxgate magnetometer, having a precision of ± 2 gammas. The instrument displays the vertical field in gammas relative to an arbitrary zero. This arbitrary zero positioning permits direct comparison with any chosen datum; in this case the fluxgate was set at 150 gammas at the Baked Mountain Hut Magnetometer Base Station.

Since the fluxgate magnetometer is a compact, light-weight instrument, easily carried and operated by a single person, it was ideal for less detailed work and for "spot readings" on a reconnaissance basis. Due to the high magnetic latitude of Katmai National Monument (magnetic inclination of 71.2 degrees) anomalies in the vertical field are comparable to anomalies in the total field.

An Elsec proton precession magnetometer type 592/132 FS was used for survey measurements of the total geomagnetic field and its vertical gradient. The recording unit displays the number of proton precessions per three second interval. This value converts to gammas of field strength within 0.1 gammas. The adjustable sensor probe support facilitated readings at two heights for determination of the vertical gradient of

the total field.

The proton precession magnetometer was read at least twice at each station to ensure that correct values were recorded and to guard against errors caused by short term fluctuations in the geomagnetic field. If the two readings were not in close agreement, the station was occupied until a steady reading was obtained. This procedure was repeated for both upper and lower probe positions if the vertical gradient was being measured.

A Brunton and a Meridian magnetic compass were used to take magnetic bearings along the traverses, and to shoot angles to prominent features for location of specific stations. Isolated "spot reading" stations, and most initial and final traverse stations, were located by triangulation on at least three well-separated landmarks, weather permitting. In the cases where low cloud cover precluded such triangulation, the location of the station was found only by reference to the U. S. G. S. map A-4, Katmai Quadrangle.

During the surveys, straight line traverses were maintained by visual sighting back along flagged stakes marking previous stations, as well as by compass bearing and fore-sighting to landmarks.

Total field stations were spaced along the surface at intervals of small integer (usually one or two) multiples of 28.05 ± 1.00 meter, which corresponds to the length of the electric cable between the sensing head and recorder of the Elsec magnetometer. When adverse topography, such as stream beds, dictated adjustment of this standard station spacing

scheme, the offset was paced or estimated.

The vertical field traverses, except for C-C' below, were paced. In the cases where the fluxgate traverses follow previous total field traverses, (e.g., B-B'', B-B''', b-b'') the distance between nearby paced vertical field stations and the flagged stakes marking total field stations was recorded. This procedure permitted the proper coincidence of the two data sets. Stations along traverse C-C' were spaced with a fifty-foot (15.2 m) length of nylon cord. This traverse, which coincides with one of the seismic survey lines (Gedney et al., 1970; seismic profile A-A'), was preceded by a transit theodolite survey. The estimated or paced distance between surveyed positions (marked with small stakes) and nearby vertical magnetometer stations was recorded, thus allowing verification of location and spacing of the magnetometer stations. It was also beneficial to correlate the elevation differences derived from the level survey with the elevation recorded by the altimeters during the magnetometer traverse.

Usually, altimeter survey accompanied the magnetometer traverses, with altimeter elevations recorded at selected stations.

The altimeter (one of two Paulin altimeters having precisions of ± 2.5 and ± 5 feet) was set to 2550 feet at the magnetometer post before each survey. Marked breaks in slope, stream beds, etc., were noted in the field notes to supplement the altimeter data in the production of elevation profiles. For logistic reasons, several of the traverses near Novarupta were conducted without an altimeter. In the cases of traverses F'-F, F''-F, F'-F'', F'-G, G'-G'', G'''-g, I-I', I'-I'', I'''-I'' and I-J,

elevations were taken from the U. S. G. S. map A-4, Katmai Quadrangle. Clearly, elevations obtained in this manner lack precision.

The time of occupation for selected stations was recorded, together with brief descriptions of the surface topography and geology, including notes on the crossings of old fumarole lines, nearby inactive fumaroles, position of snow fields, etc.

Several photos were taken in conjunction with the conduct of the magnetic survey (and collection of susceptibility samples). These were an invaluable aid in the months of analysis following the field operations.

The reduced magnetometer data and other various details of the ground survey are given in Appendix A.

CHAPTER II

MAGNETIC SUSCEPTIBILITIES FOR ROCKS

FROM THE KATMAI AREA

2.1 Purpose of Magnetic Susceptibility Determination

The parameter distinguishing rock type in magnetometer surveys is the magnetization. In recent deposits such as the Valley of Ten Thousand Smokes pyroclastic flow, the magnetization can be assumed to be in the direction of the present geomagnetic field, thus the definitive property of the rock types in the study area is their magnetic susceptibility.

An invaluable aid in deducing the structure and composition of geologic bodies responsible for observed magnetic anomalies is computer modeling. The magnetic susceptibility assigned to the model body producing an anomaly like the observed anomaly implies a composition. Obviously, for the interpretive method used in this study, it would be most convenient were each rock type in the region to possess a unique susceptibility. Model studies could then distinguish the rock type responsible for the observed anomalies.

Hand samples were collected in the Valley region of 1969. Among these are samples of banded Novarupta rhyodacite, Lethe River vitroclastic tuff, Nakenk sediments and surficial Valley deposits. Unconsolidated ash was collected in polyethylene bags from a cut bank along Knife Creek, the eastern stream cut in Broken Mountain Valley, and a pit fumarole in the fumarole area in Broken Mountain Valley. Locations of these sampling sites are shown in Figure 2.1. Subsequent sampling in 1970 and 1971 has

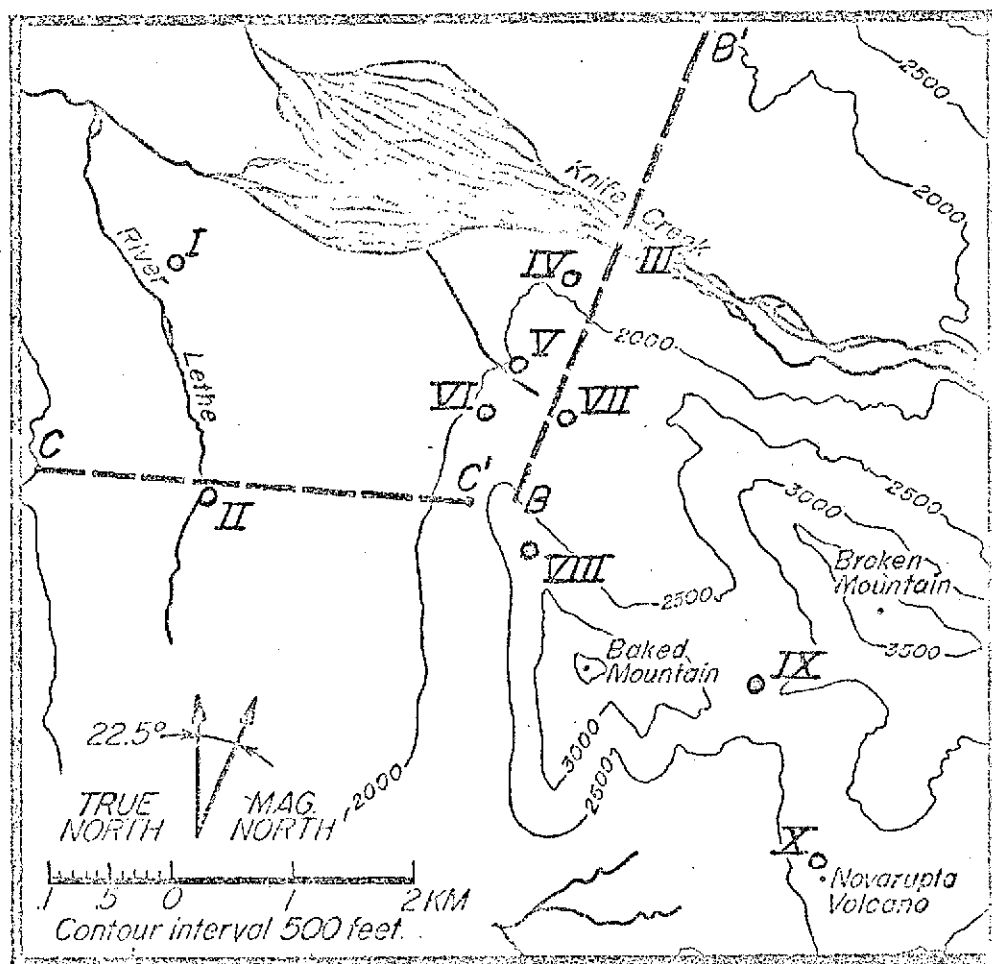


Figure 2.1. Location of magnetic susceptibility sampling sites I through X. For data from individual sites, refer to Table 2.1.

made available more types of rocks from additional sites for susceptibility determination. The susceptibility data are given in Tables 2.1 and 2.2.

2.2 Determination of Susceptibility

Magnetic susceptibilities were measured on a susceptibility bridge developed from that described by Collinson et al. (1963). Bulk susceptibilities down to about 5×10^{-8} emu/cc can not be measured with this system. The field in which the rocks are measured is in the range of 1 to 25 oersteds, so that in general only the initial susceptibility is measured (Stone, personal communication and Collinson et al., 1963).

The susceptibility meter used for the above samples was calibrated for samples of 2.54 cm diameter and 1 cm height. The rock samples were cored and sliced into discs of these dimensions. The number of discs obtained from each sample varied according to the size, shape, and character of the original sample.

Some of the hand specimens were too friable to withstand coring. Among these are: IV-2, V-1, V-2, V-3, and VII-1. These samples were impregnated by immersion in plexiglas dissolved in ethylene dichloride, methylene dichloride, or dichloro-ethane. Additional solution was poured over these rocks as they dried. This method, described by Noltmeier (1967), has the advantage of being an endothermic reaction thus eliminating the chance of introducing a thermal component of magnetization. After impregnation these samples could be cored and cut into discs of appropriate size.

The unconsolidated samples had settled severely during transportation from Katmai to College. Therefore, to insure that any given small portion of the sample was representative of the whole, a splitting technique was required. This was accomplished by applying the method discussed by

Müller (1967, pp. 42-44). The final splits of the unconsolidated samples were placed in plexiglas holders of inner diameter 2.54 cm and depth 1 cm and weighed using an Ainsworth analytic balance; accuracy ± 1.0 mg. Because it was not possible to measure densities while in the field, an average density has been assumed for conversion of measured bulk susceptibilities to representative volume susceptibilities. Both Griggs (1922, p. 293) and Kienle (1969, p. 128) determined an average density for Valley ash of 1.03 gm/cm. Using this density and letting K represent the measured bulk susceptibility of a sample of mass M, the standardized volume susceptibility, K', can be found by:

$$K' = 5.22 (K/M).$$

A representative volume susceptibility for each original field specimen was calculated by simply averaging all 2.54 cm x 1.0 cm samples from each field specimen. This is a satisfactory technique, except in the cases of the samples from sites 11 and X, which are bimodal. Refer to Tables 2.1, 2.2, 2.3, and 2.4 and Figure 2.3.

2.3 Discussion of Results

a) Naknek Sediments

Beyond the northern terminus of the Valley, the Naknek section has been sampled by several investigators (refer to Table 2.2). Although the susceptibilities of these samples range considerably, of the series collected by Packer (personal communication, 1971) on Mount Katolinat, about one-fourth clustered near 20×10^{-6} emu/cc. The present study has also determined an average susceptibility of 20×10^{-6} emu/cc for altered Naknek sediments in the Valley.

A small aromatic fumarole located on the first Naknek outcrop above the Baked Mountain camp is still active; immediately adjacent to the vent

Table 2.1

Susceptibility Studies of Rocks from the
Valley of Ten Thousand Smokes

Sample	Susceptibility* ($\times 10^{-6}$ emu/cc)			Total Discs	Approx. Depth (feet)	Rock Type	Color	Comments
	High	Low	Average					
I-1	406.9	322.8	364.5	8	0	P	G	surface rubble
I-2	8.6	0.9	4.9	4	0	IA	W	fumarole cap
II-1	1743.8	980.3	1348.2	9	0	IA	G**	Lethe indu- rated ash
II-2	1755.5	834.6	1310.8	7	0	IA	G**	same
III-1	1376.0	1255.0	1323.8	2	2	UA ¹	G	air-fall from Knife Creek cut bank
III-2	1177.0	1107.4	1142.2	2	3	UA ¹	G	same
III-3	1120.1	1061.6	1090.9	2	4	UA ¹	G	same
III-4	1461.2	1303.4	1382.3	2	4	UA	G	same
III-5	1141.4	976.7	1053.3	2	6	UA	G	same
III-6	1370.6	1021.3	1196.0	2	6	UA	P	same
III-7	985.6	980.6	983.1	2	8	UA ¹	Y	same
III-8	1284.2	1193.8	1246.8	2	8	UA	P	same
III-9	72.7	65.0	69.0	2	9	UA ¹	R	same
III-10	60.5	49.5	55.9	2	11	UA	G	same
III-11	228.0	222.4	225.7	2	11	UA ¹	G	same
III-12	1175.7	1044.4	1110.1	2	11	UA ¹	Y	same
IV-1	1.7	0.0	0.5	9	0	IA	W	fumarole cap
IV-2	83.9	37.3	51.1	5	0	FA	B	same
V-1	10.5	7.0	9.1	6	10	FA	W	stream- dissected fumarole
V-2	465.1	42.0	197.2	7	10	FA	B	same
V-3	92.1	0.0	18.8	8	10	FA	O	same
V-4	1318.1	1040.5	1172.2	2	3	UA ¹	O	nearby air-fall
V-5	1128.0	913.9	1010.2	4	6	UA	G	same
VI-1	314.6	305.9	310.2	2	15	UA	B	stream- dissected fumarole
VI-2	624.1	534.6	577.1	2	15	UA	B	same
VII-1	23.3	15.2	19.5	12	1	FA	R	pit fumarole in fumarole grid
VII-2	50.2	39.1	43.9	2	1	UA ¹	Y	same
VII-3	37.4	26.7	31.7	2	2	UA ¹	R	same
VII-4	69.2	57.6	64.3	2	3	UA ^{1,1}	B	same

Table 2.1 (continued)

Sample	Susceptibility* ($\times 10^{-6}$ emu/cc)			Total Discs	Approx. Depth (feet)	Rock Type	Color	Comments
	High	Low	Average					
VII-5	38.4	22.2	31.1	2	4	UA'''	W	pit fumarole in fumarole grid
VIII-1	552.0	533.4	539.7	4	0	IS	G	Naknek, 1st outcrop above BMH
VIII-2	22.5	18.0	20.1	5	0	IS	G	Naknek, 2nd outcrop above BMH
VIII-3	22.0	19.3	20.7	4	0	IS	G	Naknek, 3rd outcrop above BMH
VIII-4	31.0	24.2	28.5	3	0	IS	G	Naknek, 4th outcrop above BMH
IX-1	----	----	5058.3	1	0	IS	R	highly- altered Naknek
X-1	1650.6	199.3	995.6	17	0	L	G***	Novarupta banded volcanics
X-2	793.8	179.5	356.4	9	0	L	G	Novarupta rhyolite

Symbols denoting rock type:

A ash
 A' ash with some lapilli
 A'' ash with some clay
 P pumice
 S sediments
 L lava
 U unconsolidated
 I indurated (firmly)
 F friable

Symbols denoting color:

W white
 G gray
 B black
 Y yellow
 O orange
 R red
 P pink

*Susceptibility is in units of 10^{-6} emu/cc.

**Refer to Table 3.5 for details.

***Refer to Table 3.4 for details.

Table 2.2

Additional Susceptibility Data for
Rocks in the Katmai Region

Reference	Sample Identification	Susceptibility*			Rock Type	Location
		High	Low	Average		
Chantry-Price	1--8	9	0	3	sediment	near Overlook
Bingham	K 1--K 6	330	190	277	sediment	along Margot Creek
Packer	KTM 112--KTM 145	340	17	94	sediment	Mt. Katolinat
Stone	GR 1--GR 8	2400	280	1200**	andesite	Mt. Griggs
Stone	KR 1--KR 23	3200	1900	2474	andesite	Mt. Katmai crater rim
Tribble	KT 11	---	---	3500	andesite	Mt. Trident 1953 flow
Tribble	Trident Cone	---	---	1933	andesite	Trident Cone
Tribble	KFM 1--KFM 2	2500	2250	2375	andesite	Falling Mtn.
Stone	S 15--S 18	3000	1400	2300	andesite	Cerberus Dome
Stone	M 1--M 6	3800	3400	3567	andesite	Mt. Mageik
Tribble	KN 3-1-65	330	230	287	rhyolite	Novarupta central dome
	KN 3-2-65					
	KN 1-3-65					
Tribble	KN 4-2-65	---	---	1180	banded lava	Novarupta east margin
Tribble	NRC 1--NRC 3	1377	704	1084**	banded pumice	Novarupta crater
Tribble	NOVA-4	---	---	2200	tuff	Novarupta Basin fumarole crater
Stone	S 10--S 14	1600	1200	1400	tuff	Fissure Lake
Stone	S 1--S 9	1200	570	826	tuff	Corner Lake, upper unit
Tribble	S 0	---	---	1230	tuff	Corner Lake, lower unit
Tribble	LR 1	---	---	720	tuff	Lethe River
Stone	KA--KI	1320	720	967	tuff	Middle Valley
Stone	J 1--J 3	753	500	658	tuff	Juhle Creek
Tribble	KPPF 2-70	---	---	1025	tuff	Peckish Springs
Packer	PFK 1--PFK 6	2600	740	1583	tuff	Upper Knife Creek
Tribble	BMVI 1--BMVI 2	1420	1007	1214	intrusive	Broken Mtn. Valley

*Susceptibility is in units of 10^{-6} emu/cc.

**Apparently bimodal.

the ground is perceptibly warm and mosses are present, although no emanation is visible. Sample VII-1 taken from this outcrop exhibits a susceptibility in excess of 500×10^{-6} emu/cc. It is assumed that exposure of elevated temperatures, as well as to fumarolic emanations, led to chemical alteration of this sedimentary section resulting in an enhancement of its magnetic susceptibility.

There have been several reports of Naknek sediments which were obviously altered as a result of the 1912 volcanic eruptions: Griggs (1922, pp. 243-244) described dull brick-red Naknek exposures in the Baked-Broken Mountain area. He attributed their "baked" look to chemical change by excessive heat and perhaps other agents. In 1923 when Fenner (1950a, p. 607) descended into Katmai crater (the lake was reduced to a small lagoon within the horseshoe island), among the rock fragments on the floor he found "much shale, some of it having a 'baked' look." Fenner (1923, p. 35) also reports the presence of many flat bits of reddish shale and sandstone throughout the tuff-flow; he describes them as follows:

"The bits of shale and sandstone in the tuff bear evidence of having been exposed to heat. The color of the Naknek sediments which underlie the Valley and form the hills and mountains outside of the volcanic range, is generally of a somber green and greenish-gray. The fragments included in the tuff are almost always reddened or blackened if of shale, and reddened or whitened if of sandstone."

Only one sample of such highly altered Naknek sediments was collected. This sample is streaked with red and yellow throughout, although the stains are darkest on the outside. This sample was part of the surface rubble of the Broken Mountain Valley slope of Greasy Pass. It possesses a magnetic susceptibility of 5058.3×10^{-6} emu/cc.

Zies (1929) points out that the volcanoes of the Katmai area have their orifices in sedimentary rocks, so that it is reasonable to expect

that metamorphic changes will have occurred at the contacts of the two types of rock. Zies also considers that the heat from the large igneous mass represented by Novarupta would be quite effective in removing the volatiles from adjacent sedimentary rocks. One could therefore expect to find extensive zones of altered Naknek rocks (which could possess high susceptibilities) adjacent the eruptive conduits throughout the valley region.

The preceding descriptions suggest that alteration is commonplace among Naknek rocks in the Valley, where surfaces of fragments have been subjected to elevated temperatures and vapor-phase contamination. For the model studies, a magnetic susceptibility of 5000×10^{-6} emu/cc (sample IX-1) will be associated with sedimentary rocks of this history.

b) Lavas

The volcanics bordering the head of the Valley are predominately lavas of intermediate composition. The similarity of these rocks is apparent from the andesitic compositions of several samples from the Valley area (Fenner, 1926, pp. 676-679; Ray, 1967, pp. 141, 145).

Forbes et al. (1969, p. 118) found that all the andesites erupted by Mt. Trident throughout the recent years are similar, and furthermore that "all andesites erupted by Alaskan orogenic volcanoes in continental settings from 1912 to the present are highly siliceous and remarkably similar in bulk composition." They propose that this material is generated by the anatexis of lower crustal material.

Table 2.2 contains measured susceptibilities for several samples of andesite from the volcanoes bordering the head of the Valley. Their average susceptibility is 2431×10^{-6} emu/cc, although one sample ranged as high as 3800×10^{-6} emu/cc. For modeling purposes, a value of 2500×10^{-6} emu/cc can be used.

Acidic volcanics were erupted in 1912, primarily from Novarupta; however, Fenner (1926, p. 676) sampled a rhyolitic boulder on the southern rim of Katmai crater. The origin of the rhyolite lava has been much debated. A complicating factor is that a considerable amount of the ejecta attributed to Novarupta, as well as the margin of the dome itself, exhibits a banded structure (refer to section 1.4b). According to Fenner (1923, p. 56), a great part of the banding is due to streaks of dark-brown or nearly black scoria which often contain great quantities of phenocrysts within a mass of light-gray glass almost without phenocrysts. Several samples of the Novarupta volcanics have been analyzed (Fenner, 1923, p. 57; Zies, 1929, p. 56; and Forbes, personal communication, 1971). Most of the investigators have identified the dark bands as andesitic (Griggs, 1922, p. 297; Fenner, 1950b, pp. 707-710; Williams, 1954, pp. 58-59; and Curtis, 1968, p. 194). The analyses of Forbes et al., (1969, p. 118), however, suggest that the basic inclusions in the mixed lava are basaltic.

The central dome of Novarupta is almost pure rhyolite. The average susceptibility of the rhyolitic lava is 304.1×10^{-6} emu/cc. The banded lava of the margin of the dome and the banded pumice found in the moat (or crater) is of higher susceptibility. This is to be expected since the dark bands contain a greater percentage of ferri-magnetic minerals than the light mass. An analysis by Fenner (1923, p. 57) shows that the light bands consist of 0.82% Fe_2O_3 and 1.43% FeO; whereas the dark bands are 3.4% Fe_2O_3 and 4.53% FeO. This dual nature of the banded rocks results in a bimodal distribution of susceptibilities for Novarupta and its banded ejecta; this distribution is seen in sample X-1 (see Table 2.3). The average susceptibility of the banded lava and pumice is 1085×10^{-6} emu/cc. For modeling purposes, a value of 1250×10^{-6} emu/cc may be used for this

Table 2.3

Bimodal Susceptibility of Novarupta Volcanics

Sample	Disc	Susceptibility ($\times 10^{-6}$ emu/cc)*	Dark bands
X-1	1	1283.40	yes
	2	230.80	no
	3	199.33	no
	4	1300.88	yes
	5	1230.94	yes
	6	1650.58	yes
	7	1265.91	yes
	8	1528.19	yes
	9	283.26	no
	10	290.25	no
	11	272.26	no
	12	1592.30	yes
	13	226.14	no
	14	1458.25	yes
	15	1353.79	yes
	16	1405.79	yes
	17	1353.34	yes

*Susceptibility is in units of 10^{-6} emu/cc.

mixed material; whereas a value of 250×10^{-6} emu/cc will be used for the rhyolitic material.

Although none of the banded pumice on the Valley floor was sampled, a piece of light gray pumice about 5 inches in diameter was obtained (sample 1-1). This gray pumice is representative of much of the surface rubble in the middle and lower Valley. Its susceptibility of 364.5×10^{-6} is close to the value for the Novarupta rhyolite from which this pumice was no doubt derived; apparently it was erupted from Novarupta while the conduit was supplying only rhyolite.

c) Glacial Deposits

In traveling the Katmai Trail during a geological reconnaissance of southwestern Alaska in 1898, Spurr (1900) traversed the valley which was to become the Valley of Ten Thousand Smokes. He describes the valley as filled with about 30 m of glacial drift consisting of stratified gravels, sand, and near Katmai Pass, boulders, too. He also reports that fragments of the Naknek sediments were included in the valley drift. It is difficult to arrive at a susceptibility representative of this glacial material. It is reasonable to assume that this detritus is predominately composed of fragments of the basic lavas from the volcanic peaks at the head of the Valley which carry many glaciers. The portion of fragments of Naknek sediments from the Valley walls included in the drift probably varies locally but is always small. If the drift were composed entirely of volcanic material, the highest susceptibility it would possess would be that of the parent lava in situ; 3800×10^{-6} emu/cc is the largest measured susceptibility for lava. At the other extreme, if the bulk of the drift were from Naknek sediments, its susceptibility could be negligible. Obviously, it is impossible to predict the susceptibility of the glacial drift lying between the pyroclastic flow and the Naknek bedrock. A further complication is that the constituents

of the drift would be expected to be in random orientation, thus remanence would alter the apparent susceptibility of the material were it analyzed under the assumption of magnetization under the present field.

The situation is further complicated by the lack of knowledge of the temperature regime during the 1912 eruption. A maximum fumarolic temperature of 645 degrees C. was measured in 1919; this occurred at fumarole No. 153 which is located in the middle Valley (Allen and Zies, 1923, p. 104). Lovering deduced that fumarole No. 1, located at the terminus of the ash-flow, had an initial temperature between 800° C and 900° C (Lovering, 1957, p. 1590). These data imply that the emplacement temperature of the pyroclastics was well over 600°C.

According to Nagata, the Curie temperature of igneous rocks can be estimated if the ratio $\text{Fe}_2\text{O}_3/(\text{Fe}_2\text{O}_3 - \text{FeO})$ is known. An average ratio of 0.45 is representative of the igneous rocks at the head of the Valley (samples 575, 568, 526, 583, and 147 of Fenner, 1926, pp. 676 and 682; sample 153b of Fenner, 1923, p. 57). This ratio corresponds to Curie temperatures in the realm of 400°C to 600°C (Nagata, 1961, p. 138). It therefore seems probable that some realignment of magnetization occurred within the fragments in the upper portion of the glacial fill of the Valley upon emplacement of the ash. Thus, the apparent susceptibility of this limited zone of reheated drift will increase slightly. Also, such a high thermal regime could result in compositional alterations within the drift. It was found that after exposure to extreme temperatures and/or volcanic fumes that Naknek sediments could attain susceptibilities as high as 5000×10^{-6} emu/cc. However, Curtis (1968, pp. 184-185) reports that of the several examples throughout the Valley, of

morainal boulders of andesite in direct contact with the tuff flow, none show the slightest sign of alteration.

In the foregoing discussion, it is clear that a singular susceptibility cannot be assigned to the glacial drift lying between the 1912 pyroclastics and the Naknek basement. Depending on the composition, proportion of components, and history of this material, its susceptibility could conceivably range from 10^{-5} to 10^{-3} cgs units. This indeterminate susceptibility must be considered in any geological interpretation of model studies.

d) Pyroclastic Flow

The top of an indurated deposit is exposed where traverse C-C' crosses the River Lethe. In the field the rock is deep gray, but upon drying it assumes a lighter color with prominent bands of brown and white. Preliminary petrographic studies show this rock to be vitroclastic, and not welded as was first assumed. A few flow structures are also present (Forbes, personal communication, 1971).

The average susceptibility for the Lethe indurated ash (samples 11-1 and 11-2) is 1330×10^{-6} emu/cc. The susceptibilities of individual samples vary from 834.6×10^{-6} emu/cc to 1755.5×10^{-6} emu/cc. Examination of the character of the tuff comprising the individual discs disclosed the correlation of colored streaks with measured susceptibility; white and brown streaks are prominent in discs of lower susceptibility, black bands are associated with the higher values (see Table 2.4).

An exposure of similar tuff was observed along the River Lethe above the falls which are in the area of sample 1-1. Other outcrops

Table 2.4

Susceptibility Studies of Lethe Indurated Ash

Sample	Measuring disc	Susceptibility ($\times 10^{-6}$ emu/cc)*	General description
11-1	1	1318.37	black
	2	980.33	brown
	3	1318.37	black, brown
	4	1085.23	black
	5	1108.55	brown
	6	1545.67	brown, black
	7	1510.70	black
	8	1522.36	black
	9	1743.84	black
11-2	1	1493.22	black, white
	2	1458.25	black
	3	1195.97	black, brown, white
	4	1755.49	black
	5	1242.60	black and white
	6	834.62	black, white prominent
	7	1195.97	black, white

*Susceptibility is in units of 10^{-6} emu/cc.

resembling the Lethe indurated tuff are to be found in connection with explosion craters in Novarupta basin and at the base of Mt. Griggs; at the base of Mt. Katmai where the indurated exposure extends beneath the Knife Creek Glaciers; along faults at the base of Mt. Mageik by Fissure Lake where the indurated section is overlain by glacial fill through which fumarole vents can be traced, and by Corner Lake where two tuff sections are exposed; at the southwest base of Baked Mountain active fumaroles expose an indurated section beneath the ash (Forbes, personal communication, 1971). Subsequent to the present study, several of these other tuffaceous outcrops have been sampled. Although individual samples possess susceptibilities ranging from 500×10^{-6} emu/cc to 2600×10^{-6} emu/cc, in general, the susceptibilities of the tuff throughout the Valley appear fairly uniform at its average of 1187×10^{-6} emu/cc (refer to Tables 2.1 and 2.2). In conjunction with the strong visual similarities of these rocks, their common susceptibilities lend support to a hypothesis of singular origin for this indurated material throughout the Valley.

In the lower Valley the deposits possess a definite pink cast and appear to be homogeneous and indurated. The composition of Lovering's (1957, p. 1593) sample (7TL53) of normal ash near the terminus of the flow is remarkably similar to Forbes' (personal communication, 1971) sample (KN 2-3-65) of Novarupta rhyodacite. Probably, the entire flow here is more rhyolitic than farther up the Valley, where the samples for this study were obtained. Unfortunately, no susceptibilities have been determined for the flow in the lower Valley. It can only be assumed that the susceptibility of this portion of the ash flow is similar to that of the rhyolitic lava of Novarupta and the uniform pumice (sample 1-1); i.e., approximately

300×10^{-6} emu/cc.

Probably the tuffs are the product of partial welding associated with the cooling, degassing, and compaction of the pyroclastic flow of 1912. The variables controlling the presence, extent, and degree of welding within a given ash flow are discussed in detail by Smith (1960). Briefly, an ash flow of sufficient emplacement temperature and/or thickness will form a central lens of indurated material of thickness and quality dependent upon the rates of welding, cooling, and crystallization peculiar to that particular deposit.

e) Air-fall Pyroclastics

Air-fall pyroclastics were collected from approximate depths of 1 and 2 meters in a stream cut in the eastern drainage of Broken Mountain Valley. The top 0.3 meter of the ash in this area appears to be reworked and was not sampled.

The re-deposited nature of the upper ash is implied by the manner in which it is draped over the gentler sloping banks of the stream. This mantle of grayish ash was probably originally deposited upstream and on the adjacent mountain slopes. Transportation of air-fall pyroclastics from these slopes was recognized by Forbes who reported that over the years great quantities of ash and pumice have been transported down the valley sides by spring melt waters, in the form of a slurry-like mass of suspended ash and ice (Forbes, personal communication, 1968).

The next layer consists of about 1 meter of orange-stained ash with a few lapilli. This is underlain by at least 2 meters of gray ash. These two layers were sampled, and probably represent air-fall. No attempt has been made to correlate these layers with the tephra section of Curtis.

More air-fall pyroclastics were collected in the southeastern branch of the Valley. Knife Creek is braided near the crossing of traverse B-B' and the valley is quite flat to the east. Not far above the traverse crossing, Knife Creek narrows, and a 4 meter cut bank rises abruptly on the western edge of the stream; it extends for about a kilometer downstream. Plate I shows the multi-colored layers of air-fall exposed by the stream cut. The layering of this cut bank should represent the air-fall history of this part of the Valley; however, it is difficult to correlate this sequence with the published sections of Fenner (1923, Table 1; and 1950, Table 2 and pp. 712-714) and Curtis (1968, pp. 162-183 and pp. 196-201). Tentative assignment of Curtis' system to the Knife Creek section is shown in Figure 2.2.

Discrepancies can be attributed to the fact that very few beds at any given outcrop have correlative value for more than a few hundred meters. The many changing conditions during an eruption such as fluctuation in intensity of eruption, the wind direction and speed, and the amount of turbulence within the rising clouds of tephra, can account for such spatial variation (Curtis, 1968, p. 167).

Samples III-9, -10, and -11 exhibit relatively low susceptibilities which have similar values to those assigned to fumarolic surface deposits. Inclusion of these values among the fumarolic susceptibilities only raises the average to 106.9×10^{-6} emu/cc, or omitting VI-1, VI-2, and III-11, 45.9×10^{-6} emu/cc (see section 2.3f). One is led to the conclusion that following deposition of this part of the Knife Creek section, there was a period of little or no air-fall during which fumarolic venting occurred from the ash en masse. The occasional overlapping of the red and white

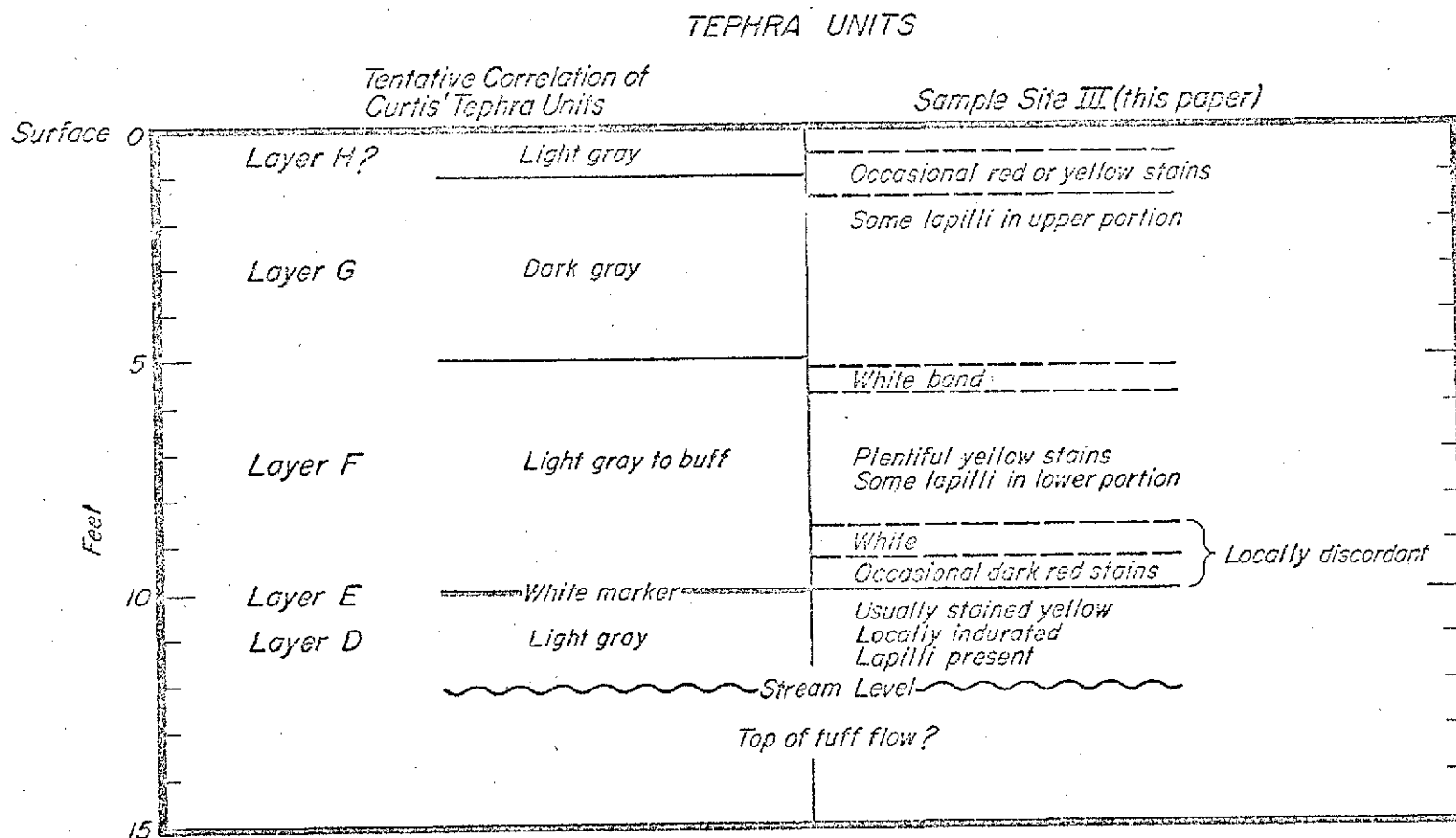


Figure 2.2. Comparative tephra sections based on Curtis (1968) and the section exposed at sample site III. Plate I is a photograph of this same site. Magnetic susceptibilities for these samples are given in Table 2.1.

layers at this depth could be indicative of fumarolic activity or of resorting by wind. The red zone might well denote fumarolic staining. Fenner (1950b, p. 712) concludes that the yellow and crimson colors at the top of certain ash layers is probably caused by gas emanations. It is also of interest to note that the zone of low susceptibility is centered about a thin white layer which has been tentatively correlated with Curtis' layer E. From his tephra study, Curtis concluded that "following the deposition of layer D was a period of relative quiescence. A thin bed of ash... termed layer E, was deposited." This period of quiescence could relate to a time of fumarolic venting as indicated by the low susceptibility ash at this depth. Curtis also deduced that at the time of the eruption of layer F, "conflicting winds must have been blowing in the vicinity of the headwaters of Knife Creek" (Curtis, 1968, p. 198). This condition could account for the overlapping at the top of the low susceptibility tephra.

The tephra section at site III contains several zones and splotches of red and yellow. The manner of such staining is discussed by Fenner (1926, p. 741):

"In thick beds of ejected pumice certain strata are deeply colored -- crimson, yellow, or yellow-brown. This is due to mere staining of the pumice with iron oxides, but the lumps are deeply impregnated. Presumably the iron was deposited by the little residual gas that oozed out subsequent to the first violent inflation of the pumice. It is remarkable that some strata show this staining and others, above and below, are free from it."

Since the anomalous low susceptibilities probably represent altered ash, they are omitted in arriving at an average susceptibility for air-fall of 1155.5×10^{-6} emu/cc.

PRECEDING PAGE BLANK NOT FILMED

Table 2.5

Magnetic Susceptibilities of Some Common Constituents
of Fumarolic Alterations Reported by
Shipley (1920), Zies (1929), and Lovering (1957)

Material	(Susceptibility $\times 10^{-6}$ emu/cc)***
sulfur	-15.5 to 700.0*
corandum	-37.0*
silica	-29.6*
opal	diamagnetic
kaolinite	diamagnetic
montmorillonite	diamagnetic
apatite	diamagnetic
halite	-30.3*
ammonium chloride	-36.7*
lead chloride	-73.8*
arsenic sulfide	-70.0*
sphalerite	-25.0*
galena	-84.0*
gypsum	-74.0*
alum	diamagnetic
lead sulfate	-697.*
barium sulfate	-71.3*

Material	Susceptibility emu/cc
pyrite	.000005 to .0002**
iron chlorides	.00998 to .01475*
iron sulfates	.0102*
FeO	.0072*
hematite	.00004 to .0001**
magnetite	.04 to 2.0**
magnetite crystals	6.3 to 24.0**
ilmenite ¹	.03 to .14**
franklinite ¹	.036**
pyrrhotite ²	.007 to .028**
specularite ²	.003 to .004**

¹Zies reported traces of Zn, Ti, & Mn in fumarolic magnetite.

²These minerals were probably present.

*CRC Handbook of Chemistry and Physics, 1965-1966, p. E-95 to E-100.

**Jakosky, 1950, p. 164 and 165.

***Susceptibility is in units of 10^{-6} emu/cc.

indicated by sharp, high, narrow magnetic anomalies which show excellent correlation with surface markings and fumarolic lineations in the fumarole grid in Broken Mountain Valley. This is discussed further in Chapter III. Sharp anomalies were observed near fumaroles along magnetometer traverses across the Valley floors as well. Unfortunately no samples were taken from below the surface in connection with these anomalous highs in the magnetic field.

Since only exposed sections of fumaroles were sampled, the study was regrettably limited to those areas which would have experienced the most leaching and weathering. The exposure of these fumaroles, as well as the diamagnetic nature of many of the incrustations, account for the low susceptibilities encountered in this study. The presence or dominance of hematite in other fumarolic samples is probably responsible for the relatively higher susceptibilities found. Those values greater than 100×10^{-6} emu/cc probably indicate the presence of some magnetic minerals.

2.4 Conclusions

Several of the rock types have indistinguishable susceptibilities (refer to Figure 2.3). Both Naknek sediments and exposed fumarolic ash can be represented by a susceptibility of 50×10^{-6} emu/cc. There is considerable overlapping of susceptibilities for air-fall pyroclastics, tuff and the banded volcanics. All three have susceptibilities near 1250×10^{-6} emu/cc. Glacial drift may well have an apparent susceptibility in this range, also. The range of susceptibility of many of the other rock types overlap, too.

The clustering of susceptibilities near 1250×10^{-6} emu/cc could

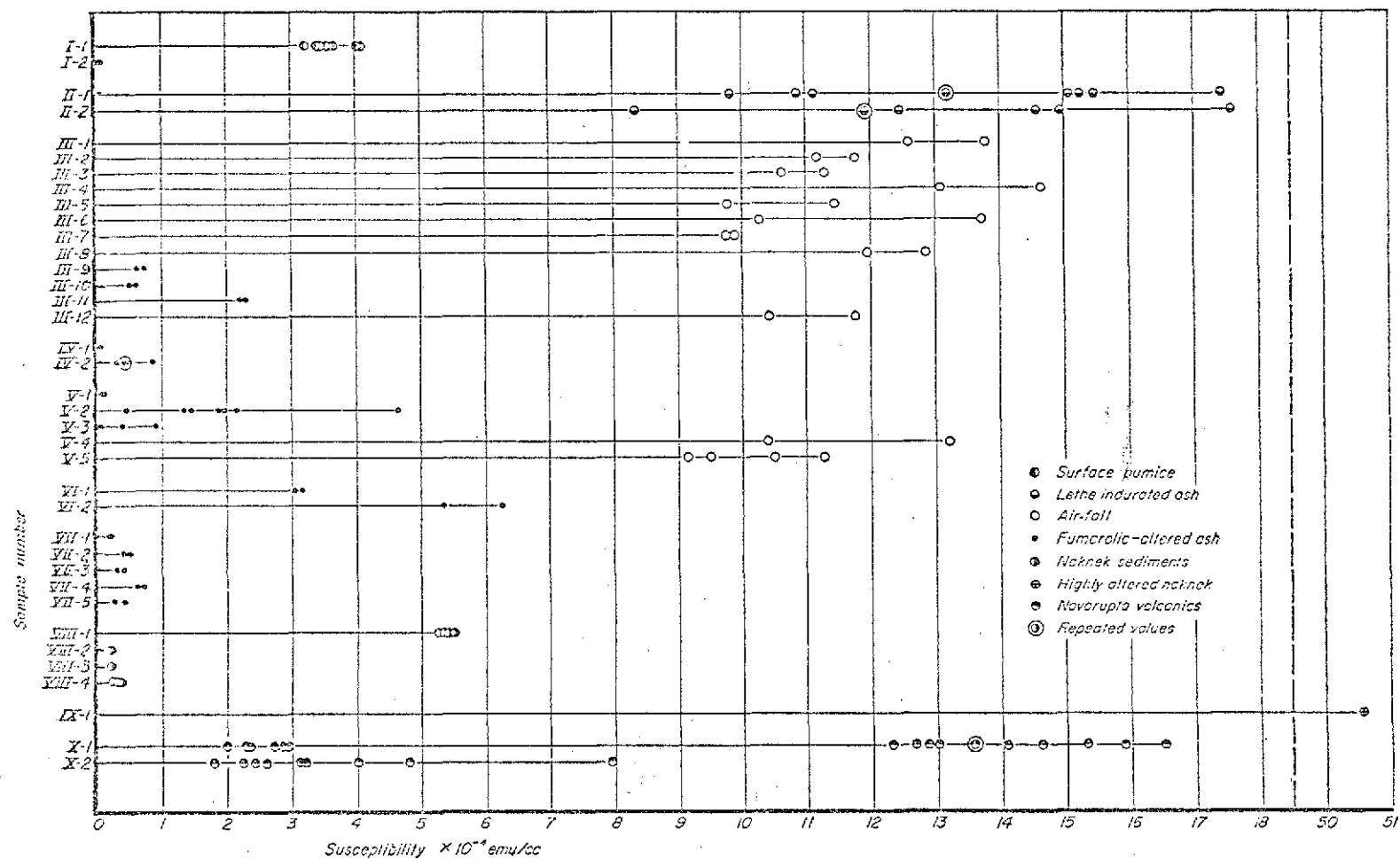


Figure 2.3. Susceptibility of individual measuring discs as function of rock type and sampling site. Refer to Figure 2.1, and Tables 2.1 and 2.6.

Table 2.6
Summary of Susceptibility Data

Material	Susceptibility ($\times 10^{-6}$ emu/cc)*			
	Measured High	Measured Low	Average	Modeling
Naknek sediments	340	0.3	94	50
altered Naknek	---	---	5058	5000
andesitic lava	3800	1400	2431	2500
mixed lava	1377	704	1085	1250
rhyolitic lava	356	230	304	250
glacial drift	---	---	---	1250?
tuff	2600	500	1187	1250
tephra	1461	913	1156	1250
fumarolic alterations	624	0	107	50

*Susceptibility is in units of 10^{-6} emu/cc.

be indicative of genetic similarity in the materials. Novarupta has been suggested as the major eruptive vent for the tuff and most of the air-fall. The similar susceptibilities of tuff, air-fall and Novarupta's banded ejecta certainly bear out this hypothesis.

The susceptibility data is summarized in Table 2.6; also given are the modeling susceptibilities which will represent each rock type in the model studies in Chapter IV. Further discussion of susceptibility as related to geological interpretation in the Valley can be found in that chapter. It appears that there is sufficient susceptibility data to test some of the previous hypotheses concerning the geologic composition of the Valley fill.

CHAPTER III

SMALL SCALE MAGNETOMETER SURVEY OVER A ZONE OF RELICT FUMAROLES

3.1 Small-scale Magnetometer Survey

A distinctive feature of Broken Mountain Valley is the colorful plaid of orange and red over tan, produced by intersecting linear zones of fumarolic markings. These bands of remnant fumaroles trend approximately parallel and perpendicular to the axis of the valley. Near the terminus of the valley, an intersection of two of these fumarole lines was chosen for detailed magnetometry. A five by ten foot (1.52×3.04 meter) rectangular grid was laid out using a 100 foot (30.5 m) cloth tape, and covered an area extending 250 feet (76.3 m) along magnetic north and 200 feet (61 m) wide. The location of this fumarole grid is shown in Figure 4.1.

A detailed sketch of the surface features of the fumarole grid is shown in Figure 3.1a, and Plate II is a view from magnetic southeast. The fumarole remnants delineated by bright splotches of fumarolic clay and discolored ash downslope, stand out sharply against the plain light ash. A three (3) meter deep crater vent with steep sides of loosely-coherent, red-stained ash is located at R-32. There is also an elongated trough in the unaltered ash; this is probably the result of collapse associated with the fumarole line which parallels it to magnetic west. At each end of this trough are minor pits, one of which is almost two (2) meters deep. Excluding these depressions, the area of the fumarole grid is relatively flat.

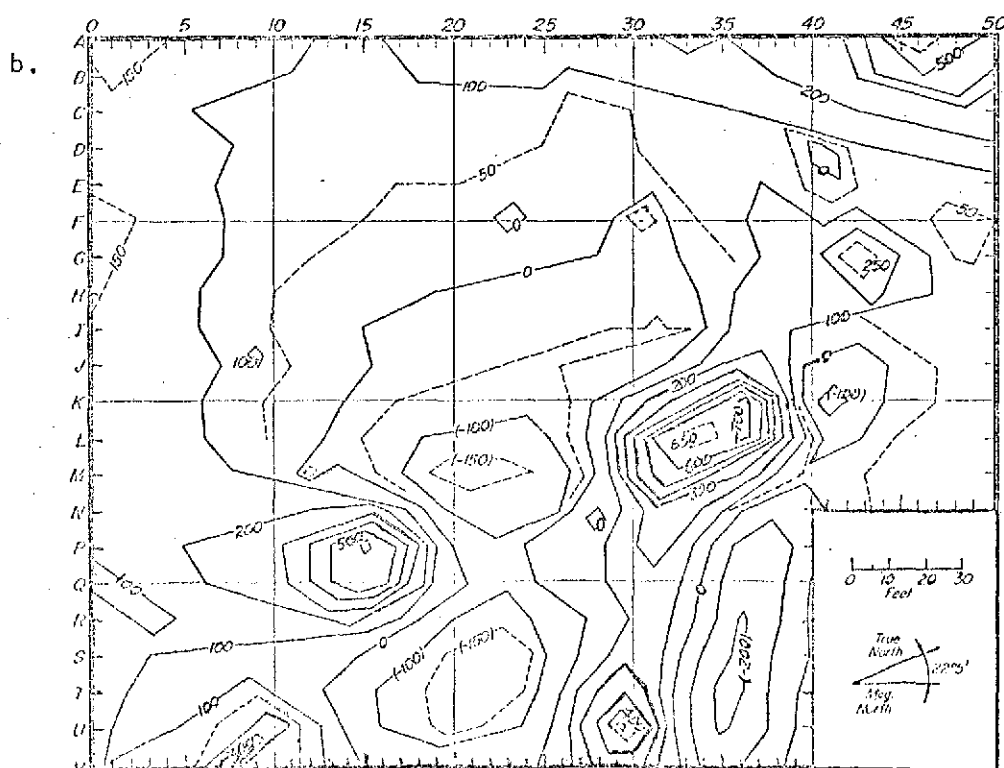
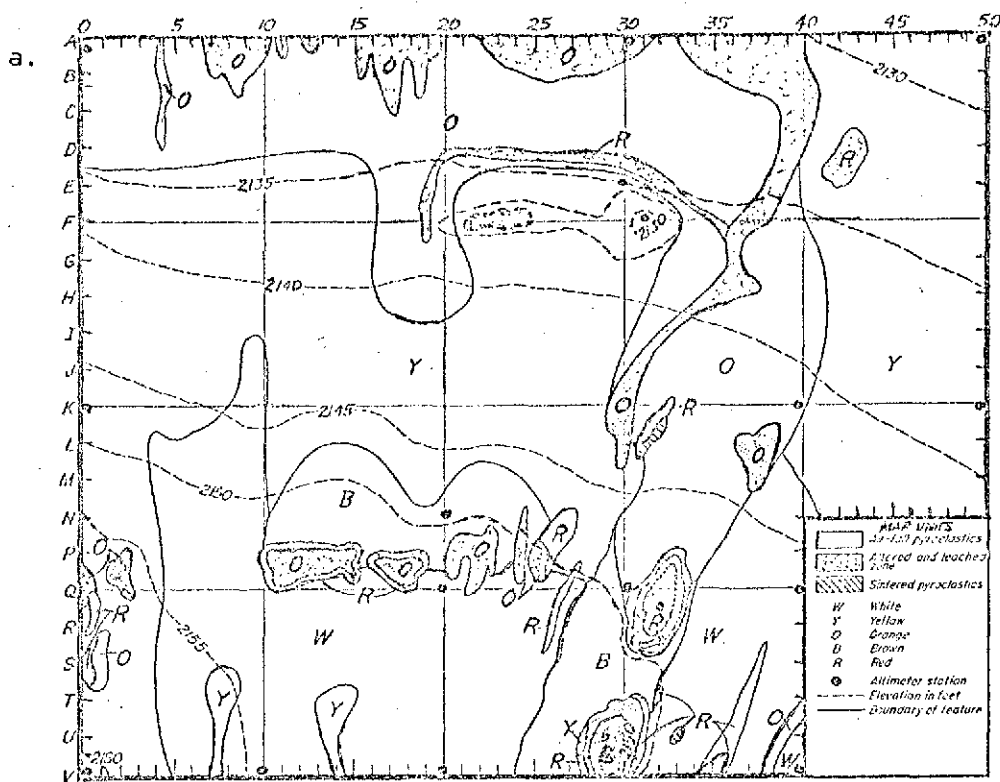


Figure 3.1a. Surficial geology of the fumarole study area. Contour interval is 5 feet. Map units designate the color and composition of the surficial deposits. Plate II is a photograph of this same area.

Figure 3.1b. Total field magnetic anomaly map over the fumarole study area. Stations 0-50 were positioned at 5 foot intervals along traverses A-V, which were 10 feet apart. Solid contour interval is 100 γ with dashed contours at 50 γ intervals. The correspondence of the large magnetic anomalies with the surficial geology (Fig. 3.1a) suggests that fumarolic magnetic minerals may be preserved at shallow depths.

The total magnetic field was measured at five foot (1.52 m) intervals along traverses A through V, which are separated by ten feet (3.04 m). The probe height was 2.07 meters. Since readings were taken in rapid succession, repeated readings generally were not made. The magnetometer readings were reduced to anomalies in the total field according to the procedure outlined in Appendix A. Figure 3.2 is a computer drawn perspective view of these anomalies from magnetic northeast. Contours of these anomalies are presented in Figure 3.1b.

Only two attempts were made to measure vertical gradients within the grid. At T-35 which is situated just outside the pit fumarole, the vertical gradient of the total field is approximately 200 gammas per meter. At M-36, which is located near a 700 gamma anomaly in a zone of orange clay and altered ash forming part of a down-valley striking fumarole line, the magnetometer failed to record a steady reading in the lower .405 meter probe position. Since the proton precession signal decays too rapidly for the magnetometer to function in fields with gradients greater than about 650 gammas per meter (Hood, 1965, p. 404), the close proximity of a disturbing body is indicated.

3.2 Analysis of the Magnetometer Data

Steep horizontal gradients of 75 to 200 gammas per meter indicate that the magnetic bodies responsible for the magnetic anomalies observed in the fumarole grid are located at shallow depths. The high vertical gradients reported in the previous section also indicate near-surface magnetic sources.

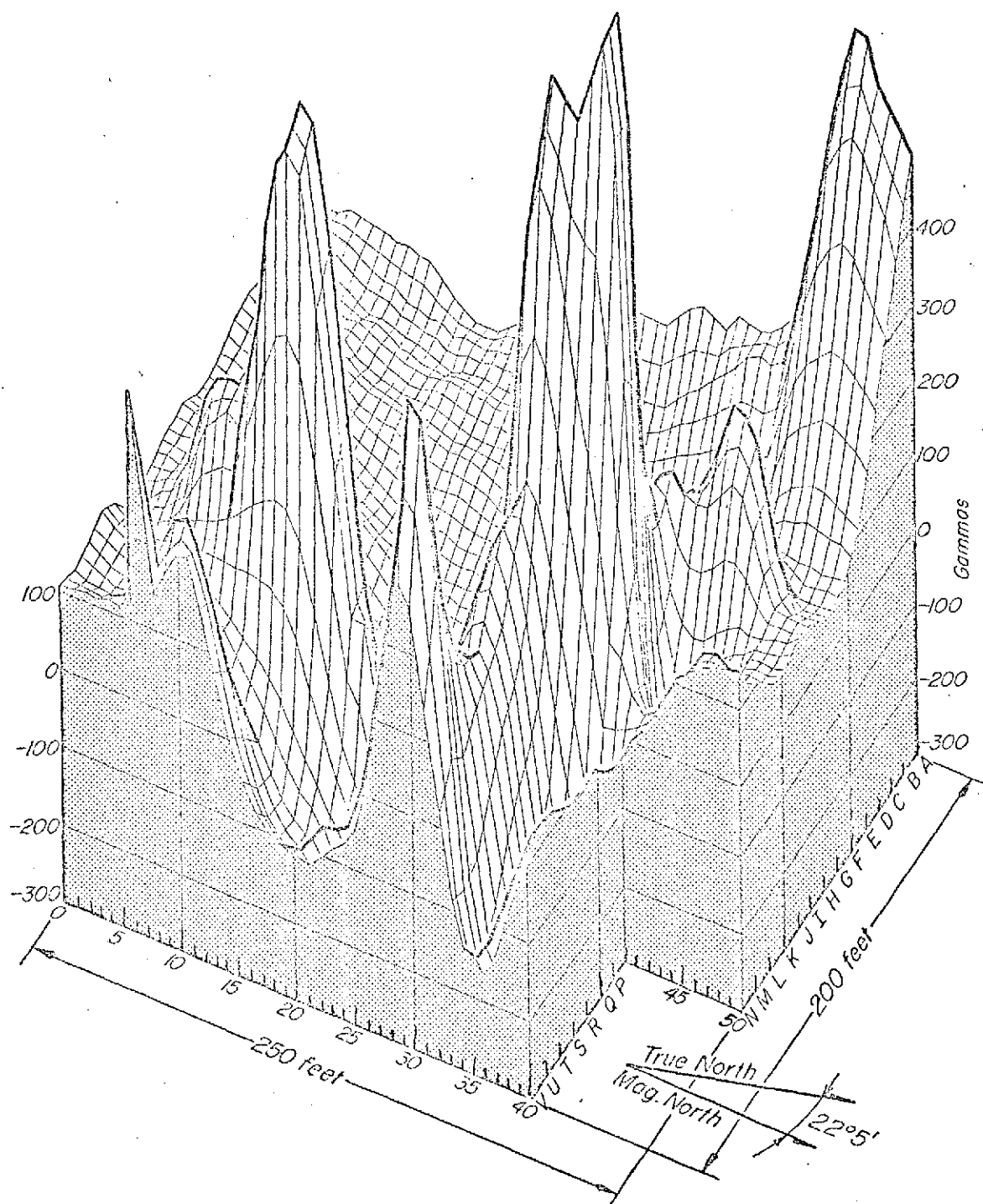


Figure 3.2. Computer drawn perspective magnetic anomaly map of the fumarole study area. Refer to contoured anomaly in Figure 3.1b.

As a rule of thumb, the width of a magnetic body cannot exceed the width of its anomaly. Thus, the bodies causing the anomalies in the grid are necessarily narrow.

The remarkable agreement between the trends of the magnetic anomalies and the linear surface expression of former fumarolic activity is apparent upon comparison of Figures 3.1a and 3.1b. The possibility of deposition and retention of magnetic minerals along fissure vents was presented in section 1.4d. The probability of occurrence of fumarolic magnetite in the area of the survey grid will be discussed in the next section.

Estimates of the depth to the top of the magnetic bodies causing anomalies in the grid were made by applying Peter's "slope" method to profiles of the total residual field (Dobrin, 1960, pp. 312-313). This technique assumes that the source is a thin vertically-magnetized, vertical dike of infinite length. Also, the width should be of the same order of magnitude as the depth and the thickness should be much greater than the depth of burial. Although the formulae are for vertical anomalies, they should be equally applicable for total anomalies at such a high magnetic latitude as the Valley. The high gradients and narrowness of the anomalies are clear evidence that the source of the anomalies is indeed thin, shallow, and linear, but the thickness of these accumulations has not been resolved. Application of this technique to individual profiles within the grid indicates that the depth to the magnetic bodies varies from one to three meters; deepest below the crater vent and shallowest near the 700 gamma anomaly of L-37.

3.3 Implied Source for the Anomalies

Although it was never the site of extensive studies, Broken Mountain Valley did receive some attention by the early investigators. In describing Broken Mountain Valley, Griggs (1922, p. 233) reports: "Its mouth is the seat of some of the most vigorous vents in the region, and smaller fumaroles occur farther up." Fenner (1923, p. 15) was also impressed by the amount of fumarolic activity in this valley. In 1919, Allen and Zies (1923, pp. 104-105) examined the emanations of ten fumaroles in Broken Mountain Valley, primarily at its terminus. Although they found the valley to be one of the hottest areas in the Valley of Ten Thousand Smokes, no exceptionally high temperatures were encountered in 1919; measured temperatures for the fumarolic gasses ranged from 94°C to 353°C. Examination of Allen and Zies' map (Allen and Zies, 1923, p. 80) indicates that the grid area was not the site of any of their fumarole studies. However, their studies in other regions of the Valley of Ten Thousand Smokes imply that such an area could have been the site of the sublimation of magnetic minerals. They report that the hottest fumaroles were small circular crater vents, "say fifteen feet in diameter and ten feet deep" (Allen and Zies, 1923, p. 91). They also found the throats of the hotter fumaroles lined with a crust of "metamorphosed pumice conspicuously colored by oxide of iron. Some of the oxide is bright red and of loose texture" (Allen and Zies, 1923, p. 97). Similar features still possessed high temperatures in 1919; temperatures from 400°C to 645°C were measured for a group of crater vents in the main Valley (Allen and Zies, 1923, p. 91). The crater at R-32 appears similar to those

studied above, so it can be assumed that this vent was probably a site for magnetic mineral accumulation.

Although crater vents often served as the principal outlets along a fissure line, sometimes the fissure itself was a line vent of considerable length. Even in 1919, temperatures above 400°C were recorded along some fissure vents (Allen and Zies, 1923, p. 91). It is thus possible that the rectilinear features of Broken Mountain Valley are filled fissures which could have been the site of sublimation for magnetic minerals.

In the early years after the eruption, Griggs reported that the fissures criss-crossing the center of the valleys were mostly filled and "usually marked only by the lines of encrustations or of small fumaroles stretched along their courses" (Griggs, 1922, p. 235). This early description is applicable to the present situation in Broken Mountain Valley. No open fissures were observed at this location; primarily the fissure pattern was revealed by lines of fumarolic clay and discolored ash. It seems reasonable that these central fissure fumaroles were closed even early in their history. In this case, metallic sublimates along their vents may have been protected from leaching by acid condensates in the latter stages of fumarolic activity and from subsequent weathering. It is proposed that the magnetic sublimates thus preserved along the fissure vents at shallow depths are responsible for the narrow, sharp, high magnetic anomalies encountered over the linear surface markings indicating earlier fumarolic alteration.

Broken Mountain Valley is much higher than the other branches of the Valley. The pyroclastic flow in this valley is also the thinnest in the region (Sbar and Matumoto, 1971). One would thus conclude that the top of the Naknek in this valley is also higher than in the other valleys. As was proposed for some of the fissures in the southern branch of the valley, settling over bedrock topographic features can result in fracturing of the pyroclastic flow. In this manner, parallel fractures could have been produced in the pyroclastics near the terminus of Broken Mountain Valley where the deposit settled over a sharp break in elevation of the underlying Naknek. Contracting and settling within the valley confines would then explain the intersecting system of fissures.

The fissure fumaroles within the grid area intersect at an angle of about seventy degrees. Similar alignment of fumarolic fissures is reported by Sheridan for the Bishop Tuff. He found that the fumarolic fractures have orthogonal intersections; for most, the dihedral angle is about sixty degrees. These joints penetrate up to 120 meters into the sheet, well within the densely welded, devitrified zone. Sheridan's studies indicate that the fracturing mechanism was complex, related to welding deformation as well as to thermal stress release, and somewhat influenced by the underlying topography (Sheridan, 1970, pp. 860, 861).

The magnetometer survey within the grid offers no proof of the extent of the fumaroles in this area but is a very strong indication. All that is demonstrated is near-surface, highly-magnetic accumulations along the fumaroles. Nothing from deeper horizons can be inferred.

3.4 Conclusions

This study has shown that narrow magnetic anomalies encountered in the vicinity of fumaroles can be directly related and probably are genetically related to the fumaroles. In the fumarole grid, the sharp anomalies are restricted along surficial zones of fumarolic alteration. Analysis of profiles over these fumarolic markings indicates the sources are necessarily shallow, narrow, and elongate. Previous studies imply that this area was one of extreme temperatures following the emplacement of the 1912 pyroclastics, thus, it was probably the site of sublimation of magnetic minerals. The existence of the anomalies implies that these fissure fumaroles were covered early in their history, thereby protecting and preserving the magnetic accumulations along their vents.

It is regrettable that samples were not collected at various depths within the fumarole grid. Samples from a few meters depth below magnetic highs would be most informative. As for now we can only speculate as to the composition and extent of the accumulations responsible for the sharp anomalies coincident with the surface fumarolic alterations.

CHAPTER IV

CROSS-VALLEY MAGNETIC PROFILES IN THE VALLEY OF TEN THOUSAND SMOKES

4.1 Magnetometer Survey in the Valley Region

Magnetometer traverses were made across each branch of the Valley of Ten Thousand Smokes (refer to Figure 4.1). It was hoped that this restricted survey could clarify some of the controversy about the structure and composition of the ash flow and its confining pre-1912 valley. Appendix B includes the details of these magnetometer traverses and the listings of the reduced data. Profiles of the various valley crossings are given in Figures 4.2 through 4.5.

The jagged nature of the valley profiles makes analysis difficult. As discussed in Chapter III, it is probable that these narrow anomalies are caused by small, near-surface pockets of magnetic minerals associated with fumarolic alterations. It is unfortunate that the present survey was a ground survey and thus particularly sensitive to the effects of these small, close features. Figure 4.6 gives two of Anna's (1972) aeromagnetic profiles which are near ground magnetometer traverses. The smoothed nature of the aeromagnetic profiles clearly demonstrate that the short period spatial variations are indeed of shallow origin.

For comparison with model anomalies in an attempt to determine the possible composition of the Valley, it is necessary to ignore these narrow anomalies. Several qualities of the present survey disqualify

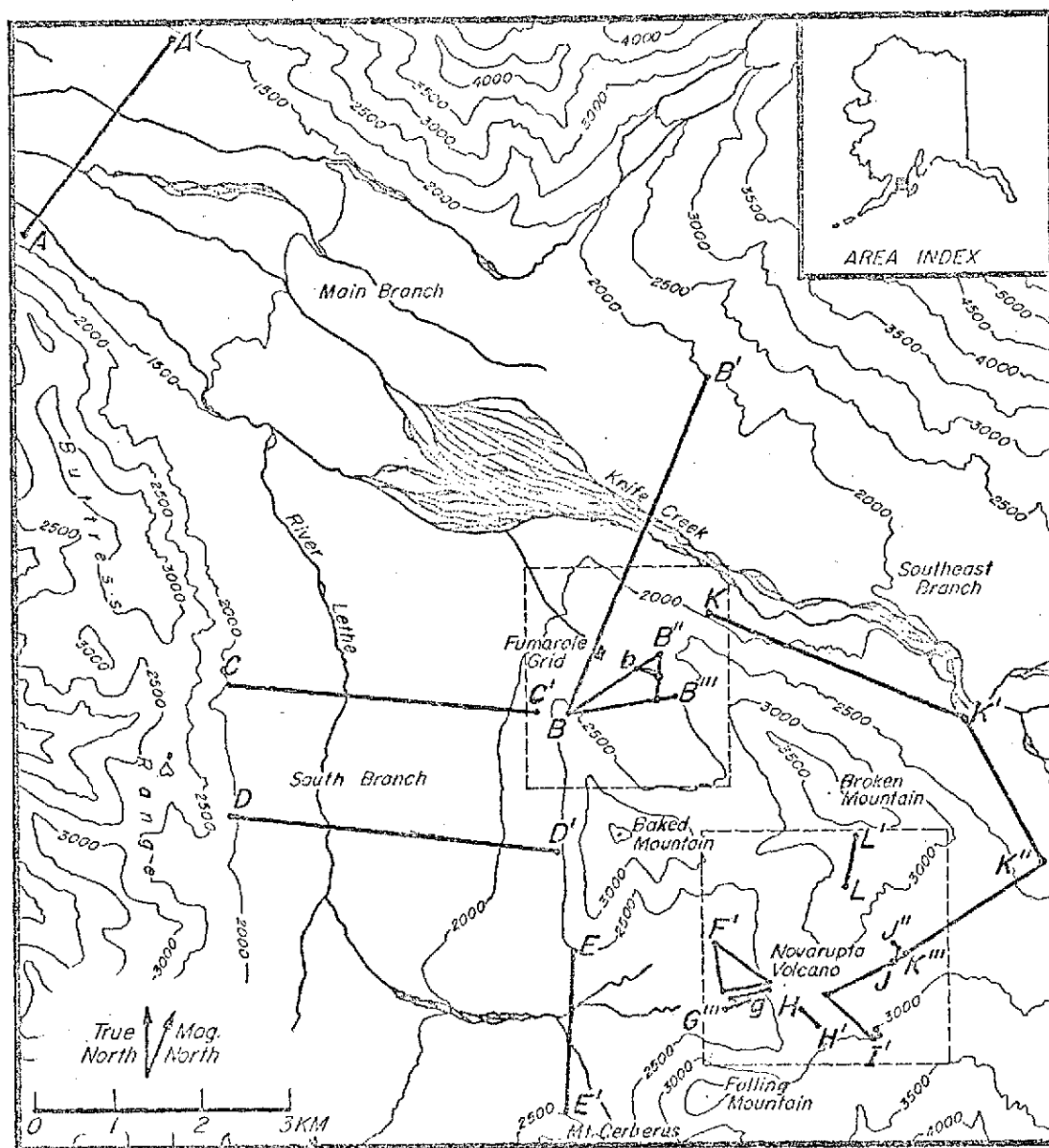


Figure 4.1. Magnetometer traverses in the Valley of Ten Thousand Smokes, Katmai National Monument, Alaska. Detailed maps of dashed areas are presented separately in Figures 4.9a and 5.3a. Elevation contour interval is 500 feet.

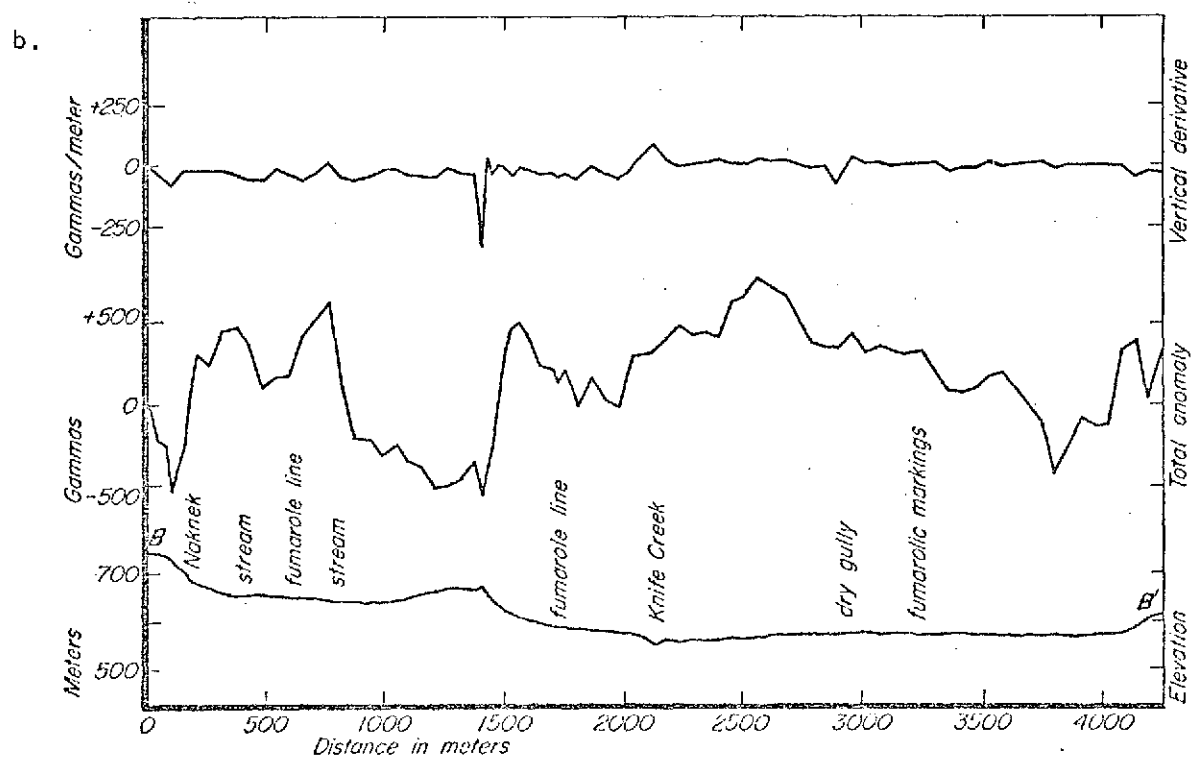
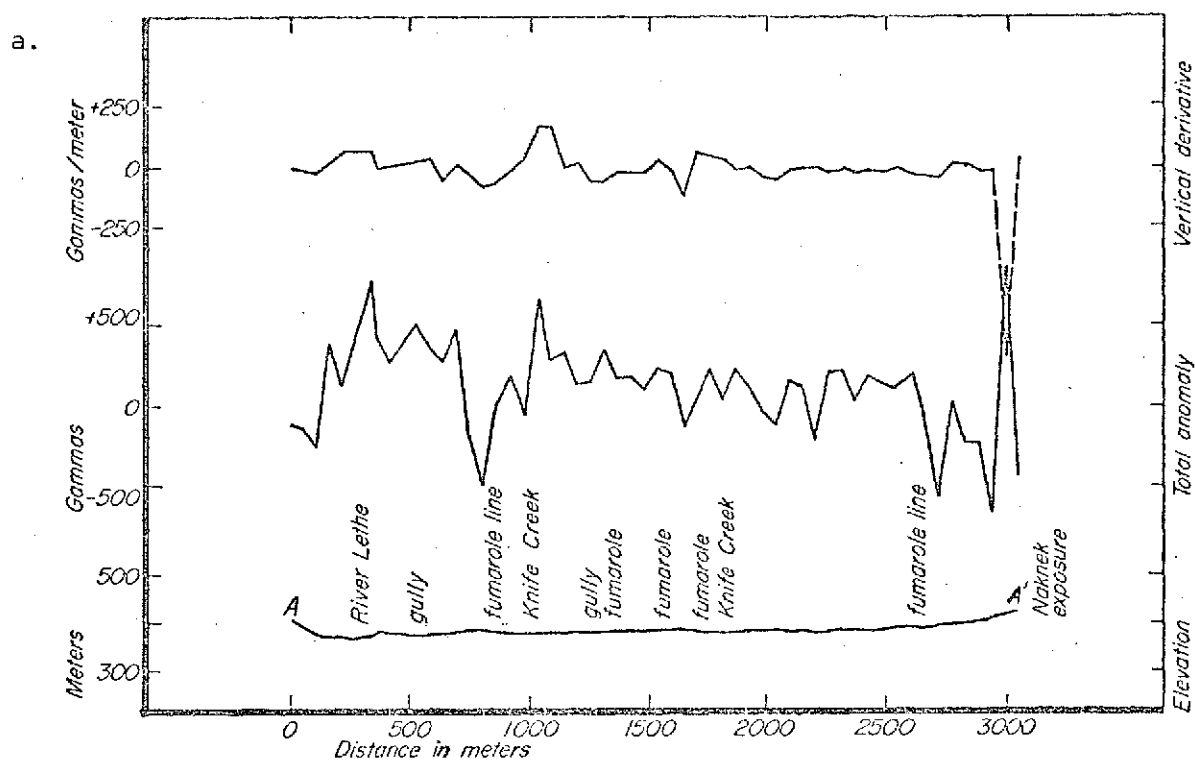


Figure 4.2a. Reduced magnetic profile data for Traverse A-A'.

Figure 4.2b. Reduced magnetic profile data for Traverse B-B'.

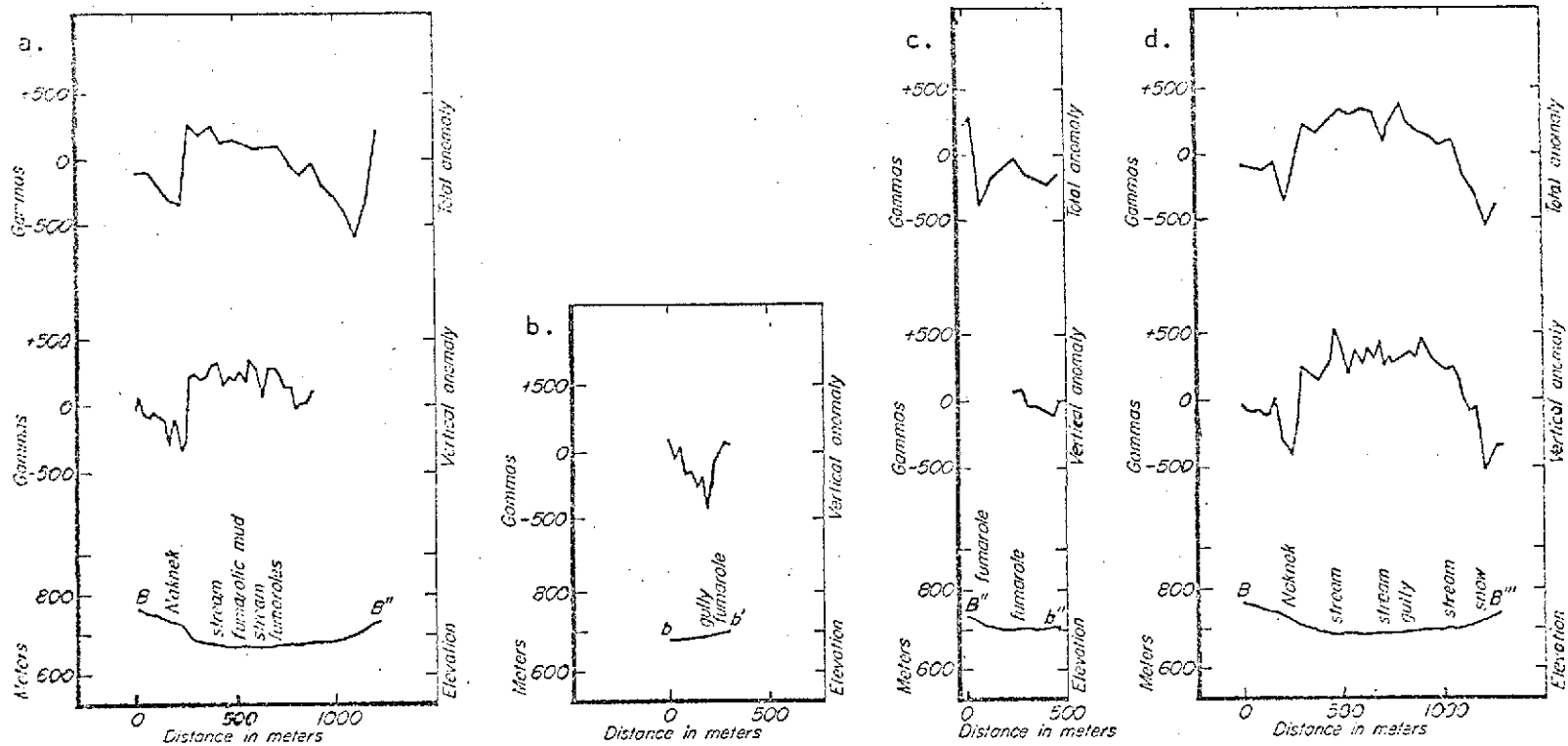


Figure 4.3a. Reduced magnetic profile data for Traverse B-B'.

Figure 4.3b. Reduced magnetic profile data for Traverse b-b'.

Figure 4.3c. Reduced magnetic profile data for Traverse B''-b''.

Figure 4.3d. Reduced magnetic profile data for Traverse B-B'''.

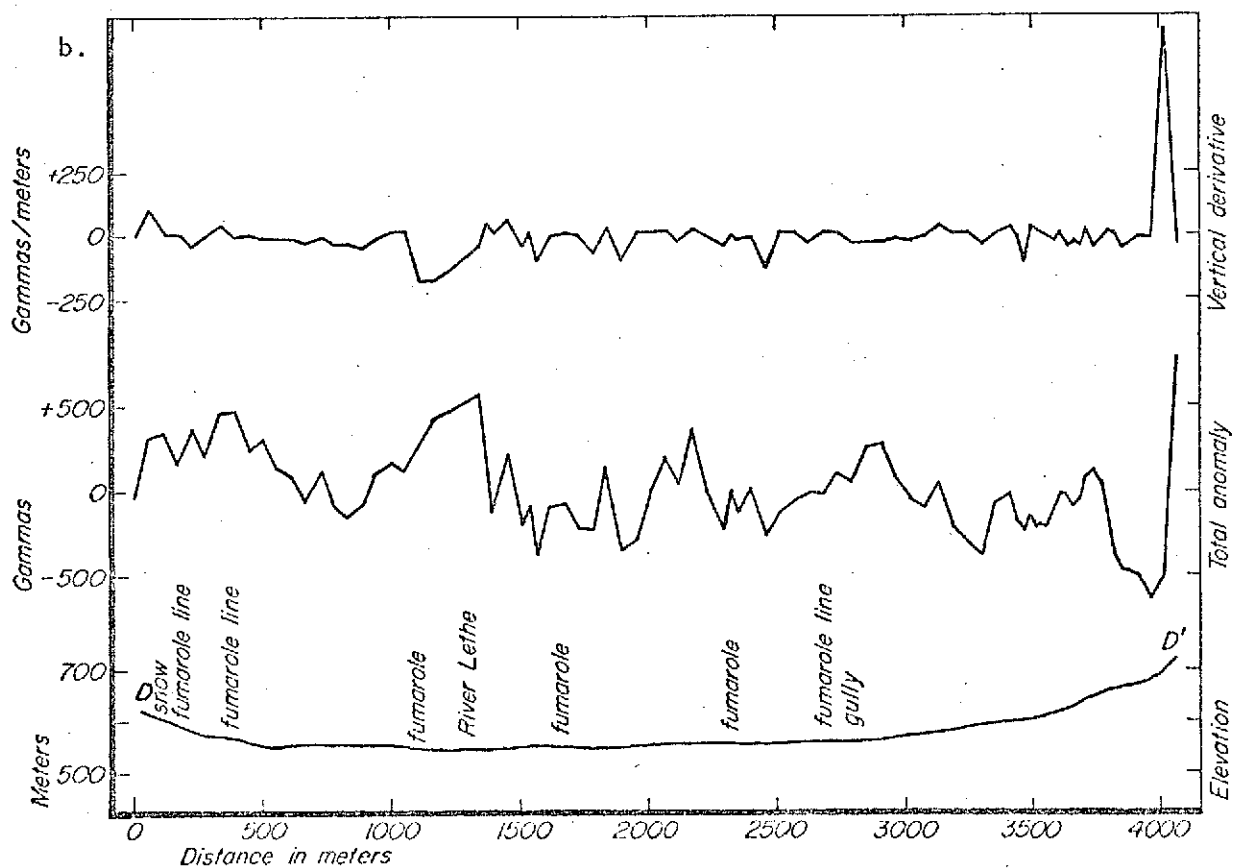
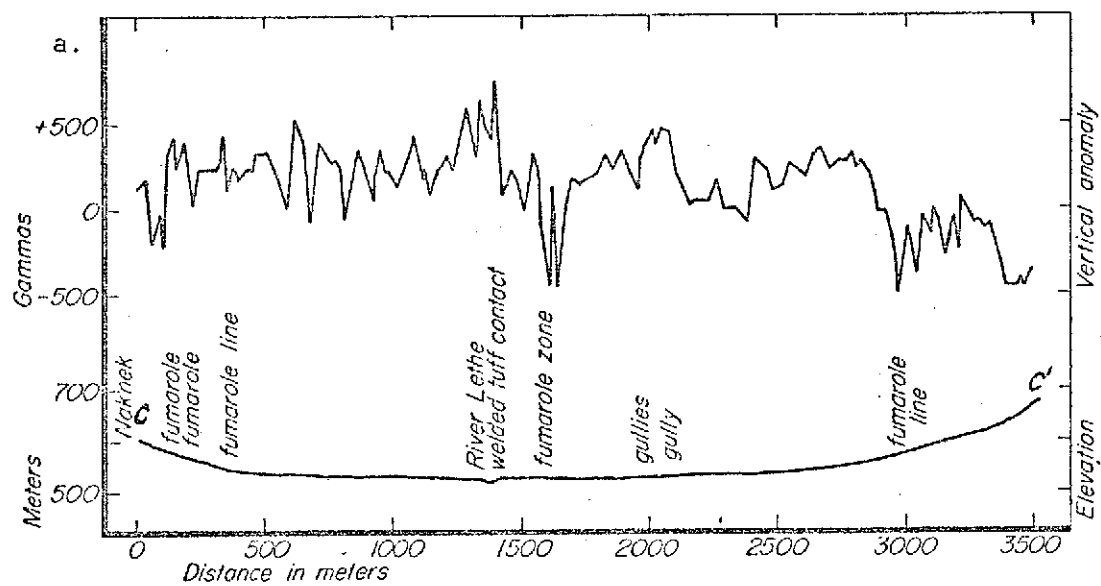


Figure 4.4a. Reduced magnetic profile data for Traverse C-C'.

Figure 4.4b. Reduced magnetic profile data for Traverse D-D'.

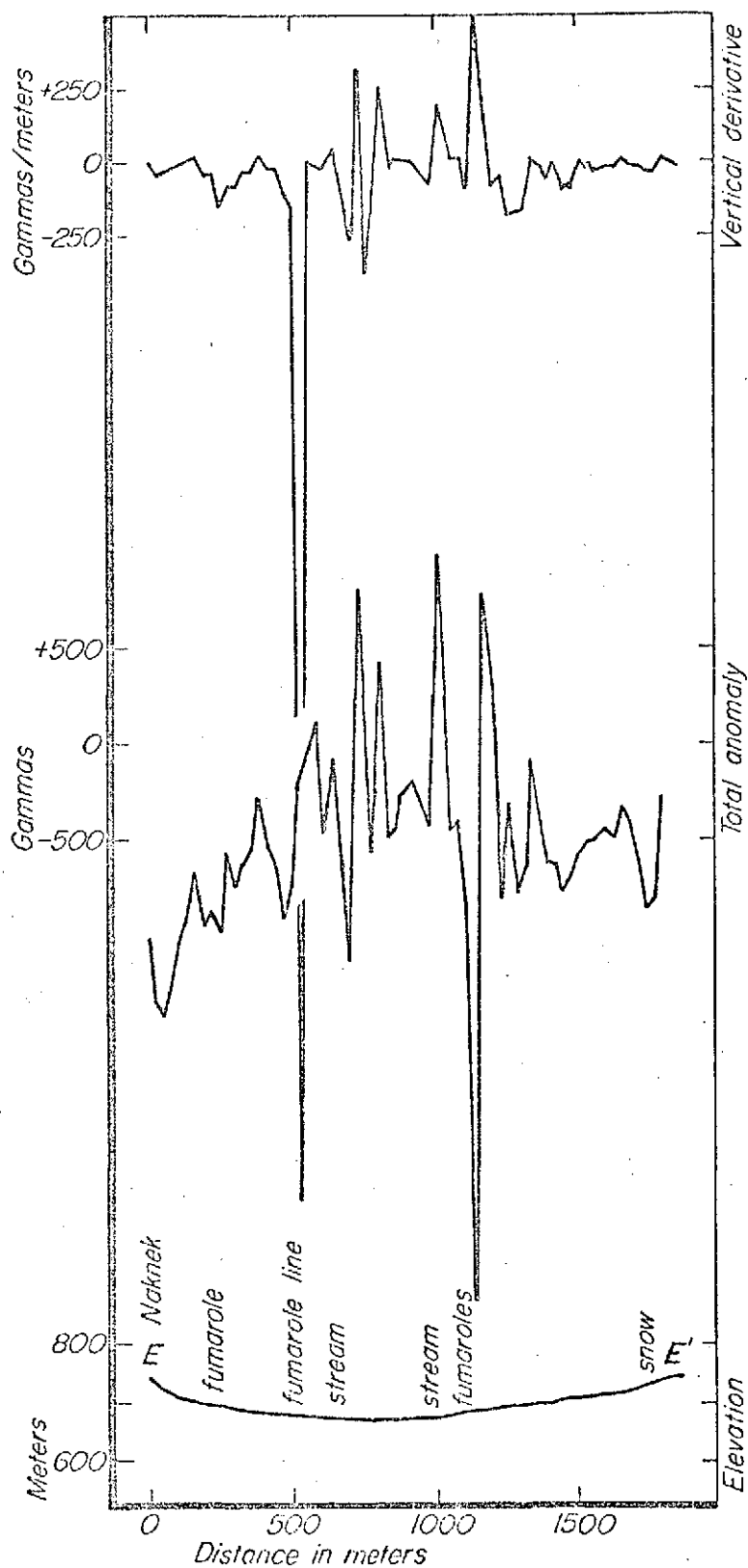


Figure 4.5. Reduced magnetic profile data for Traverse E-E'.

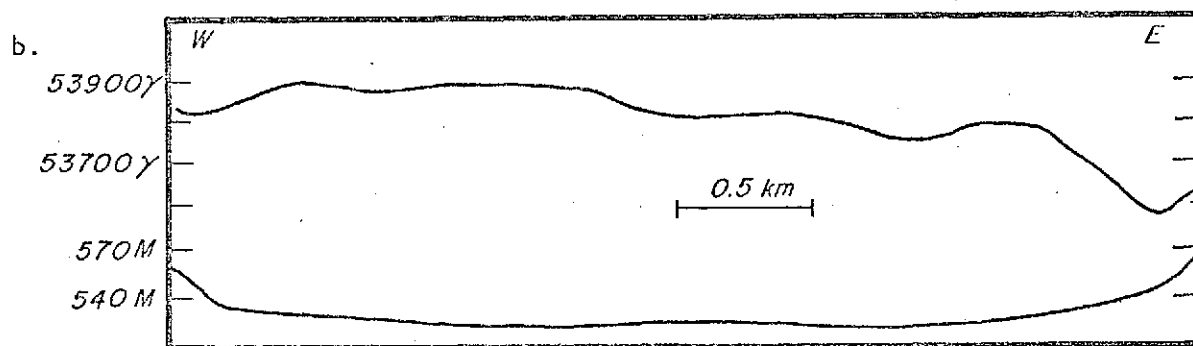
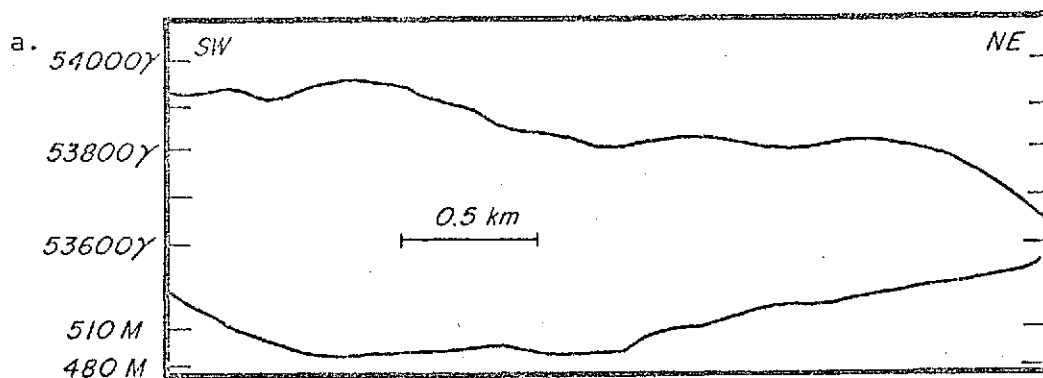


Figure 4.6a. Total magnetic intensity profile along Anna's (1972) flight line 31NW in the lower valley near Tribble's profile A-A'. Flight elevation was 550 meters.

Figure 4.6b. Total magnetic intensity profile along Anna's (1972) flight line 15E in the southern branch near Tribble's profile C-C'. Flight elevation was 610 meters.

the data from being "smoothed" by most mathematical techniques. First, the readings are not evenly-spaced; although along the surface the station spacing was fairly regular, it was irregular horizontally. This variance violates a prerequisite for most smoothing methods. The second failure of the survey lies in the probable structure of the narrow anomalies which are to be removed. These anomalies are likely caused by fumarolic encrustations along compaction fractures in the pyroclastics, thus they can justifiably be termed neither "random" nor "periodic". Furthermore, the sparseness of the data was a handicap which prevented removal of erroneous readings and regional trends by association with adjacent profiles. Since the data cannot be assumed to be of any specific mathematical form, no method of smoothing the data by fitting to a polynomial is justified. The only analysis technique which is justified in this study is the gross visual comparison of the observed data with profiles of model anomalies.

Nowhere, with the exception of the fumarole grid, is the data sufficiently concentrated to justify an attempt at three-dimensional analysis. However, a specific type of two-dimensional analysis is suggested by the character of the observed anomalies. A preliminary examination of the valley profiles indicates that the causative bodies tend to be linear, i.e., of length significantly greater than width. This linear trend is evident throughout the study area; within the individual branches of the Valley the anomalies are easily correlated among adjacent traverses, e.g., parallel profiles C-C' and D-D' in the southern branch of the Valley; E-E' and N'-N''' in Novarupta Basin; and

the several profiles in Broken Mountain Valley (Figures 4.7, 4.8 and 4.9, respectively). The continuance of individual anomalies from one traverse to the next also demonstrates that the bodies causing these anomalies parallel the axis of the valley.

The mathematical formulation of a computer program designed to calculate anomalies for linear magnetic bodies for comparison with observed profiles, based on the methods of Sharma (1966) and Heirtzler et al. (1962), is presented in Appendix E. In the model study, susceptibilities have been assigned under the assumption of uniform magnetization in the present field.

It should be noted that an erroneous interpretation could result if the remanence, which can be sizable in rocks of volcanic origin, is significant in any of the Katmai sequences.

In the present study, remanence is undoubtedly insignificant in the recent volcanic deposits, but it could be a factor in the apparent susceptibility of glacial drift and Naknek sediments. Since the susceptibility of the Naknek rocks is so small, alteration of the orientation of its magnetization would be relatively inconsequential. The glacial drift, which is surely primarily composed of randomly oriented volcanic material, could be expected to display an apparent susceptibility much lower than that of its parent igneous mass. Also, the volcanics probably lost much of their heavier magnetic minerals as they were eroded and deposited by glacial action. Therefore, if during the pyroclastic eruptions of 1912 this mass had been heated above the Curie point of its components, its apparent susceptibility would increase, but not to

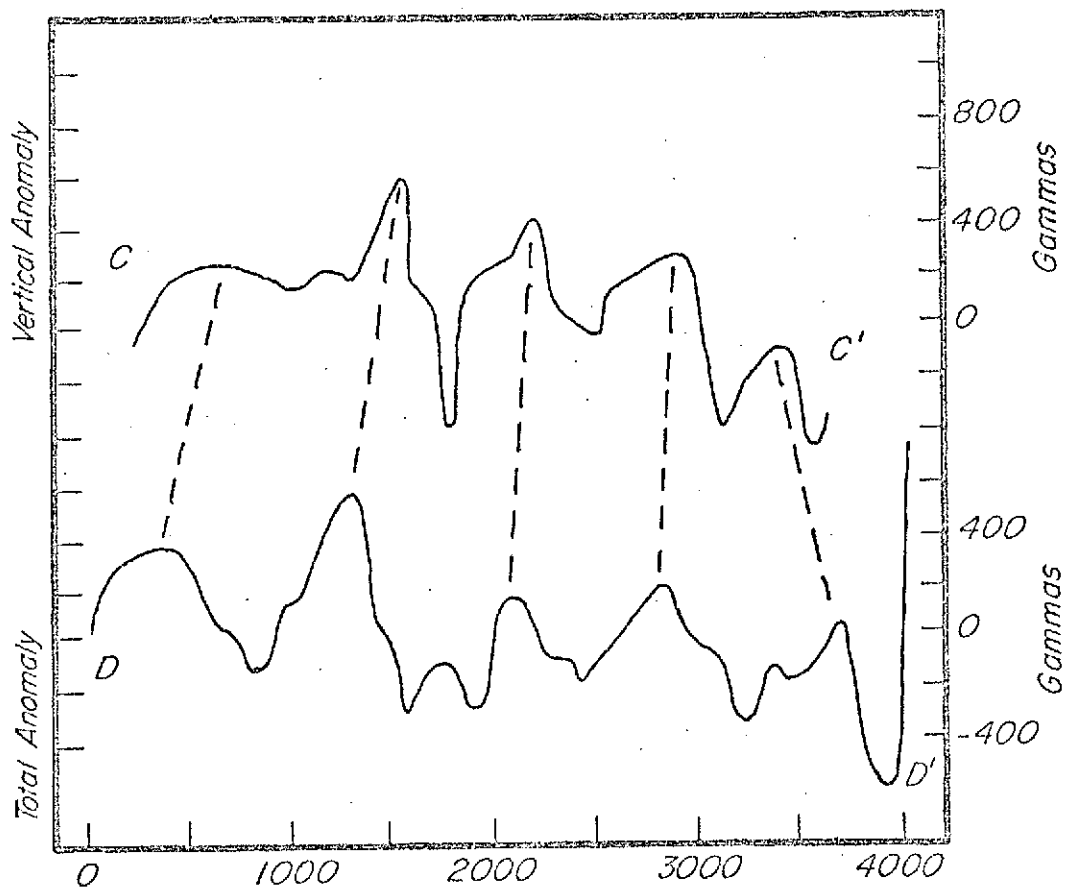


Figure 4.7. Comparison of smoothed magnetic anomaly profiles along adjacent traverses in the southern branch of the valley (refer to Figures 4.1 and 4.4).

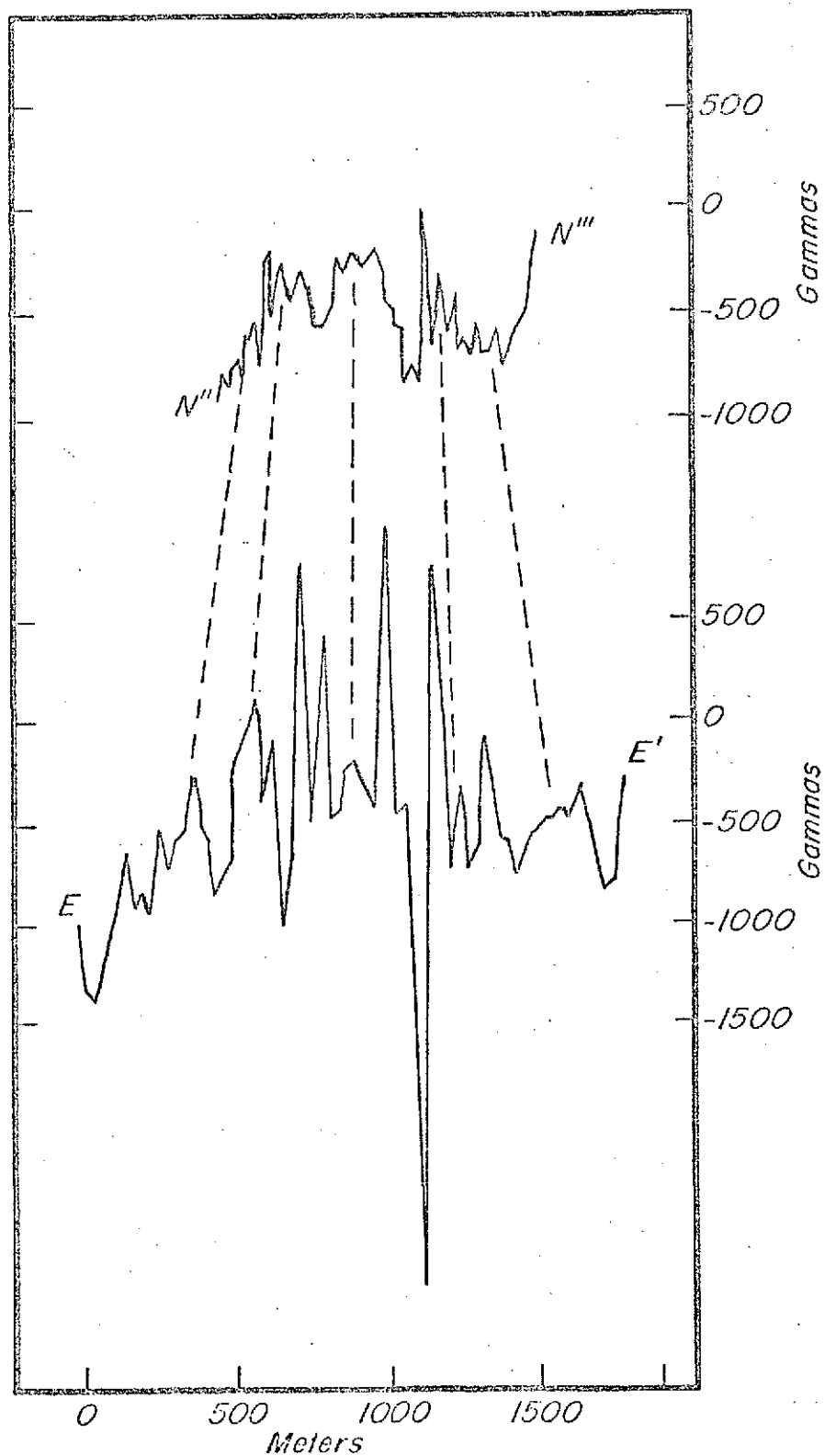


Figure 4.8. Comparison of smoothed magnetic anomaly profiles along adjacent traverses in Novarupta Basin (refer to Figures 4.1 and 4.5).

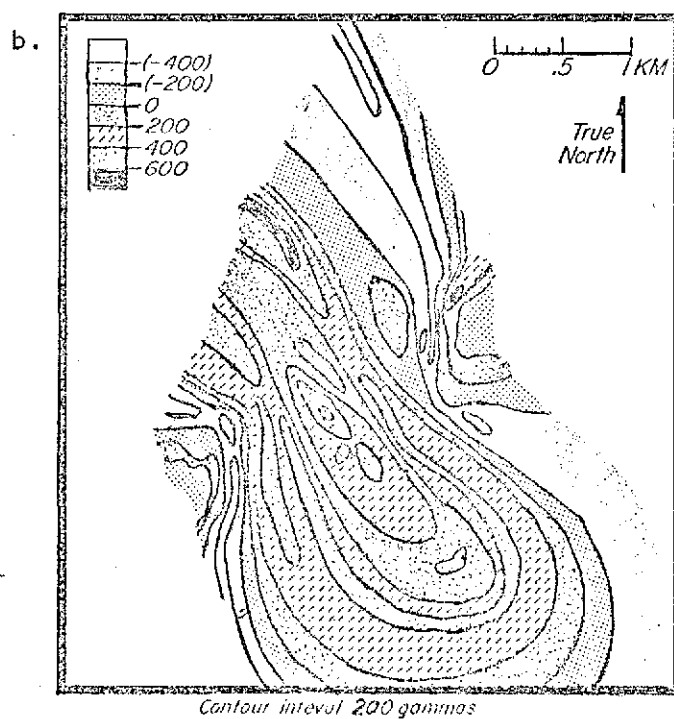
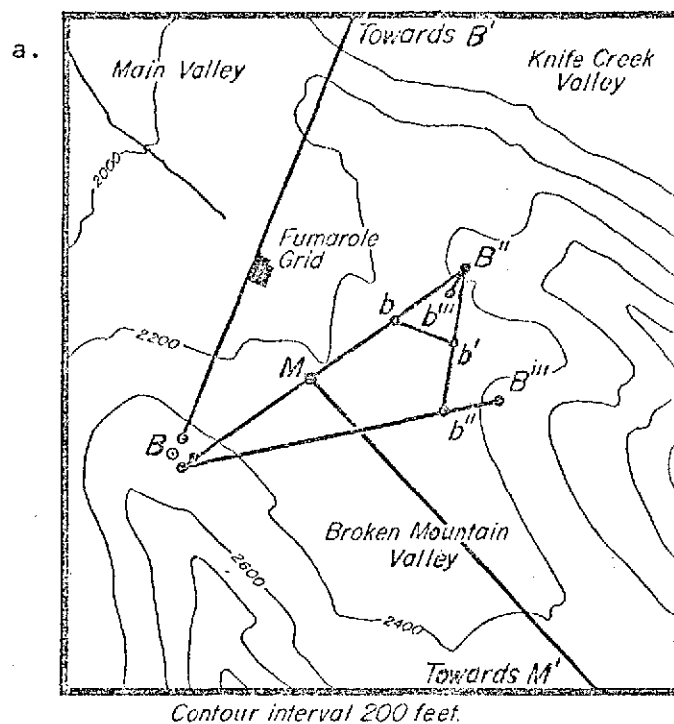


Figure 4.9a. Location of magnetometer traverses in Broken Mountain Valley (refer to Figure 4.1). Elevations contoured at 200 ft. intervals.

Figure 4.9b. Magnetic anomaly map of a part of Broken Mountain Valley. Contour interval is 200 γ . Note the continuity of the anomaly pattern throughout the Valley.

the value of the undisturbed parent volcanics. This possibility was dealt with previously and was taken into account in Table 4.3.

4.2 The Character of the Flow

An important property of the flow which has been detected by several geophysical techniques is its heterogeneity. Not only is the flow zoned vertically, as would be expected had it undergone welding, but it is variable laterally as well. And greater proximity to the eruptive vent(s) apparently even further increases the cross-sectional heterogeneity. It is very difficult to analyze the geophysical profiles, they are so very complicated. Elsewhere, the trends of adjacent geophysical profiles suggest that the relief of the old Valley floor is in large part responsible for the development of the lateral and vertical variations in the flow.

In order to propose plausible magnetic models of the flow, it was necessary to examine all of the geophysical data taken in the Valley. The magnetic susceptibility measurements (Tables 2.1, 2.2 and 4.3) and density determinations (Appendix C and Table 4.1) given in this paper serve as the basis for transforming the gravity, seismic and magnetic data into probable geological relationships.

There have been relatively few density determinations made on rocks from the Katmai region. Appendix C lists the accumulated data to date. Although most of the rock types have a fairly small range of densities, the density of the tuff is found to vary from values comparable with tephra to values comparable with the banded lava of Novarupta. Also, the densities measured for the tuff throughout the valley show a strong tendency to decrease with increasing distance from Novarupta. The density data are summarized in Table 4.1.

Table 4.1

Summary of Density Data
(refer to Appendix C for details)

material	density (gm/cc)		
	low	high	average
tephra	0.98	1.09	1.03
tuff	1.15	1.94	varies*
banded lava	1.70	2.22	1.91
rhyolite glass	2.25	2.30	2.28**
andesitic lava	2.44	2.55	2.48
Naknek sediments	2.48	2.75	2.62

*Density of tuff increases as one approaches
Novarupta.

**Mean, not average.

One of the first tasks in analyzing the previous geophysical information was to re-examine the available seismic data. If travel-time curves were presented in the literature, these data were individually reduced to compressional velocities and thicknesses for each seismic layer (Dobrin, 1960, pp. 70-83); otherwise, the smoothed data as presented by the original investigator was used. A composite of this seismic information is presented in Appendix D and summarized in Table 4.2.

It should be understood that the reduction of seismic refraction data assumes that each successively deeper layer possesses a greater compressional velocity than the overlying layer. If this condition is not met in nature, then the depths and thickness for any layers below such a low velocity layer will be in error since the thickness of the low velocity layer has not been taken into account.

Since it is suspected that at least a portion of the flow is welded, the general nature of welding within an ash flow should be understood. According to Smith (1960, p. 831), a single ash flow (one cooling unit) may display three basic zones. These three types are: no welding, partial welding, and dense welding. Emplacement temperature and flow thickness are critical factors in determining the character of the zoning. Usually, when dense welding occurs in a unit, it is enveloped in a zone of partial welding, which in turn is surrounded by unwelded material. The lower zones of no welding and partial welding are thinner than their upper counterparts. Special or extreme conditions of temperature and pressure can cause some of the zones to be locally absent.

Therefore, since the degree of welding is directly proportional

Table 4.2


Summary of Seismic Parameters

Seismic Layer Number	Probable Composition	Highest Compressional Velocity (km/sec)	Lowest Compressional Velocity (km/sec)	Number of Velocity Readings	Average Velocity (km/sec)	Number of Thickness Readings	Average Thickness (m)
1	weathered layer	0.29	0.1	13	0.16	13	1.2
2	air-fall	0.59	0.25	30	0.38	30	5.7
3	zone of no welding	0.74	0.43	28	0.61	28	26.6
4	zone of partial welding	1.2	0.8	18	0.98	13	41.4
5	zone of dense welding	2.44	1.5	30	1.94	13	48.4
6	glacial drift	3.36	2.5	17	2.88	--	---
7a	Naknek bedrock	3.8	3.68	6	3.73	--	---
7b	igneous bedrock	4.6	4.4	2	4.5	--	---

to the density within the flow, and seismic velocity is directly proportional to the density, it is probable that the zones of welding serve as seismic layers. Furthermore, the depth and thickness of seismic layers beneath a welded zone can be expected to be in error, for the thin lower border of less welded or unwelded material (less dense and of lower velocity) would not be detected by seismic refraction. Should the flow consist of more than one cooling unit (be underlain by a previous welded flow(s) of greater age), then the hierarchy of welded and unwelded zones could become complicated. The multiple low velocity layers which could be entrained in such a section would greatly decrease the accuracy of a thickness determined by seismic refraction.

There are at least eight different seismic velocity layers represented in the Valley. In a few cases an uppermost thin (1.2 meters) layer of very low velocity (average 0.16 km/sec) material was observed. Surely this covering is composed of uncompacted secondary deposits of a (wind and water) weathered nature. Although probably present throughout the Valley, this layer went undetected along most profiles due to its thinness, the depth of the shot and the spacing of the first few geophones.

In most cases the top seismic layer which was detected has an average velocity of 0.38 km/sec. In each case where 0.16 km/sec material was detected, it was underlain by a layer of 0.38 km/sec material. This second layer is probably air-fall. Again it is a relatively thin section (averaging 5.7 meters thick) in most cases. Along a few profiles it was not detected (the cause is probably the same as that cited for the common failure to detect the first layer).



Usually the third layer had an average velocity of 0.61 km/sec. (However, in a few cases the next layer was of 0.98 km/sec or 1.94 km/sec material; and, on the bench on the western side of Baked Mountain, 30 meters of 0.30 km/sec material is underlain by a section of 3.2 km/sec material.) The 0.61 km/sec layer is relatively thick and probably constitutes an unwelded zone within the pyroclastic flow. Generally, this zone is underlain by 0.98 km/sec or 1.94 km/sec material, or both; the exceptions are a few places in the southern branch where velocities of 2.5 to 3.0 km/sec are observed for the next layer, and along one profile in Novarupta Basin where 73 meters of 0.65 km/sec material overlies a section of 4.4 km/sec material.

When detected, the 0.98 km/sec layer is usually overlying 1.94 km/sec material. In the southern branch there are a few instances where the velocity of the next layer ranged from 2.5 to 3.1 km/sec, and near the terminus of the flow the bottom layer has a velocity of 3.8 km/sec. The conspicuous columnar jointing within the flow near the terminus is indicative of partial welding. In this area, the bulk of the flow possesses a seismic velocity near 1.0 km/sec. It is thus logical to assume that the layer with an average velocity of 0.98 km/sec represents a zone of partial welding within the pyroclastic flow. The average thickness observed for this layer is 41.4 meters.

The presence of dense welding is probably indicated by velocities in the range of 1.94 km/sec. Often this seismic layer was the deepest horizon detected by the refraction surveys; however, in the few instances

when deeper sections were observed, it is possible to determine that this zone can range from 33 meters to 73 meters thick.

The uniqueness of the upper five layers (1--0.16 km/sec; 2--0.38 km/sec; 3--0.61 km/sec; 4--0.98 km/sec; and 5--1.94 km/sec) is demonstrated in Section 5b of Sbar and Matumoto's Profile 2 in the south branch of the Valley; elsewhere, layers 1 through 4 and 2 through 5 are encountered along individual sections (refer to Appendix D). The failure to detect the uppermost layers along some profiles is no doubt due to their thinness relative to the surveying parameters. The absence of 1.94 km/sec material indicates that conditions within that section of the flow were not conducive to the formation of a densely welded zone. The absence of both the fourth and fifth layers shows that no welding occurred in that portion of the flow. The absence of layers three and four above a layer of 1.94 km/sec material indicates that this part of the flow was the site of extreme temperature or pressure conditions.

The sixth seismic layer encompasses quite a range of velocities and is probably the glacial drift mantling the Naknek bedrock. Across the southern branch of the Valley, the velocity of the deepest horizon detected by Gedney et al. (1970) ranged from 2.62 to 3.0 km/sec. Similar velocities were encountered elsewhere in the southern branch, in the middle Valley, and in the lower halves of Broken Mountain Valley and Novarupta Basin. Since no deeper horizons were ever observed beneath this material, its thickness can not be determined. When present, this glacial drift constitutes layer six.

Curtis (personal communication, 1971) claims that seismic velocities

of 2.8 km/sec are not out-of-line for densely welded tuffs. If this conjecture is expanded to include all of layer 6 (average velocity 2.88 km/sec), it is evident that the pyroclastic flow might be substantially thicker than previously assumed. If layer 6 is actually the densely welded zone in an earlier cooling unit, it would probably be enveloped in lower density, less-welded material (which would constitute low velocity layers and would not be detected by seismic refraction surveying) and the total thickness of the deposits may be great indeed.

The bedrock in the region of the Valley is the Naknek sedimentary strata. Near the end of the flow, it is exposed along the river gorges beneath less than 50 meters of pyroclastics. In this area, Matumoto and Ward (1967, p. 121) detected a base horizon of 3.8 km/sec at a depth of 46 meters. Similar seismic velocities were observed below zones of dense welding in the upper half of Broken Mountain Valley and near the edge of the bench along the western flank of Baked Mountain in the southern branch of the Valley. Since it is likely that the glacial accumulations were slight in these two places, it seems probable that seismic velocities near 3.7 km/sec are indicative of the Naknek sedimentary horizon. The density of the Naknek sediments (2.6 gm/cc) is in accord with such a seismic velocity (Grant and West, 1965, p. 200). Only twice were higher velocities observed. Near Novarupta, Sbar and Matumoto (1971) recorded velocities of 4.4 and 4.6 km/sec. Nearby igneous rocks have densities near 2.5 gm/cc, which could possess seismic compressional velocities in this range. It is proposed that in these two instances, Sbar and Matumoto penetrated to an igneous stratum or bedrock. Thus, the bottommost horizon is the Naknek bedrock which composes

layer 7a; or, near the volcanoes, the igneous horizon acts as layer 7b.

A few general statements can be made about the thickness of the pyroclastic deposits. The possible inclusion of low velocity layers means that the seismic information can serve only as minimum estimates of the flow thickness. This restriction should be kept in mind throughout the following discussion.

The minimum thickness of the flow increases from approximately 50 meters at the terminus to about 70 meters in the middle and southern branches, to 100 meters in Broken Mountain Valley and Novarupta Basin, and perhaps even more in the southeast branch. Generally the air-fall pyroclastics constitute less than 10 meters of the pyroclastic flow. On the bench on the west of Baked Mountain the air-fall layer is some 25 meters thick. These unusually thick deposits are probably in part due to slumping of the ashy material from the adjacent steep slopes.

Unfortunately, there is no case where a profile containing all three zones of tuff extends to horizons 6 or 7. Therefore, we do not have thicknesses for all 3 zones within any one section. The available profiles, however, permit some conclusions concerning the zoning within the flow. Where underlain by layer 4, layer 3 averages about 15 meters thick; layer 4 ranges from 24 to 62 meters thick in this case; the absence of layer 3 makes no discernible difference in the recorded thicknesses for layer 4; where layer 5 is in immediate contact with layer 3, the latter layer averages nearly 25 meters thick; there is no marked difference in the thicknesses detected for layer 5 whether or not it is overlain by layers 3 or 4 (it varies from 33 to 73 meters in

both cases); and where not underlain by either layers 4 or 5, layer 3 was observed to reach thicknesses of up to 73 meters.

Layer 4 was not observed in Broken Mountain Valley, although the flow is thick, and possesses a zone of dense welding. Assuming that an ancestral Novarupta (refer to Chapter V) stood higher than Greasy Pass, one could assume that Broken Mountain Valley would receive a large portion of the flow, and at a higher temperature than the more distant branches of the Valley. The high emplacement temperature could be responsible for the absence of layer 4. The flow is thinner in the southern branch and farther north. The seismic evidence for the southeast branch is inconclusive since layer 5 was the deepest horizon detected, but here, too, layer 4 is absent. Curtis (1968) showed that most of the tephra eruption was directed northeast away from Novarupta; this would be into Broken Mountain Valley and the southeast branch. If the expulsion of the tuff was similarly directed, the accumulations would be thicker and hotter in this branch as well as in Broken Mountain Valley. This supposition agrees well with the meager seismic evidence. According to this hypothesis, the portion of the tuff which flowed down Novarupta Basin and thence into the southern branch was somewhat cooler, and cooled further with travel. The presence of layer 4 in these areas and farther north supports this idea.

Kienle's profile D-D' shows no layer 3. The high temperature near Novarupta apparently indurated most of the flow. Closest to the dome the flow consists of 16 meters of partial welding and 73 meters of dense welding; whereas about halfway out of the basin, the ratio has reversed

to 43 meters of layer 4 over 33 meters of layer 5. In the southern branch, layer 3 is often present as well as layers 4 and 5. And, near the terminus of the Valley where the flow was the thinnest and coolest, there is no evidence of dense welding.

The direction of the eruption and distances from the eruptive vent affected the thickness and temperature of the flow, and thus the character and extent of the welding. The thicker and/or hotter the flow, the more extreme and extensive the welding.

Comparison of magnetic and gravimetric data along adjacent traverses (refer to Figures 4.10, 4.11 and 4.12) clearly demonstrates correspondence --usually the two data forms appear as mirror-images of one another with a gravimetric low corresponding to a magnetic high and vice versa. One explanation for this feature would be to assume that the pyroclastics deposits and the glacial drift above the bedrock (Naknek sediments are of high density and low susceptibility) are of uniform thickness along any one profile, with lateral groupings of dense material of low susceptibility. Such a situation is contrary to density and susceptibility measurements to date, i.e., the denser pyroclastic material has a tendency to be of higher susceptibility.

Generally, the pyroclastics in the Valley tend to be of relatively low density and high susceptibility in comparison with their surroundings. Increasing the thickness of the underlying deposits therefore increases the magnetic anomaly and decreases the gravimetric anomaly. In fact, variable thickness is probably the primary cause of the anomalous gravimetric and magnetic trends across the various branches of the Valley.

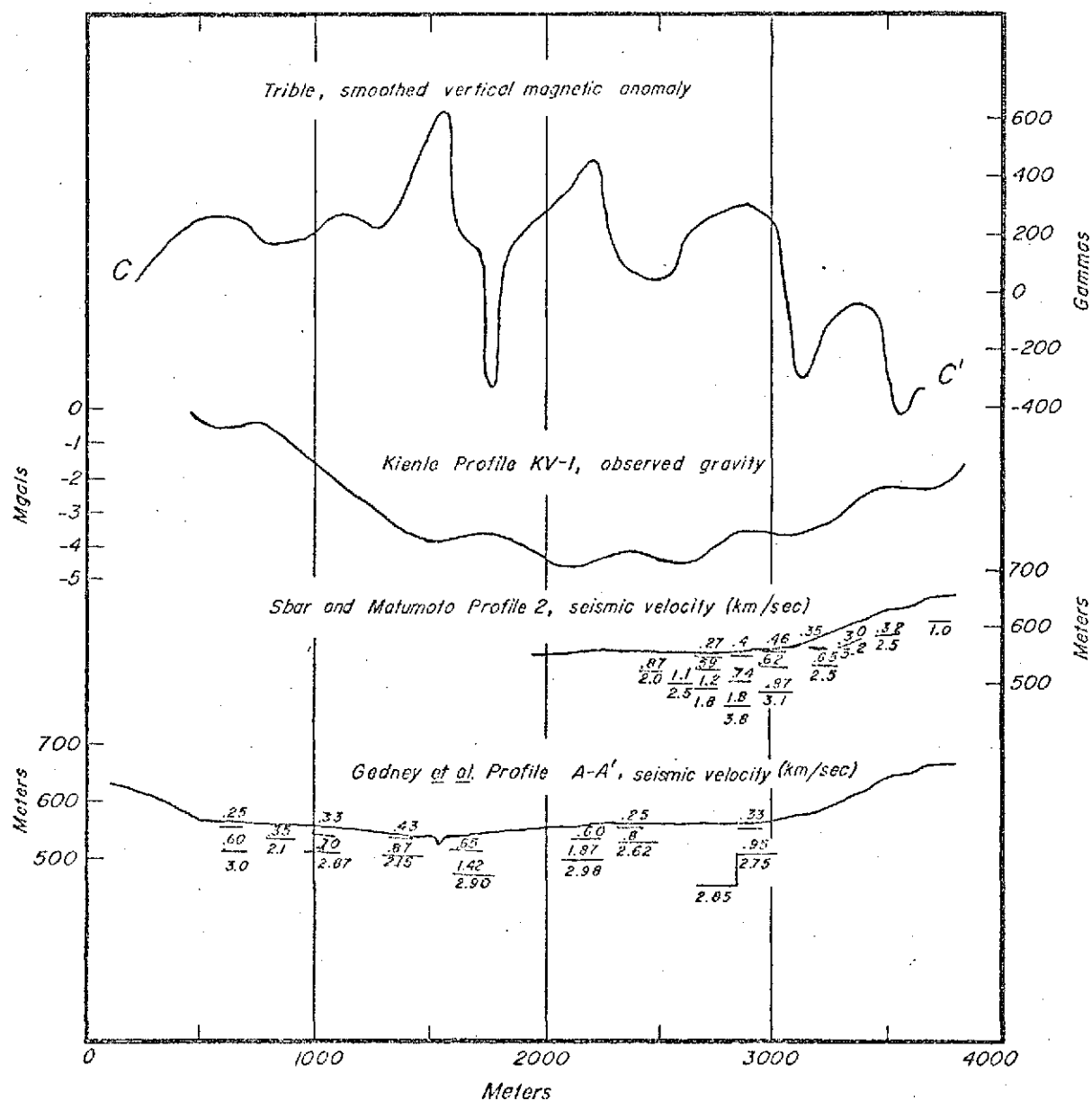


Figure 4.10. Correlation of adjacent geophysical profiles in the southern branch of the Valley. Refer to Figures 1.3 and 4.1.

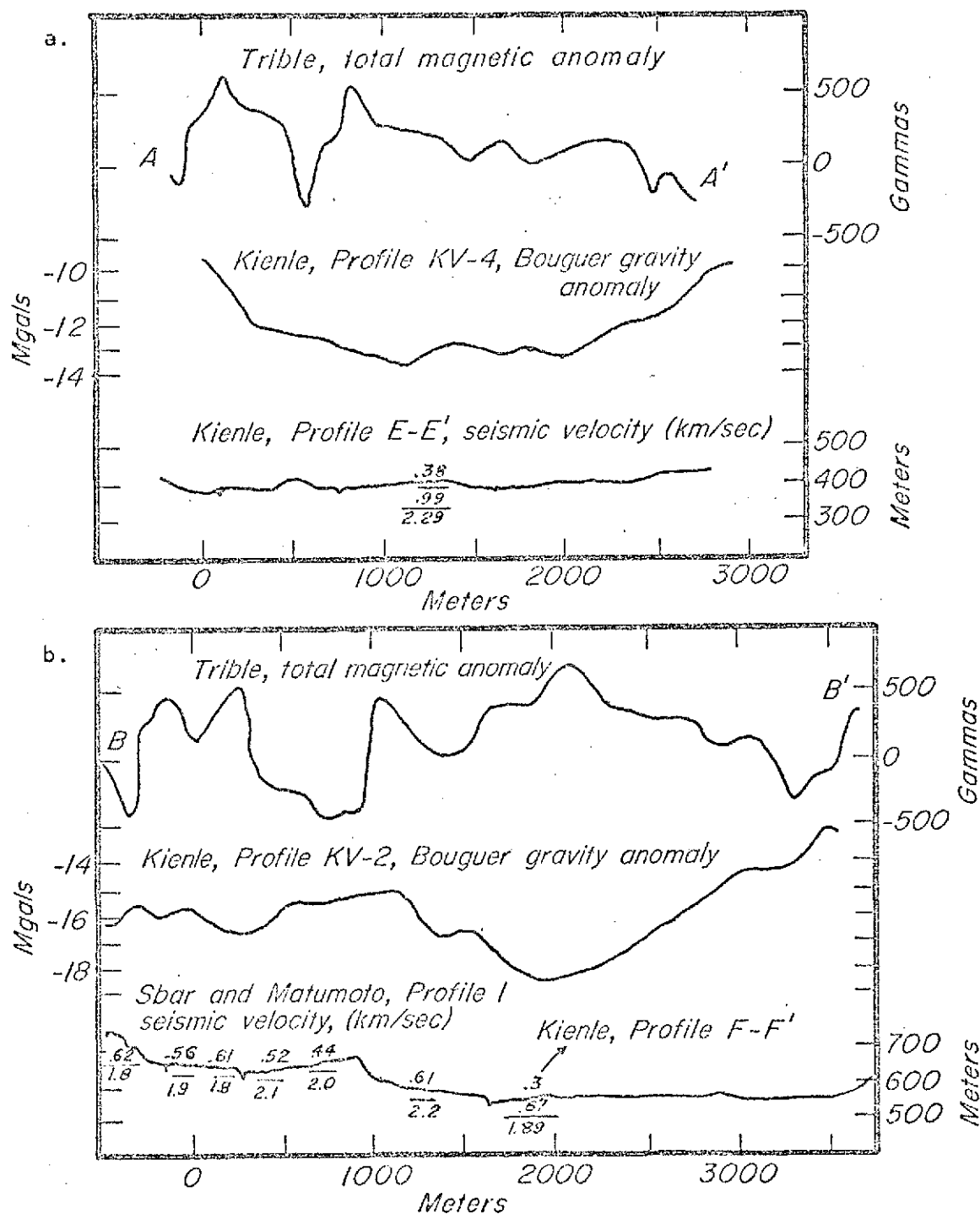


Figure 4.11a. Correlation of adjacent geophysical profiles in the lower valley. Refer to Figures 1.3 and 4.1.

Figure 4.11b. Correlation of adjacent geophysical profiles in Broken Mountain and Knife Creek Valleys. Refer to Figures 1.3 and 4.1.

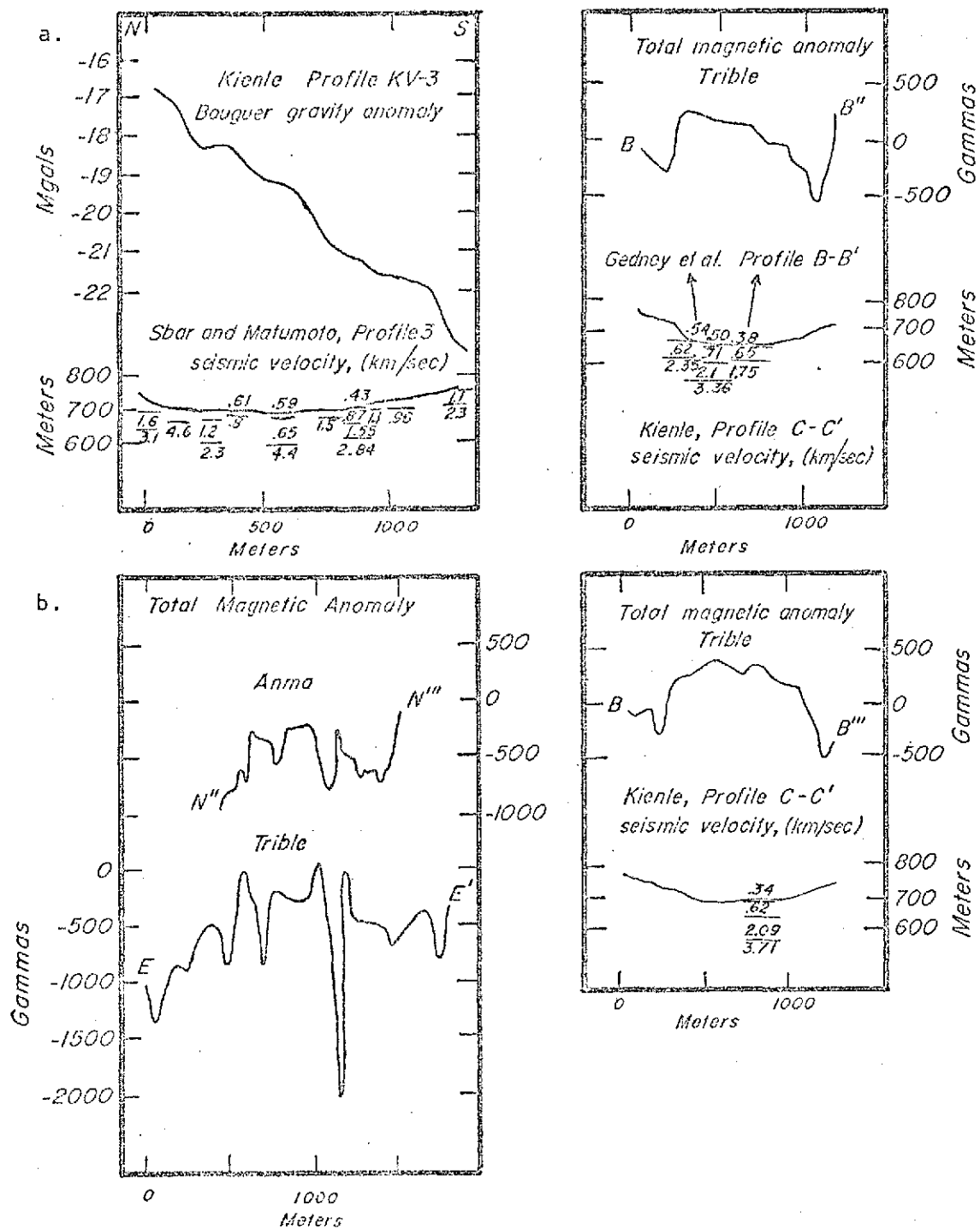


Figure 4.12a. Correlation of adjacent geophysical profiles in Novarupta Basin.

Figure 4.12b. Correlation of adjacent geophysical profiles in Broken Mountain Valley.

Since the top of the flow is quite level, the geophysical anomalies imply that base has considerably relief. In all cases, the greatest anomalies occur in the vicinity of the present streams. This evidence supports the suggestion of previous investigators (Kienle, 1970, p. 6657; Curtis, 1968, p. 186) that the present streams overlie the pre-existing stream channels. It would seem then, that the gravimetric and magnetic anomalies can serve to delineate the configuration of the pre-1912 valley floor. The undulating nature of the anomalies in the southern branch may indicate faulting previous to the final emplacement of the flow.

Cursory examination of the seismic profiles corresponding to the gravimetric and magnetic profiles shows greater tuff thicknesses and higher degree of welding in conjunction with the magnetic highs. This complementary evidence is further proof that in profile the base of the flow is not level and that the buried deeply incised stream channels underlie the present streams.

Kienle (1969) determined two possible models capable of producing the observed gravimetric anomalies (refer to Figure 4.13). The density contrast between the flow and bedrock for his model P now appears to have been too great (1.59 gm/cc), as a density of about 1.6 gm/cc is normal for the tuff, and Naknek sediments have an average density of 2.6 gm/cc. The flow is probably separated from the Naknek bedrock by glacial drift, which would, however, be of lower density than the sediments. Kienle's model F with a density contrast of 0.75 gm/cc probably more nearly represents the actual situation. The tuff thicknesses suggested by model F correspond well with Curtis' (1968) estimates based on geomorphologic extrapolation (refer to Table 1.3).

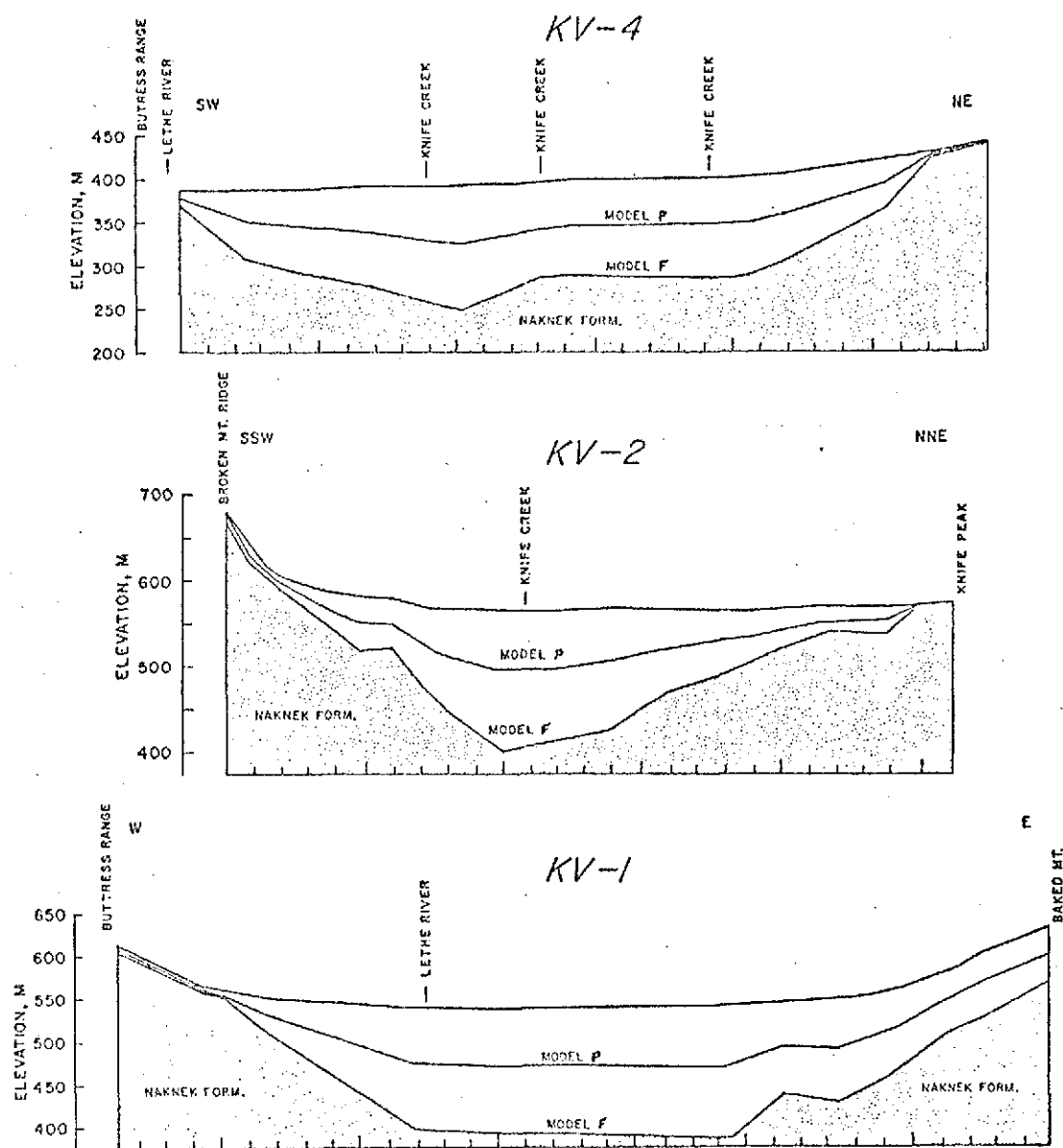


Figure 4.13. Summary of Kienle's (1969) structure sections derived from gravity data.

In most branches of the Valley, the seismically indicated flow thicknesses are less than Curtis and Kienle calculated. Perhaps the seismic sections are too thin for they have not allowed for undetectable low velocity layers of substantial thicknesses; perhaps seismic layer 6 is also part of the pyroclastic flow. On the other hand, the seismic data show thicker pyroclastic sections in Broken Mountain Valley than Curtis and Kienle predict. Curtis had no base control for this branch of the Valley and apparently he did not appreciate the depth of the base in this area. Although Kienle's data were poor in Novarupta Basin and Broken Mountain Valley, his preliminary thickness estimates for these branches seem anomalously low. Higher emplacement temperatures for the flow near Novarupta (e.g., these two branches) would result in the flow being more densely welded and therefore more dense. The tuff densities were found to increase with proximity to the dome, with the highest (1.96 gm/sec; Kienle, personal communication, 1971) from Novarupta Basin (refer to Appendix C). Thus, in these two branches the contrast between tuff and bedrock is lower than Kienle's model F; i.e., the flow is thicker than suggested by model F.

4.3 Magnetic Models of the Flow

Some of the parameters remained constant in all of the computer models. A total field of 53,800 gammas, with declination of 21.5°E and inclination of 71.2°, was used. All the magnetic bodies were assumed infinite along an average valley axis of 30°W.

Four widths were used in modeling the anomalies: 250, 500, 750 and 1000 meters. Most of the observed anomalies have a lateral extent com-

parable to one of these values. The depths and thicknesses of the modeling bodies are based on the seismic layers. The probe of the magnetometer was approximately 2 meters above the surface of the flow. The air-fall deposits generally account for an upper section of about 3 meters, below which the body of the tuff amounts to 25 meters or more. A 10 meter wedge below 50 meters could represent a thermally-altered zone of glacial drift and/or Naknek bedrock. Additional wedges of 50 and 100 meters (representing greater flow thickness, internal zoning and/or a layer of glacial drift) permit calculation for total thicknesses of up to 300 meters (or, of up to 900 meters for 750 meter wide bodies).

As is clear from the derivation in Appendix E, magnetic susceptibility is a constant, altering only the magnitude of an anomaly, not its form. If all other factors are static, it is possible to calculate the amplitude of the anomaly over an identical body of different susceptibility by merely multiplying by the ratio of the newly-assigned susceptibility to the previously-assigned susceptibility (refer to Table 4.3). Of course, the converse scheme permits the deduction of the susceptibility required to produce an anomaly of specific magnitude if all the other parameters of the body are constant.

Since a susceptibility of 1250×10^{-6} emu/cc aptly represents air-fall and tuff, and may well approach the apparent susceptibility of the glacial drift, it was the best choice for the initial model studies. Appendix E.3 lists the total magnetic anomalies at increments of 20 meters across various wedges of 1250×10^{-6} emu/cc material. The central anomalies of these wedges is summarized in Table 4.4.

Table 4.3

Rock Types in the Valley of Ten Thousand Smokes,
 Their Modeling Susceptibilities, and Conversion
 Factors (for Calculating the Magnitude of the
 Magnetic Anomaly Due to Susceptibilities
 Other than 1250×10^{-6} emu/cc
 from Appendix E.3)

Material	Susceptibility*	Conversion Factor
Naknek sediments	50	0.04
fumarolic altered ash	50	0.04
rhyolite	250	0.20
air-fall	1250	1.00
tuff	1250	1.00
banded volcanics	1250	1.00
glacial drift	(1250?)	1.00
andesite	2500	2.00
altered Naknek	5000	4.00
altered drift	(5000?)	4.00

*Susceptibility is in units of 10^{-6} emu/cc.

Table 4.4

Summary of Central Total Anomalies (in Gammas) for
 Computerized Magnetic Bodies of
 Susceptibility = 1250×10^{-6} emu/cc
 at a Depth of 2 Meters
 (refer to Appendix E.3)

Thickness (m) →	3	28	53	63	103	203	298
Width (m) ↓							
250	253	328	364	378	423	488	519
500	250	294	316	324	355	414	451
750	250	297	312	318	340	389	426
1000	249	292	303	308	325	365	398

Unfortunately, it is not possible to derive the unique thickness, susceptibility and depth responsible for an anomaly of specified width and amplitude. Therefore, these parameters must be studied separately within the reasonable limits of the other two parameters.

Initially, the reduced magnetic anomalies were examined by dividing the profiles into as few laterally separated anomalies as seem probable, and taking their magnitude relative to the regional magnetic field only (refer to Figure 4.14). Table 4.5 lists these values. As is clear from Appendix E.3, the magnetic anomalies at the high magnetic latitude of Katmai and along the specified traverse orientations die off rapidly beyond the wedges. It is therefore possible to neglect the contribution of neighboring wedges without markedly influencing the quality of the results. First, it was assumed that each anomaly was due to a wedge of 1250×10^{-6} emu/cc material at a depth of 2 meters and of the modeling width nearest the width of the observed anomaly. From this, the nearest modeling thickness capable of producing the observed anomaly was determined. In several instances the observed anomaly was of insufficient magnitude to be the resultant of even a 3 meter thickness of 1250×10^{-6} emu/cc material at a depth of 2 meters. In these cases, the top of the causative body is assumed to be at a depth of 5 meters. Increasing the depth of the wedge requires a sizeably greater thickness to produce the same magnetic anomaly.

It is clear from Table 4.4 that the susceptibility of the uppermost few meters is critical; e.g., the anomaly caused by a 3 meter thick by 250 meter wide wedge at a depth of 2 meters is approximately equal to

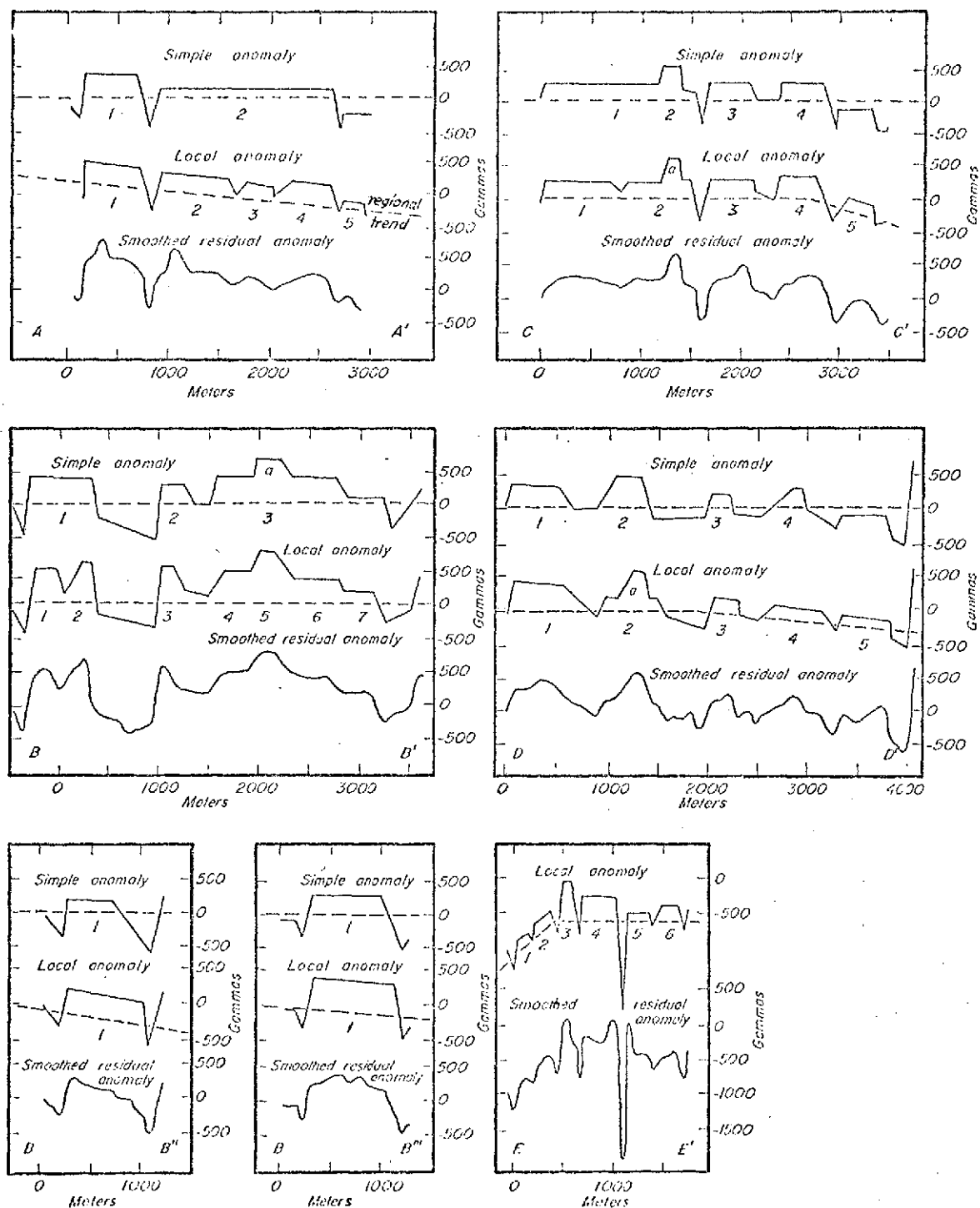


Figure 4.14. Smoothed residual magnetic anomalies and their corresponding simple and local anomalies along the valley traverses (see text).

that from a 295 meter thick by 250 meter wide wedge at 5 meters, and a 3 meter thick by 750 meter wide wedge at 2 meters yields an anomaly similar to that due a 595 meter thick by 750 meter wide wedge at 5 meters depth.

If fumarolic leaching was especially prevalent in the upper portion of the flow, one would expect the material to be of very low susceptibility. In such a case, the top few meters would contribute a negligible amount to the magnitude of the anomaly; this situation could be responsible for the unusually low anomalies. It is unreasonable however to expect that such leaching should be restricted to the precise region of the lower anomalies. If the leaching is widespread, the implication is that ridiculously thick sections of 1250×10^{-6} emu/cc material would be responsible for all the anomalies. The initial determination of the thickness of the flow (given the approximate width, depth and probable susceptibility) yields some erratic results across various branches of the Valley. These models do suggest, however, that the flow may be some 300 meters thick.

Another method of analysis is to assume a specific thickness, depth, and width for the causative body. Two estimates of the thickness of the flow in each branch were chosen from the conclusions of previous investigators (refer to Table 4.5); the depth to the top of the flow was taken as 2 meters and the modeling width nearest the width of the observed anomaly was used. Given the above factors and the magnitude of the observed anomaly, it is possible to calculate the magnetic susceptibility required of the body to produce the anomaly. The calculated susceptibilities

Table 4.5

Simple Magnetic Anomalies and Three Computer Models

Traverse	Anom. #	OBSERVED PARAMETERS			MODEL I		MODEL II	MODEL III		
		Anomaly Width (m)	Anomaly Magnitude (γ)	Nearest Modeling Width (m)	D (m)	(D+DD) (m)	(D+DD) (m)	K (emu/cc $\times 10^{-6}$)	(D+DD) (m)	K (emu/cc $\times 10^{-6}$)
A-A'	1	600	400	750	2	250	55	1620	155	1366
A-A'	2	1200	200	1000	5	>300	55	826	155	725
B-B'	1	650	400	750	2	250	55	1602	105	1470
B-B'	2	300	300	250	2	30	155	841	250	746
B-B'	3	1350	400	1000	2	300	155	1449	250	1312
B-B'	3a	350	650	250	2	>300	155	1822	250	1616
B-B''	1	850	150	750	5	250	55	600	105	552
B-B'''	1	900	300	1000	2	55	55	1238	105	1154
C-C'	1	1100	250	1000	5	>300	55	1032	155	906
C-C'	2	250	500	250	2	250	55	1717	155	1401
C-C'	3	500	250	500	5	>300	55	990	155	812
C-C'	4	500	250	500	5	>300	55	990	155	812
D-D'	1	600	300	500	2	30	55	1187	155	974
D-D'	2	550	425	500	2	250	55	1681	155	1380
D-D'	3	250	200	250	5	205	55	686	155	561
D-D'	4	350	250	250	5	300	55	858	155	710
E-E'	-	---	---	all negatives	-	---	--	---	---	---

Model I: given susceptibility = 1250×10^{-6} emu/cc; width = nearest modeling width, and the magnitude of the observed anomaly, and specifying the depth to the top (D), what is the required thickness, i.e., what is the needed nearest modeling depth to the base (D+DD)?

Models II and III: given width = nearest modeling width, the magnitude of the observed anomaly, and the depth to the top of the body = 2 m., and specifying the depth to the base (D+DD), what is the required susceptibility (K)?

are all within the range of the measured susceptibilities, but it is difficult to explain such lateral alteration in the magnetic properties of the flow. Evidently, there may be down-valley and cross-valley compositional changes in the flow.

A casual inspection of the profiles of the residual field shows that the regional trends are significant along several profiles. Kienle (1969) was able to remove the regional gravity trends because he had bedrock stations at the ends of his traverses. Such a technique is not possible in the present magnetometer study. Neither are the magnetometer traverses sufficiently dense to permit delineation and removal of the regional field by mathematical techniques. Instead, the regional trends have to be arbitrarily, visually removed in order to obtain the local magnetic anomalies. Figure 4.14 exhibits the regional trends and the resulting local anomalies. These anomaly parameters are listed in Table 4.6.

These anomalies were analyzed as above; first, to determine the necessary thickness of 1250×10^{-6} emu/cc material, and next to determine the necessary susceptibility in two cases. The results were no more satisfying than those from the examination of the residual anomalies in Table 4.5. The few instances in which seismic data is available near magnetic profiles permits a check on the plausibility of the magnetic models. Table 4.7 presents these correlated data. Comparisons of the computerized magnetic models with the seismic information reinforces many of the earlier indications of Tables 4.5 and 4.6.

If the seismic thicknesses are assumed to be reasonable estimates

Table 4.6.

Multiple Local Anomalies and Three Computer Models

Traverse	Anom. #	OBSERVED PARAMETERS		Nearest Modelling Width (m)	MODEL I		MODEL II	MODEL III	
		Anomaly Width (m)	Anomaly Magnitude (γ)		D (m)	(D+DD) (m)	(D+DD) (m) K (emu/cc $\times 10^{-6}$)	(D+DD) (m)	K (emu/cc $\times 10^{-6}$)
A-A'	1	620	285	500	2	30	55	1125	155
A-A'	2	780	230	750	5	500	55	922	155
A-A'	3	350	170	250	5	105	55	584	155
A-A'	4	600	285	500	2	30	55	1125	155
A-A'	5	200	55	250	5	30	55	189	155
B-B'	1	400	455	500	2	300	55	1800	105
B-B'	2	300	585	250	2	>300	55	2050	105
B-B'	3	250	515	250	2	300	155	1442	250
B-B'	4	400	455	500	2	300	155	1473	250
B-B'	5	350	740	250	2	>300	155	2038	250
B-B'	6	550	340	500	2	105	155	1104	250
B-B'	7	350	170	250	5	105	155	477	250
B-B'	1	850	340	750	2	105	55	1362	105
B-B'	1	920	455	1000	2	400	55	1879	105
C-C'	1	750	285	750	2	30	55	1142	155
C-C'	2	750	230	750	5	500	55	922	155
C-C'	2a	200	585	250	2	>300	55	2010	155
C-C'	3	450	270	500	2	30	55	1069	155
C-C'	4	530	340	500	2	105	55	1345	155
C-C'	5	400	170	500	5	205	55	672	155
D-D'	1	650	400	750	2	250	55	1602	155
D-D'	2	650	170	750	5	300	55	681	155
D-D'	2a	350	570	250	2	>300	55	1958	155
D-D'	3	300	200	250	5	250	55	686	155
D-D'	4	750	170	750	5	300	55	681	155
D-D'	5	550	115	500	5	105	55	488	155
E-E'	1	200	115	250	5	55	105	340	155
E-E'	2	250	170	250	5	105	105	503	155
E-E'	3	150	585	250	2	>300	105	1729	155
E-E'	4	400	340	500	2	105	105	1198	155
E-E'	5	250	115	250	5	55	105	340	155
E-E'	6	280	230	250	5	250	105	679	155

(The models are based on the same requirements as given in Table 4.5.)

Table 4.7

Correlation of Four Computerized Magnetic Models with Observed Local
Magnetic Anomalies and Nearby Seismic Refraction Profiles

Location	Traverse	Anom. #	Modeling Width Nearest Observed Width (m)	Magnitude of Local Anomaly (γ)	Thickness of Seismic Layers (m)*							Modeling Thickness Nearest Total Seismic Thickness (m)	Model I (D+DD) (m)	Model II Magnitude of Anomaly (γ)	Model III K (emu/cc $\times 10^{-6}$)	Model IV (D+DD) (m)
					1	2	3	4	5	6	7a					
Lower Valley	A-A'	2	750	230	()	2	7	37	?	---	?	---	<5	---	---	---
Southeast Branch	B-B'	3	250	515	()	1	18	---	?	()	()	---	300	---	---	105
Southeast Branch	B-B'	5	250	740	()		22	---	?	()	()	---	>300	---	---	300
Broken Mtn. Valley	B-B'	1	500	455	1	2	25	---	?	()	()	(105)	300	355	1605	130
Broken Mtn. Valley	B-B'	2	250	585	1	2	25	---	?	()	()	(105)	>300	423	1729	155
Broken Mtn. Valley	B-B''	1	750	340	3	5	25	---	58	?	()	105	105	340	1250	65
Broken Mtn. Valley	B-B'''	1	1000	455	2	7	22	---	73	---	?	105	400	325	1750	205
Southern Branch	C-C'	1	750	285	()	1	47	---	---	?	()	55	30	312	1142	---
Southern Branch	C-C'	2	750	230	()	4	43	---	---	?	()	55	<5	312	922	---
Southern Branch	C-C'	2a	250	585	()	2	14	25	?	()	()	---	>300	---	---	155
Southern Branch	C-C'	3	500	270	()	5	31	---	33	?	()	65	30	324	1041	---
Southern Branch	C-C'	4	500	340	()	2	---	105	---	?	()	105	105	355	1198	---
Southern Branch	C-C'	5	500	170	()	25	---	---	---	?	()	30	<5	297	723	---

* --- not detected

? detected, but no thickness information

() suspected

Model I: given depth to top = 2 m, susceptibility = 1250×10^{-6} emu/cc, width = nearest modeling width, and the magnitude of the observed anomaly, what is the required nearest modeling depth to the base, (D+DD)?

Model II: given depth to top = 2 m, susceptibility = 1250×10^{-6} emu/cc, width = nearest modeling width, and (D+DD) = modeling thickness nearest the total seismic thickness, what is the resultant magnitude of the anomaly?

Model III: given depth to top = 2 m, (D+DD) = modeling thickness nearest the total seismic thickness, width = nearest modeling width, and the magnitude of the observed anomaly, what is the required susceptibility K?

Model IV: given a body of the nearest modeling width at a depth of 2 m extending to 30 m and of susceptibility = 1250×10^{-6} emu/cc, directly underlain by a body of the same width but of susceptibility = 2500×10^{-6} emu/cc, what is the nearest modeling depth to the base, (D+DD), of the second body in order that the anomaly be of the observed magnitude?

of the true thickness of the flow along the traverses, then one must conclude that the susceptibility of the flow is variable. Clearly, the alterations in the flow thickness are insufficient to be the sole cause of the local magnetic changes.

Concentrations of material of substantially lower susceptibility than 1250×10^{-6} emu/cc are to be found in the Lower Valley, near the borders of the flow in all branches of the Valley, and in Novarupta Basin.

It should be understood that the modeling susceptibility (1250×10^{-6} emu/cc) for the flow was based on air-fall and tuff samples from the upper regions of the flow only. No samples were obtained from the Lower Valley where the flow has changed in appearance and is more homogeneous and more rhyolitic.

It has been found that the susceptibility of rhyolitic material is relatively low. Obviously, were an appreciable amount of the flow primarily rhyolitic, the resulting magnetic anomalies would be far smaller than those calculated for a flow comprised entirely of the modeling susceptibility. Thus, the more rhyolitic composition of the flow near its terminus is responsible for its lower susceptibility and resulting lower magnetic anomalies. Extensive pockets of rhyolitic material near their source, Novarupta, could account for the indicated low susceptibilities in Novarupta Basin.

A different explanation for the longitudinal pockets of low susceptibility material along the borders of the Valley is probable. Much of the ash along the borders is thought to be weathered debris which has slumped from the adjacent steep slopes. Perhaps the prolonged weather-

ing of these portions of the flow which were originally deposited on the steep slopes has leached the ash sufficiently to decrease its susceptibility almost by half, as is suggested by the magnetic modeling studies.

As was previously stated, it is doubtful that fumarolic leaching could be extensive enough to account for the observed anomalies. Fumarolic activity was never observed to be continuous over areas as large as those outlined by the magnetic anomalies. On the other hand, in many cases a seismically-determined thickness of 1250×10^{-6} emu/cc material is insufficient to produce the observed local magnetic anomaly; greater thickness and/or higher susceptibility is required.

Frequently the highest magnetic anomalies were encountered near streams. If greater thickness is assumed responsible, then one would conclude that the previous streams must underlie the present gorge. Spurr (1900) reported that the previous streams were incised about 30 meters into the old valley floor of glacial drift. But even an extra 50 meters of the modeling material below a minimal flow thickness of 50 meters cannot produce the observed anomaly. A wedge 250 meters wide at a depth of 55 meters could increase the anomaly by 95 gammas; far less than the difference of about 200 gammas frequently found near the streams. The models in Tables 4.5, 4.6 and 4.7 show that increased thicknesses of over 100 meters are required to account for the "stream" anomalies, if the susceptibility remains at 1250×10^{-6} emu/cc throughout the flow. Therefore, one must conclude that at least a portion of the flow must be of greater susceptibility than the modeling susceptibility.

There has been some speculation that magnetite concentrations along

the present stream beds are responsible for the high anomalies encountered nearby. Certainly even a thin wedge, with a susceptibility as high as has been measured for magnetite, could easily account for the magnitude of the observed anomaly, were the accumulations not too deep (even taking into consideration the void of 1250×10^{-6} emu/cc material above the stream). However, the gorges are not nearly as wide as the observed anomalies. Perhaps magnetic accumulations along the buried, possibly wider previous channels could be in part responsible for the highs associated with the present streams.

It was frequently noted that fumarolic activity was particularly concentrated along the streams. Assuming that the present waterways are indeed above the previous channels, it is clear that they outline the major site of accumulation for both ground and surface waters. Thus the neighborhood of the streams could provide abundant steam to be expelled by the fumaroles and to aid in their transport of metallic constituents from the flow. The stream area would also be expected to undergo a greater amount of settling and fracturing since it is the thickest portion of the flow. Such conditions are favorable for the establishment of fumarolic vents. Welding would also be more likely to occur in the deeper sections of the flow; the degassing would further add to the fumarolic emanations. The chance of concentration and retention of magnetic minerals along fumarole vents has been discussed. Since such accumulations are restricted to the immediate vicinity of the vents, and are infrequently preserved, it is doubtful that fumarolic magnetite could form a substantial zone the width of the observed magnetic anomalies.

The susceptibility of one of the samples of welded tuff was nearly 2500×10^{-6} emu/cc. If the densely welded zone within the flow is of this susceptibility, then the thickness of the flow required to produce the local anomalies is closer to that indicated by the seismic data. (Model IV of Table 4.7 lists the depth to the base of the flow assuming that the densely welded section is overlain by 30 meters of 1250×10^{-6} emu/cc material.) It therefore seems possible that the welding process can double the apparent susceptibility of the flow.

Another method of increasing the magnitude of the model anomalies is to consider that there may be a substantial thickness of high susceptibility glacial fill beneath the flow. Fifty meters of 2500×10^{-6} emu/cc material below a typical flow thickness would not sufficiently increase the model anomaly: if it is 250 meters wide and 55 meters deep, the increase equals almost 120 gammas; if 100 meters deep, the increase is only about 70 gammas. Even if the upper 10 meters of the drift had been thermally-altered during emplacement of the flow such that its susceptibility had been enhanced to 5000×10^{-6} emu/cc, the increase in the model anomaly would only be about another 50 gammas for a 50 meter thick flow underlain by glacial drift. In addition, there is no reason to expect either of these features to be restricted to the stream areas. A previous andesitic lava flow of similar susceptibility (2500×10^{-6} emu/cc) and thickness might have been restricted to the stream channels, but there is no geologic evidence for such a stratum.

In practice, the magnetic model studies tend to imply that the glacial drift below the flow is either relatively thin or of negligible apparent susceptibility. To model the larger anomalies requires the

flow itself to be of higher susceptibility than 1250×10^{-6} emu/cc. Assuming higher susceptibilities for the welded zones is an effective means of increasing the value of the model anomalies to the observed magnitudes.

Were Fenner to examine the geophysical data, he would no doubt construe it as support for his hypothesis of the eruption. The undulating bedrock profiles would indicate the collapse of the old valley floor following the expulsion of the tuff flow from fissure feeders. The multiple anomalies across each branch would outline the portions of the flow originating from separate feeders. The increased magnetic anomalies in these areas would be due to compositional variations outward from each vent and alterations within the glacial drift and bedrock through which the tuff was erupted. Since the valley floor would have been thinnest and therefore weakest along the stream channels, then the greatest alteration would be expected here, accounting for the highest magnetic anomalies in this area.

Assuming that a typical valley cross-section consists of 50 meters of tuff over 50 meters of drift, the total magnetic anomaly for a 250 meter width (of 1250×10^{-6} emu/cc) is 423 gammas. If the character of the emplacement of the flow had been so encompassing as to realign the magnetization vectors throughout the drift, its apparent susceptibility might be about doubled, which could increase the anomaly by 60 gammas. Assuming that the drift underwent extreme alteration capable of doubling its susceptibility again, the anomaly could be increased by yet another 120 gammas. Had the Naknek bedrock been

similarly altered and its susceptibility enhanced to 5000×10^{-6} emu/cc throughout a 50 meter section, the anomaly would be greater by almost 300 gammas. Of course such extensive alteration is extremely unlikely.

4.4 Conclusions

The pyroclastic flow in the Valley of Ten Thousand Smokes is not a simple, uniform unit. Not only does it possess the vertical zonation typical of flows which have undergone welding deformation, but it is variable laterally as well. As would be expected, cross-sections of the flow become increasingly complex as one nears Novarupta.

The presence of several individual anomalies along each profile suggests that some of the parameters of the flow are also variable laterally. Correlation of these anomalies among adjacent profiles within any one branch of the Valley shows that the causative variations are more or less continuous, and are parallel to the axis of that branch of the Valley. This apparently linear nature of the anomalous magnetic bodies permits a specific type of two-dimensional analysis. Adaptation of this model analysis technique to the computer allows the calculation of several possible geologic models of the flow. Comparison of the anomalies produced by the models, with the observed anomalies, enables limitations of the probable flow parameters.

The excellent "mirror-image" correspondence of gravimetric and magnetic anomalies along adjacent traverses suggests that the primary cause of both anomalies is variable thickness of the low-density, high-susceptibility pyroclastic material above the dense, low-susceptibility Naknek sedimentary bedrock. Since the top of the flow is essentially flat, this proposition requires that the base of the flow have considerable

relief. In most cases, the deepest sections are indicated beneath the streams, implying that the present streams are above the pre-1912 channels. Generally, the indicated base relief can be reconciled with a plausible pre-1912 valley configuration; however, in the southern branch, the undulating nature of the anomalies may outline faulting of the bedrock prior to the final emplacement of the pyroclastics in 1912.

The sparse seismic data available to date reinforces the conclusion based on the other geophysical evidence that the base of the flow has high relief. Several intermediate layers within the flow are exposed by the refraction profiling. These seismic layers are probably caused by zones of differing degrees of welding. As would be expected, were Novarupta the eruptive source, the zones of dense welding become more prominent as one nears Novarupta, where the flow would have been the hottest; and there and elsewhere, the degree of welding is greater in the thicker sections of the flow.

The inability of magnetic models (using thickness based on the gravimetric, geomorphological and seismic evidence, and a susceptibility based on the average of the present studies) to produce the observed anomalies suggests that variable thickness is not solely responsible for the multiple magnetic anomalies encountered along each profile. It is necessary that the susceptibility also vary across the flow. Model studies suggest that the high anomalies may be due to increased susceptibility in the welded section. The lower than average susceptibilities suggested for the borders of the flow are thought to result from weathered ash which has slumped from the adjacent steep valley walls. Fumarolic

leaching could also decrease the susceptibility of the flow, but its effects are thought to be restricted in depth and width. The longitudinal (from south to north) compositional change of the flow from more andesitic to more rhyolitic is the probable cause of the lower susceptibilities indicated in the lower Valley. Pockets of this more rhyolitic ash near the eruptive vent, Novarupta, are thought to be responsible for the low susceptibilities suggested by the magnetic models for Novarupta Basin.

The preparation of a model magnetic profile and Valley cross-section based on the ground magnetometer survey traverses alone is unjustified. The complicated inter-relationships of changing thickness, composition and history (both weathering and fumarolic) throughout the flow precludes any such model profile. If used in conjunction with other geophysical data, however, the magnetometer data can help place limits on the various parameters of the flow.

The magnetometer survey data are in agreement with the flow thicknesses suggested by Curtis (1968), Kienle (1969, Model F) and Kienle's recent seismic refraction profiles. In fact, the magnetometer data may indicate even greater thicknesses for some branches of the Valley. According to Curtis (1968, p. 207), such thicknesses show that the total volume of the eruption(s) in 1912 was great enough to equal the collapse of Katmai crater, the subsidence surrounding Novarupta, and a substantial amount of other regional subsidence.

CHAPTER V

RECONNAISSANCE MAGNETOMETER SURVEY IN THE VICINITY OF NOVARUPTA VOLCANO

5.1 Description of Novarupta

Six miles west and 780 meters below Katmai Crater is the volcanic dome, Novarupta. Present hypotheses consider Novarupta as the primary vent for the 1912 pyroclastic eruption. Supposedly this vent enlarged throughout the eruption, passed through a violent stage, and finally extruded a mass of viscous lava as a dome (Fenner, 1950b, p. 708). Other sources of the flow deposits are assumed to have been a series of eruptive fissures at the head of the Valley of Ten Thousand Smokes, with vents concentrated along a southeast-trending zone, approximately parallel to that marked by the line of Falling and Cerberus Mountains, and the domes at the base of Mount Mageik (Williams, 1954, p. 58).

The dome of Novarupta is circular, approximately 400 meters in diameter and 91.5 meters high. It is surrounded by a high wall or "corona" of ejected pumice and glass blocks. The height of this crater rim rises continuously from a low point of 61 meters above the general level outside the corona on the western side until it merges with the gouged-out face of Stumbling Mountain on the northeast, where Naknek sediments are exposed. Mild gas emission still occurs along the crest of the rim, and many of these fumaroles are far too hot to touch.

The strata of the crater rim dip away from the dome at moderate

angles, but on the inward side are cut off sharply, presenting a steep face to the dome. The intersection of this face with the surface of the dome generally makes a V-shaped trough or moat, but locally the moat has a flat bottom.

Novarupta dome itself consists of glassy though slightly porous lava. In forming the dome, the viscous lava congealed to a glass while it was still being thrust upward, resulting in a great portion of it being shattered. Much of this shattered material has remained on the slopes of the dome, although some blocks have dropped into the encircling moat.

Flow banding is exhibited by the dome. On all sides the banding can be seen dipping toward the center of the dome (Curtis, 1968, p. 192). Fenner attributes this orientation to the overturning of the outer layers as the central mass was pushed up (Fenner, 1950, p. 719). The flow banding itself is due in part to alternations of glassy and cellular material but some is due to alternations of light-gray rhyolitic glass and dark-brown andesitic scoria (Fenner, 1923, p. 56). The dark bands of andesitic composition are particularly common on the northeast side of the dome, while the central part is much closer to pure rhyolite (Curtis, 1968, pp. 192, 194). At the summit of Novarupta dome is a trough (Fenner, 1925b, p. 219).

5.2 Patterns of Subsidence Around Novarupta

In general, the pattern of subsidence in the upper Valley is concentric to Novarupta dome. Most of the faults in the vicinity of Novarupta seem to display simple vertical throws; others are step-like (Fenner, 1925b, p. 202). All the faults appear to record settling

toward Novarupta. Gräben structures separate Stumbling Mountain from Broken Mountain. On a smaller scale, fissures intersect the edge of the dome itself. Thick deposits of pyroclastics conceal any offsets in Novarupta Basin. The prominent subsidence features are outlined in Figure 5.1.

Curtis (1968) estimates that the circular scarp at a radius of approximately 2 km centered just northeast of Novarupta, has a downthrow towards the dome of at least 150 meters. The major structural features on the border of this scarp are the northern face of Falling Mountain, the faulted lower northern slope of Mt. Trident, Fenner Ridge, the faulted southeastern slope of Broken Mountain, and Greasy Pass.

The sharp scarp face of Falling Mountain bears witness that a huge rock slide probably preceded or accompanied the pyroclastic eruption. The irregularities of the landslide debris are not visible, as they are smoothed over by the pyroclastic deposits. Curtis (1968, p. 190) supposes that the northern part of Falling Mountain collapsed into a void as subsidence of Novarupta began. Fenner (1926, pp. 197-198) reported a line of crater vents located at the base of the falling cliff which he attributed to a deep fissure. Many small fumaroles issued from the bare rock face of the mountain in the early years (Griggs, 1922, p. 242). Fenner (1920, p. 586) discovered that the fumarolic emanations were actively altering the igneous rock composing Falling Mountain, resulting in a loss of cohesive strength, and thus contributing to the numerous landslides which characterized this mountain from the beginning.

The faults which shattered the lower slopes of Mt. Trident were the scene of strong fumarolic activity shortly after the eruption

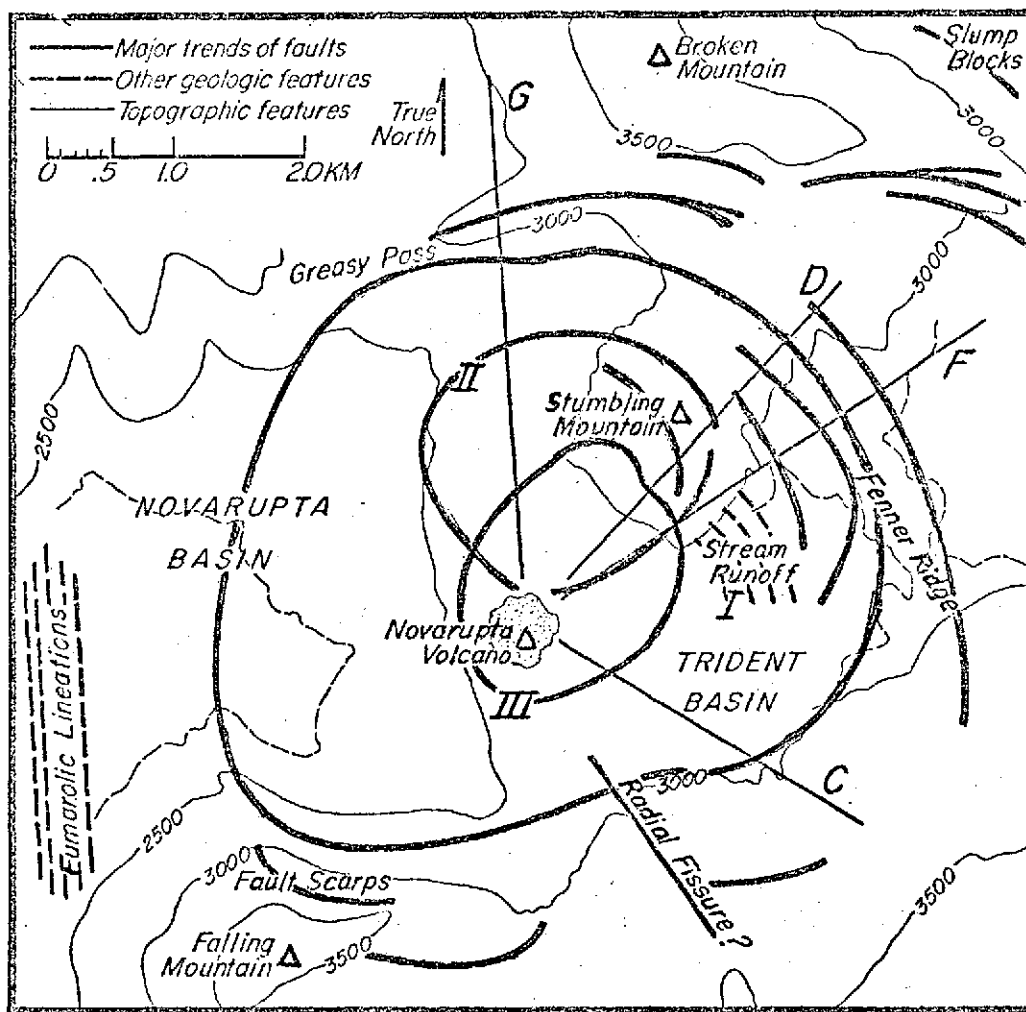


Figure 5.1. Map of structural features in the vicinity of Novarupta Volcano. In all instances, the faults are downthrown towards the dome. Radials correspond to the major axes of the patterns of tephra distribution given by Curtis (1968). Refer to Figures 5.2 and 5.3b. Elevation contour interval is 500 feet. Based on aerial photos from Curtis (1968, Plate 5) and U.S.G.S., Katmai Quadrangle, aerial photos 136 and 137.

(Fenner, 1925b, p. 199). In 1969, quiet steaming still occurred along the deep fissures along Fenner Ridge and the slump blocks on the southern slopes of Broken Mountain. Throws of almost 30 meters have been recorded for the larger faults on Broken Mountain (Fenner, 1925b, p. 217). And, Fenner (1950b, p. 716) has estimated the total downthrown displacement of these faults to be about 90 meters, but the total bedrock displacement is probably much greater. The undisturbed appearance of the pumice beds overlying these faults prove that the present observable offsets record only gradual readjustment after the deposition of the pyroclastics. The initial fracturing could have been violent and more extensive than the present exposures indicate (Fenner, 1925b, p. 218). Even without allowing for burial of its base beneath the pyroclastic flow, Greasy Pass is over 90 meters above the top of the flow in Novarupta Basin.

The major circular scarp just described is very prominent in aerial photos of the head of the Valley. There are three oval depressions within the scarp which are also quite conspicuous in aerial photos. The outline of each of these resembles that of the crater rim of Novarupta dome, which is the most obvious of the oval features. The major axis of the ovals is about 2 km and they all intersect to the northeast of the dome near the center for the outer circular scarp.

The crater of Novarupta is the clearest of the oval features; a second oval depression is offset to the north, barely intersecting the lava dome, and most visible where it cuts the crater rim of Novarupta and breaks the summit of Stumbling Mountain. To a viewer

standing on Novarupta dome, the cuts in the rim would appear as "radial" fissures. They are the site of continuing fumarolic activity. Trident Basin, located a little southeast of the dome, also has this same general outline. The basin heads at Fenner Ridge on the east and is separated from Novarupta Basin by a slight rise to the west. Apparently surface runoff was disrupted by the sinking of Trident Basin; several small lakes are now situated in this basin. Reportedly, a stream from this drainage area has cut a gorge through the rise and into Novarupta Basin. This last feature implies that the stream was able to cut through the pyroclastics while the basin was sinking.

Each of these small collapse ovals could outline the top of the Novarupta vent during a major eruption stage. Then the location of an oval would be directly related to a specific conduit orientation. The sequence of orientations is implied by the "freshness" of the collapse. The crater rim (oval III) is clearly the most recent. Trident Basin (oval I), although recording substantial subsidence, has no distinct fissures like those of oval II which cut the corona and Stumbling Mountain. Thus it appears that Trident Basin (oval I) predates oval II, which predates the crater rim (oval III).

If the collapse ovals do record previous orientations of the Novarupta conduit, they should correlate with the isopachus tephra trends as measured and contoured by Curtis (1968) (refer to Figure 5.2). Radials from Novarupta along the main axis of the tephra contours are superimposed on the subsidence features in Figure 5.1. The first layer contoured by Curtis is C. Its distribution is elongate over oval I.

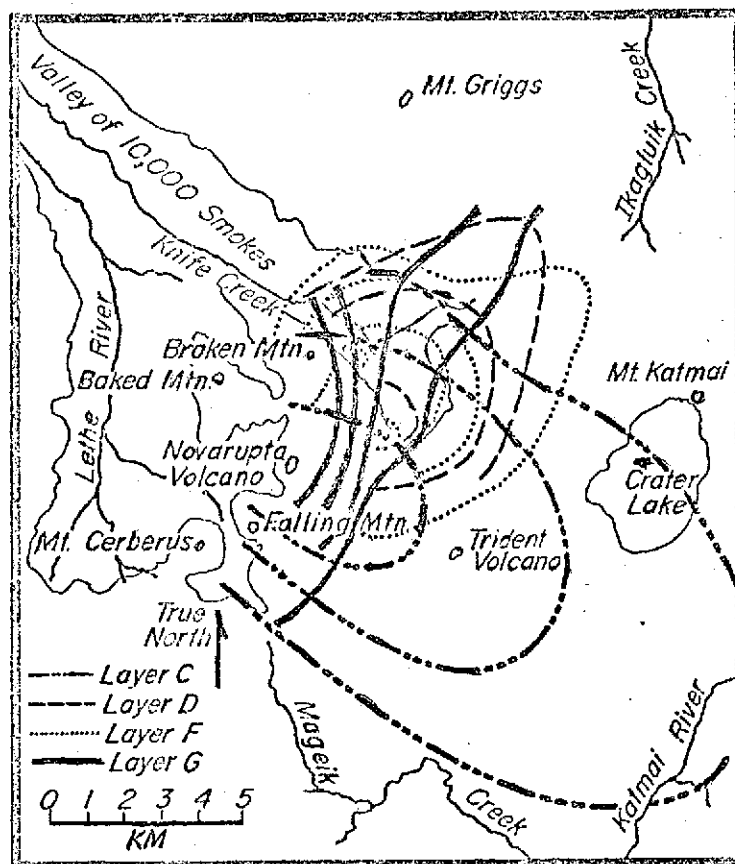


Figure 5.2. Isopachs of tephra layers C, D, F and G. (After Curtis, 1968, Figures 8, 11, 12 and 13). Refer to Figure 5.1.

Radials for layers D and F actually correspond to the latest oval, No. III. Layer G, from the last major eruption of Novarupta (Curtis, 1968, p. 198), is strongly directed northward over oval II. Thus there is some evidence that Novarupta's conduit underwent changes of position throughout the eruption. Some of these previous positions have been preserved in oval features intersecting the lava dome.

Beyond the major circular scarp are several arcuate faults on Broken Mountain and on the lower slopes of Mt. Trident, and the parallel fumarolic lineations near the mouth of Novarupta Basin. Quiet steaming characterizes many of the concentric and arcuate features. Surely these denote subsurface fractures related to the family of concentric fractures about Novarupta.

The oval patterns of subsidence close to the dome probably record the sequence and direction of the changes in the orientation of the eruptive vent of Novarupta. The larger circular scarp was probably formed as the overall area collapsed in response to the removal of vast amounts of magma from the underlying reservoir. The oval features and surrounding concentric and arcuate fractures therefore probably outline an underlying intrusive body related to the erupted pyroclastics and the extrusive dome of Novarupta. The presence of this cooling mass is also indicated by the continued fumarolic activity, which is restricted to the head of the Valley.

5.3 Magnetometer Survey Around Novarupta

It was hoped that magnetometry could be used to delineate the igneous subsurface at the head of the Valley. To test the applicability

of this method of detailed subsurface mapping within the ground magnetometer regime of the Valley, several reconnaissance ground magnetometer traverses were conducted around Novarupta. Most of these traverses were oriented radially to the dome. In addition, a few spot readings were taken in the immediate vicinity. All work was accomplished with the vertical field magnetometer. The locations of these stations and traverses are shown in Figure 5.3a.

A contour map of the anomalous vertical field in the vicinity of Novarupta is presented in Figure 5.3b. A 500 gamma contour interval shows well the concentric pattern of the anomaly about a high centered just northeast of the dome itself. Two interesting features of this anomaly are its gentle horizontal gradients and insignificant distortion by local topography. These features indicate that the source is both deep and thick. As for the shape of the anomaly: near the dome, the concentric oval contours correspond beautifully with the outline of the crater rim; farther out, the contours are elongate more down valley, and are similar in shape to the outer collapse oval of Figure 5.1. Inspection of total field anomalies along 1970 traverses N-N'' and N'''-n reveals that the contours extending off the left of Figure 5.3b curve back around to the south, then southeast, essentially paralleling the 500 gamma contour in that quadrant of the figure.

The elongation of the contours and the outer oval down-valley may indicate structural control. It is along this same bearing that Curtis defines the axis of the Naknek anticline, which is slightly offset from the volcanic line (see Figure 1.1). Williams also felt that the eruptive

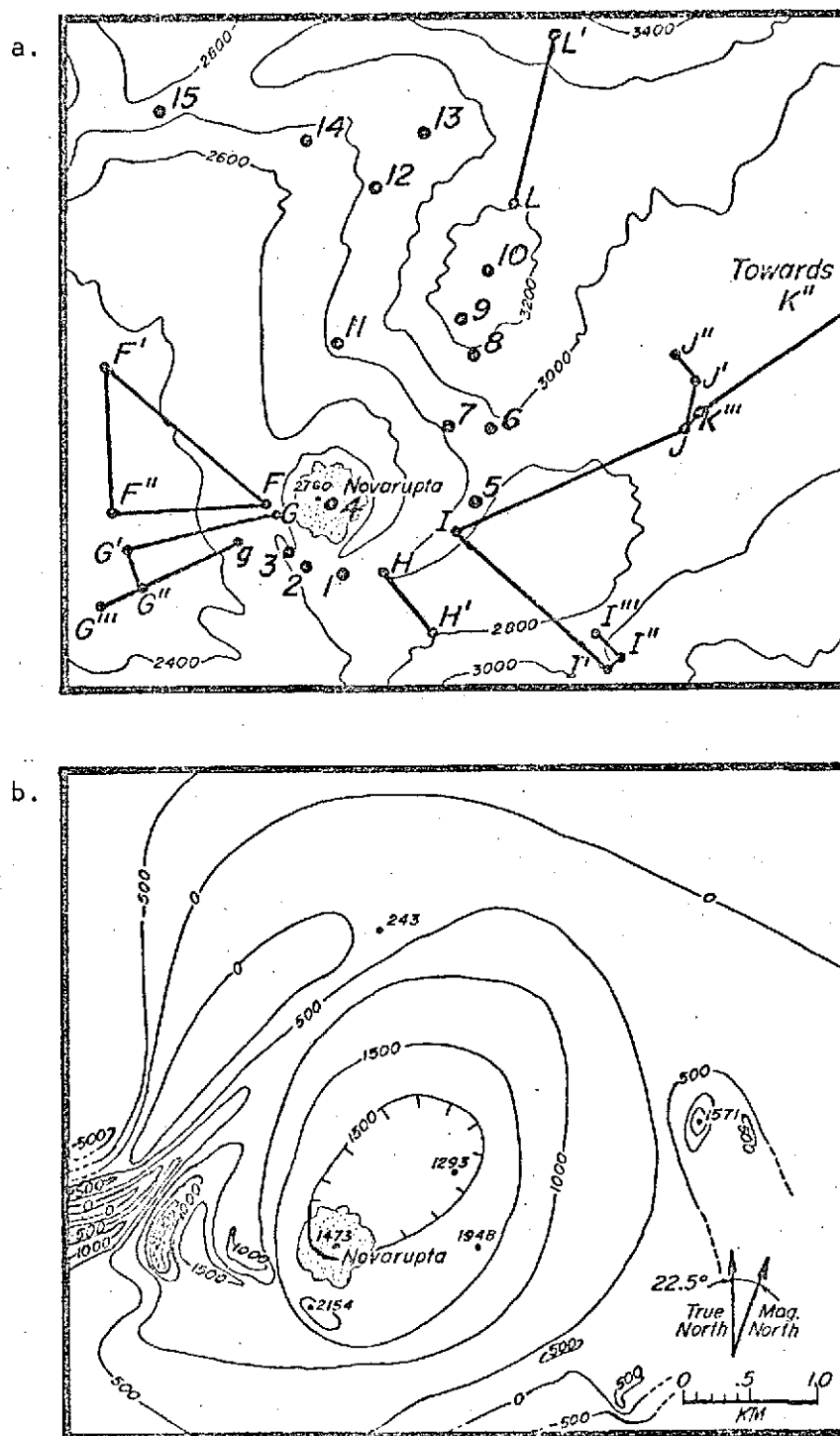


Figure 5.3a. Location of magnetometer traverses and isolated readings in the vicinity of Novarupta dome. Refer to Figure 4.1. Contour interval is 200 feet.

Figure 5.3b. Anomalous vertical magnetic field near Novarupta dome, contour interval is 500 γ . Note the correspondence of these contours with the subsidence features of Figure 5.1.

fissures were aligned along this trend. The elongation may overlies the bedrock contact of Naknek sediments to the north from volcanics to the south. Or, the elongation may merely reflect the control of confining mountains bordering both sides of Novarupta Basin.

A more extensive survey will be required to follow the magnetic anomalies westward beyond Falling Mountain and past Mageik Basin. Such exploration could reveal a relationship of these collapse areas and the hypothesized bedrock contact. A more encompassing survey might also yield more information about possible contemporaneous settling of the Baked-Broken Mountain complex.

The magnetic low just northeast of the dome in the center of the otherwise inwardly increasing anomaly is based on two spot readings only; one on the summit of Novarupta, the other on the gouged-out western face of Stumbling Mountain. Perhaps the abrupt terrain affected the recorded field. However, Anna (1972) observed the same low as he crossed the dome in his aeromagnetic survey. This inner low may indicate that some central portion of the Novarupta intrusive is still near the Curie temperature of the magnetic minerals, since the magnetic susceptibility of volcanic rocks is drastically reduced as this temperature is approached. The continued fumarolic activity in this area only is proof that considerable heat is still present in this subsurface. But since rocks are above their Curie temperatures long before they are molten, and the affected volume of rock in this instance is probably small and also shallow, one would not expect detection of this zone of anomalous temperatures by the seismic method of Berg and Kubota (1967).

A more plausible explanation for this central low may be based on the composition of the dome: the central zone of Novarupta is of almost pure rhyolite, whereas the margin has been contaminated by streaks of more basic material. Susceptibility studies show that the banded lava has a susceptibility of 1085×10^{-6} emu/cc, compared to only 304×10^{-6} emu/cc for the rhyolite. The fact that the larger conical anomaly centered on Novarupta seems to be caused by higher susceptibility material supports Forbes' hypothesis that magmatic differentiation was responsible for the variable ejecta of the 1912 eruption. Accordingly, as the rhyolitic magma was erupted by Novarupta, the remainder of the magma in the reservoir would have become increasingly basic; consequently, it had the potential of attaining relatively higher susceptibilities. The banding observed at the margin of the dome suggests that some of this higher susceptibility material was dragged up along the vent contacts during the expulsion of the rhyolitic plug at the end of the eruptive stage of Novarupta. The small concentration of low-susceptibility rhyolite forming the central dome of Novarupta as contrasted to the mass of higher susceptibility material remaining in the subsurface can account for the magnetic low observed directly over the dome.

Anma (1972) has suggested that this central low is caused by adjacent dipoles underlying Novarupta and Stumbling Mountain (which would correspond to collapse ovals II and III). However, the complete encirclement of high values about the rim of Novarupta's crater is contrary to his model and tends to discredit this hypothesis.

The local high anomaly directly west of the dome corresponds to a

zone of previously intense fumarolic activity. The local high at the northern end of Slippery Pass is marked by a large area of quiet steaming and bright, multicolored clay, bounded on the east by a sizeable fissure. A magnetic low is also indicated along the "valley" extending northeast of the dome from Novarupta Basin to Broken Mountain.

The individual profiles in the Novarupta region are jagged with minor peaks and troughs imposed on the overall dome-shaped anomaly. There seems to be some correlative value of anomalies between adjacent radial traverses (refer to Figure 5.4). Such correlation indicates near-surface features concentric about Novarupta. Fractures in the pyroclastics, and possibly fumarolic alterations along these, could account for the narrow, shallow anomalies.

Broader breaks in slope along the magnetic profiles, like those clearly exhibited along traverses G''-g and I-I', could indicate bedrock structure. Major subsidence faults could be responsible for these offsets.

No evidence for fractures radial to Novarupta were revealed by this survey. However, the nature of magnetic profiling precludes the detection of anomalies paralleling traverses.

5.4 Anomalous Geophysical Parameters in Novarupta Basin

Adjacent total magnetic anomaly profiles across the lower half of Novarupta Basin (E-E' and N'-N'') possess a similarity (Figures 4.8 and 4.12) which suggests that multiple, linear magnetic bodies paralleling the axis of the basin are their sources.

Model studies (refer to Table 4.6) show that the material causing

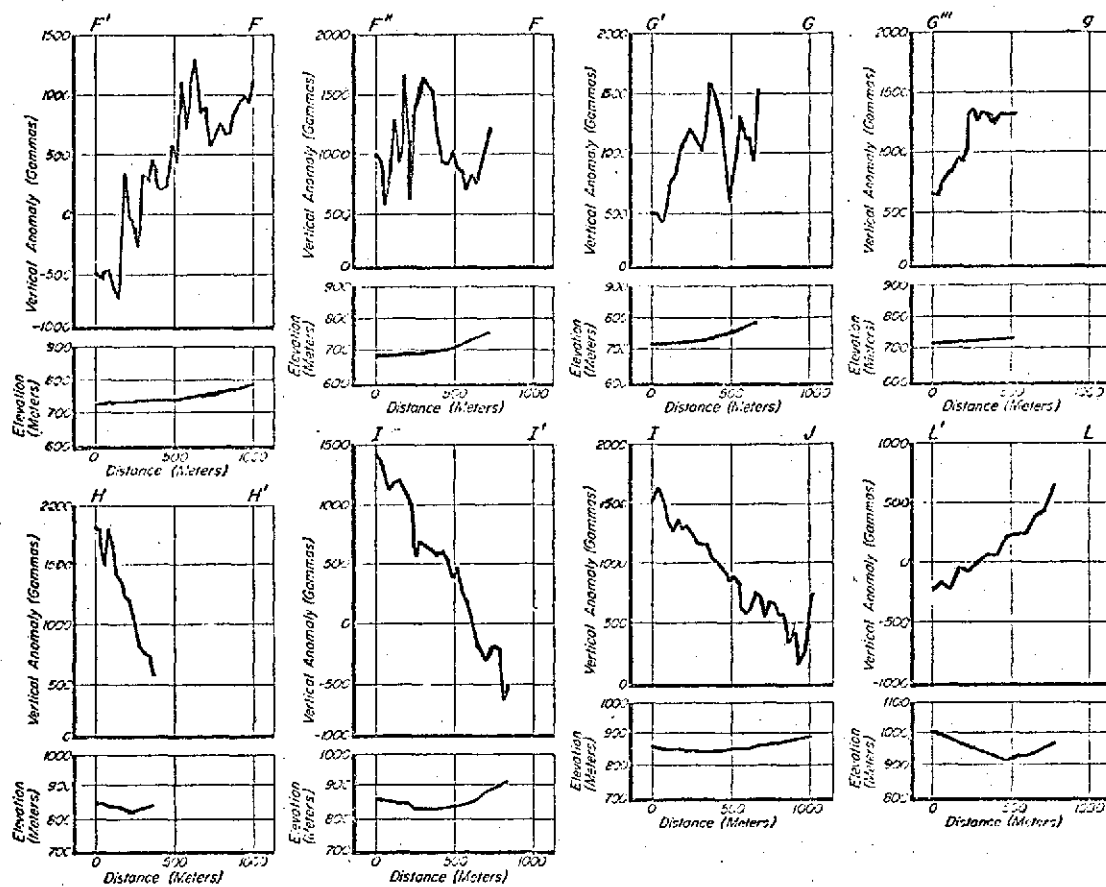


Figure 5.4. Vertical magnetic anomaly profiles radial to Novarupta Dome. Refer to Figure 5.3a for locations.

several of the local anomalies must be of quite low susceptibility, even if the flow is only 100 meters thick as has been indicated by seismic measurements (Table 1.3). It was proposed (Section 4.3) that pockets of predominately rhyolitic material might be responsible for the small local anomalies.

Another unusual property of these magnetic profiles is the abrupt change in the regional trend about half-way across the basin (refer to Figures 4.8, 4.12 and 4.13). Perhaps this feature reflects the encroachment of a wedge of volcanics related to the volcanic peaks of the Aleutian Range into the Naknek sedimentary province.

Yet another conspicuous quality of the magnetic profiles in the lower half of Novarupta Basin is their negative values relative to the overall regional geomagnetic field. It has been suggested that this magnetically-low zone may represent the low of the dipole field due to Novarupta, perhaps including contributions from the other neighboring igneous masses, too; but the magnitude is too great to substantiate this proposition, and the alignment of the anomaly is not that expected of a dipole at Novarupta dome. Another remotely possible explanation for this zone would be the presence of a reversely-magnetized body beneath the flow in this area.

Anomalous lows in other parameters have been recorded in this same portion of Novarupta Basin. Zeis and Allen (1923) measured relatively low fumarolic temperatures in this zone in 1919. Their data has been contoured and is shown in Figure 5.5. There are too few data on the composition of the early emanations from the fumaroles in this particular

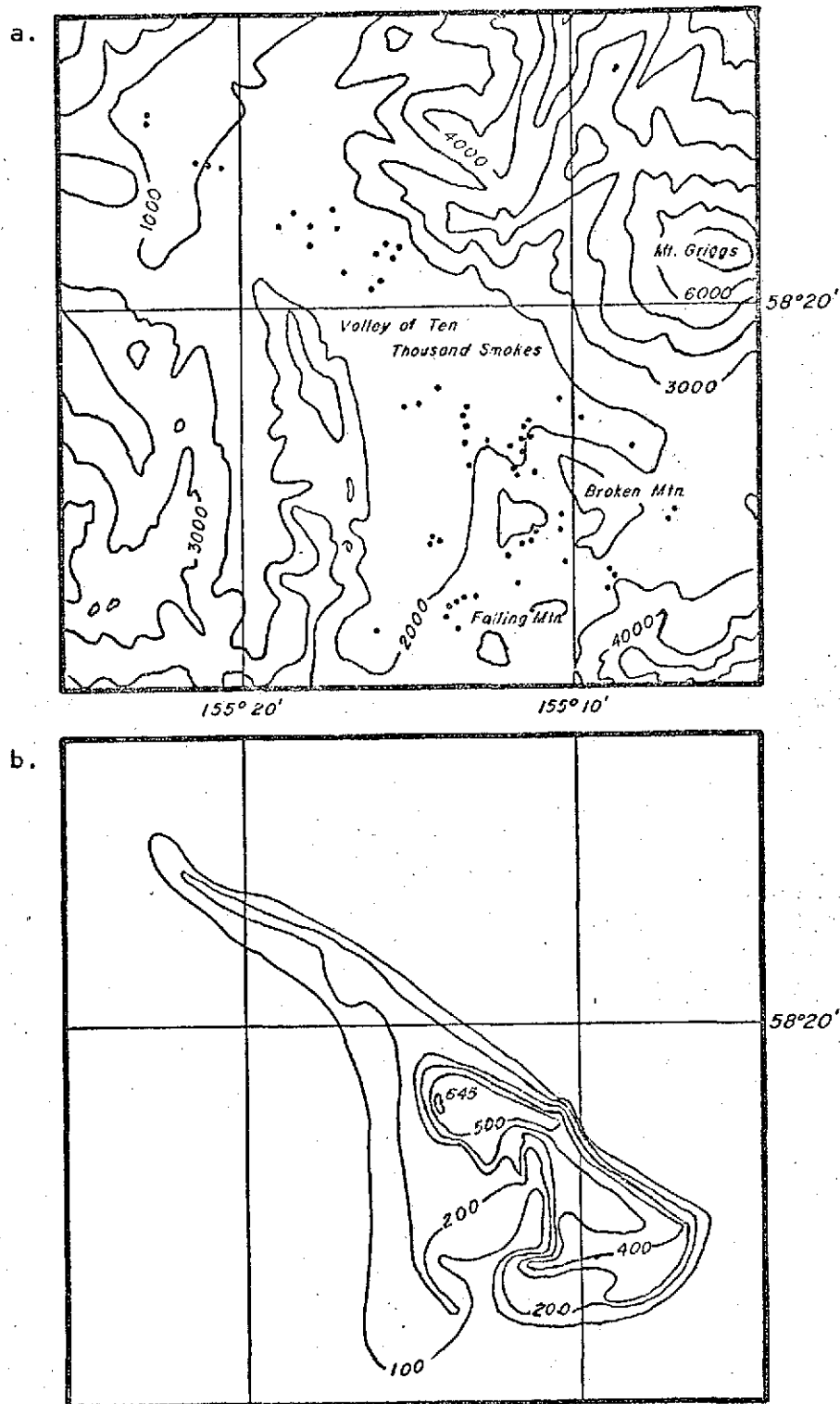


Figure 5.5a. Location of fumaroles studied by Allen and Zies in 1919 (Zies, 1929, pp. 2-3). Contour interval is 1000 feet.

Figure 5.5b. Isothermal map of fumarole vapor temperatures as measured by Allen and Zies in 1919 (1923, pp. 104-106). Contour interval is 100°F.

area of the Basin to permit any predictions as to their most probable primary source. Perhaps the gasses vented here were of a secondary nature, in contrast to the fumes high in CO_2 and the sulphur gasses which characterized the high temperature vents at the head of the Valley, and were indicative of connections with a deep seated source (Lovering, 1957, p. 1588).

The area of the relatively low fumarolic temperatures observed in 1919 lies beyond the prominent collapse features in Novarupta Basin (beyond the larger collapse oval shown in Figure 5.1). If this area is located beyond the bedrock faults related to the deflation of ancestral Novarupta, it would not have been as accessible to the heat and vapors from the deep seated source as were the fumaroles within the disturbed areas closer to Novarupta. The same isolation would hold true were this area between widely spaced bedrock fractures; another major fault caused by the subsidence of the Baked Mountain-Broken Mountain-Novarupta complex is thought to be aligned with the western face of Baked Mountain, which would be to the west of this zone.

In this same portion of Novarupta Basin, Kienle (1969, pp. 126-127) took gravity measurements. He found the regional field in the basin to be quite different from that encountered in the other branches of the Valley. The regional gradient which plunges almost 7 mgals from Baked Mountain to Falling Mountain is almost twice the regional gradient observed elsewhere in the Valley, and the field is some 6 mgals more negative.

In all probability, the distinctly negative nature of both the

magnetic and gravity fields in Novarupta Basin can be explained in terms of regional tectonics. The alignment of these features might be structurally controlled by a deep seated fault with the northern side down-thrown by some 3 km relative to the southern side (Kienle, 1969, p. 23). The Naknek section also thickens as one approaches the range from the north. Magma reservoirs have been located at relatively shallow depths below the volcanic peaks (Kuboto and Berg, 1967). All three of these structural possibilities are capable of reducing the observed gravity and magnetic fields because they increase the amount of low-density, low-susceptibility material between the stations on the surface and the dense, high-susceptibility volcanic basement. These arguments are particularly applicable if the lower portion of Novarupta Basin is a relatively undisturbed block within the area-wide subsidence towards Novarupta.

Unfortunately the seismic profiles are not complete in this area; however, seismic profile D-D' (refer to Appendix D) shows the flow to thin from 95 meters to 80 meters from the base of Novarupta towards the center of the basin. Since the top of the flow is relatively level along this profile, the data suggest that the bedrock dips towards Novarupta. Such an interpretation is in keeping with the often recorded pattern of subsidence towards Novarupta dome. The flow thickness suggested by Kienle (1969, Model F) for gravity profile KV-4 seems unusually low, only 50 meters (refer to Table 1.3). The lack of bedrock stations for reference may have led to an erroneous value; or, since the tuff is considerably denser here near its source than farther down valley (refer to Appendix C) it would make a lower density contrast

with the bedrock than assumed in Model F (a lower density contrast would have the effect of increasing the gravimetrically-indicated thickness). Kienle's 1970 seismic refraction profile D-D' shows the flow to be about 80 meters thick near this area. Profile 3 of Sbar and Matumoto is very erratic but it does suggest that the flow is from 40 to 70 meters thick along the same line as Kienle's profile (refer to Appendix D and Figure 1.3).

If the bedrock here is actually higher relative to the general subsidence closer to Novarupta, then the nearly level surface of the flow would require that the pyroclastics are thinner in this anomalous area than on either side. Such an interpretation would also be in keeping with the relatively small magnitudes of the smoothed local magnetic anomalies.

5.5 Conclusions

Preliminary magnetometry in the vicinity of Novarupta Volcano indicates the presence of a broad, dome-like structure underlying the head of the Valley. The nature of the major anomaly indicates that the causative body is both deep and thick. Generally, the magnetic anomalies decrease radially from the dome. The contoured anomalies form concentric ovals centered just northeast of the dome itself. The direction of elongation of these ovals parallels the Aleutian Range, and is probably related to the overall structure of the area. The inconsistent central low is caused by the small concentration of low susceptibility rhyolite forming the central zone of Novarupta dome. Minor anomalies superimposed on the main anomaly imply bedrock faulting

as well as fracturing of the overlying pyroclastics and possible fumarolic alteration.

Oval topographic depressions intersecting Novarupta dome may preserve a record of conduit orientations. Alteration in orientation of the vent at Novarupta could account for the varied patterns of distribution displayed by successive tephra layers. Partial agreement of extensions from Novarupta along the direction of elongation of the tephra contours with the major axis of the collapse ovals supports such an hypothesis.

The radial orientation of the traverses precluded detection of radial features. The survey can therefore give no evidence of a suggested relict conduit connecting Mounts Katmai and Trident with Novarupta.

The impressive agreement of the shapes of the magnetic contours and the subsidence features indicates that both outline the intrusive body beneath. A more comprehensive magnetometer study at the head of the Valley could produce a detailed map of the intrusive body which is expressed at the surface by Novarupta and its concentric fault system. Aerial surveying would reduce the complication caused by near surface anomalies.

The unusually negative values recorded for both gravity and magnetic fields in the lower half of Novarupta Basin are related to their proximity to the volcanic axis of the Alaska Peninsula. Increased Naknek thicknesses and shallow magma reservoirs are probably the principal causes of the regional trends adjacent to the volcanic peaks. The

anomalously low fumarolic temperatures in this area in 1919 may mean that this region did not have the connections with the deep-seated source responsible for the hotter emanations observed closer to Novarupta in a structurally-more disturbed area. It is proposed that the lower half of Novarupta Basin may be a relatively upthrust block between two major faults: one caused by the settling encompassing the entire Baked Mountain-Broken Mountain-Novarupta complex, and the other by the more localized collapse around Novarupta itself.

The amount of subsidence recorded in faults about Novarupta can account for an ancestral Novarupta of sufficient altitude to allow deposition of pyroclastics in all areas where they are to be found. Spurr mapped a high, conical structure situated at the head of the Valley in 1898. It is proposed that this mountain was ancestral Novarupta. The present Novarupta volcano is the last remnant of this mountain, and the arcuate and circular collapse features preserve the pattern of its deflation.

CHAPTER VI

SUMMARY OF THE GROUND MAGNETOMETER SURVEY

Magnetic susceptibilities were determined for many samples collected from the Valley of Ten Thousand Smokes. It was found that the pyroclastic flow, the air-fall pyroclastics, and the banded lava and pumice all have susceptibilities near 1250×10^{-6} emu/cc. The average susceptibility of the andesitic lava is close to 2500×10^{-6} emu/cc, but the susceptibility of the rhyolitic material is an order of magnitude smaller. Naknek sediments normally have susceptibilities less than 50×10^{-6} emu/cc, but if subjected to extreme heat and volcanic emanations, the altered sediments can attain susceptibilities of 5000×10^{-6} emu/cc. It is difficult to predict the susceptibility of the glacial drift, as none was sampled. Probably the drift is primarily composed of randomly-oriented, andesitic debris. Its susceptibility is most likely less than 1250×10^{-6} emu/cc.

A small scale total field magnetometer survey was conducted over a zone of relict fumaroles near the terminus of Broken Mountain Valley including both crater vents and filled fissure vents. It was found that the large, narrow total magnetic anomalies show spectacular agreement with the surficial geology. The close association of the anomalies with the fumarolic markings is a strong indication that pockets of magnetic minerals have been preserved along the vents at shallow depths. Sharp anomalies were often encountered near extinct fumaroles in all branches of the Valley. It is thus proposed that the preservation of such accumulations of magnetic minerals along fumarolic

vents is common throughout the Valley.

In general, the vertical magnetic anomalies in the vicinity of Novarupta Volcano increase as one approaches a point just northeast of the dome. The contoured vertical anomaly is in fact composed of nearly concentric ovals. Evidently, the dome is simply the surficial expression of a sizeable, conical-shaped intrusive, probably of andesitic composition. The inconsistent low in the center of the Novarupta magnetic anomaly is probably caused by the small concentration of rhyolitic lava forming the central zone of the dome. Corresponding offsets in the magnetic anomalies among adjacent traverses radial to Novarupta suggest that there is concentric faulting about the dome. This faulting apparently includes fractures in the bedrock as well as in the pyroclastic flow, and would be related to the general pattern of subsidence around Novarupta.

As one approaches the volcanic peaks at the head of the Valley, the magnetic anomalies tend to be increasingly more negative. Increased thickness of the Naknek sediments as well as shallow magma chambers are no doubt the principal causes of this regional trend.

Cross-valley magnetometer traverses were made in each branch of the Valley. The pattern of individual anomalies along adjacent, nearly-parallel traverses is very similar. Evidently, the magnetic bodies responsible for the anomalies are linear, and trend parallel to the axis of each branch of the Valley.

The mirror-image correspondence of magnetic and gravimetric anomalies along nearby cross-valley profiles suggests that the primary cause of both anomalies is variable thickness of high-susceptibility,

low-density pyroclastics above the low-susceptibility, high-density Naknek sedimentary bedrock. Since the top of the flow is relatively flat, this proposition requires that the base of the flow must have considerable relief. In most cases, the implied base relief can be reconciled with a plausible pre-1912 valley configuration. Since the deepest sections are usually indicated beneath the present streams, it follows that the streams have been established above the pre-1912 channels. The wavy pattern of the anomalies in the southern branch of the Valley probably outline major bedrock faulting which probably occurred prior to the final emplacement of the pyroclastic flow.

Using thicknesses based on the gravimetric, seismic and geomorphological evidence, and a susceptibility based on the average for the pyroclastics sampled for this study, it is impossible to model the observed anomalies. Clearly variable thickness is not the single cause of the multiple magnetic anomalies encountered along the cross-valley traverses. It is necessary that the susceptibility of the flow also varies laterally. The susceptibility studies do suggest that the denser welded tuff can possess much higher susceptibilities than were observed for the unconsolidated airfall pyroclastics. Welding is also more prominent in the thicker sections of the flow. If the welded portion of the flow in the thicker sections of the flow is of higher susceptibility than the average measured for the pyroclastic flow to date, then reasonable thicknesses can be used to model the flow. To model the small anomalies over the

sections of the flow near the valley walls often requires lower than average susceptibilities. It is thought that the slumping of weathered ash from the adjacent steep slopes could be responsible for the lower susceptibilities. The highly rhyolitic composition of the flow in Novarupta Basin and in the lower valley has been cited as the cause of the low susceptibilities suggested for these areas by the magnetic model studies.

In conclusion, if used in conjunction with other geological and geophysical data, the magnetometer data can set limits on estimates of the thickness and composition of the pyroclastic flow.

APPENDICES

APPENDIX A

REDUCTION OF MAGNETOMETER SURVEY DATA

A.1 The Reduction Technique

Reduction of ground magnetic survey data to magnetic anomaly values along metrically-described traverses involves data selection, interpolation, conversion and correlation.

Ground survey data include the magnetometer reading(s), surface station spacing, time of occupation, altimeter reading, and field notes. A unique magnetometer reading must be selected for every station where multiple readings were made. Because time and elevation were only noted intermittently, values of these parameters had to be interpolated and assigned to each station. These interpolated values were then utilized in correcting for diurnal variations and for calculating the horizontal station spacing, respectively.

a) Reduction of Total Field Data

The Lamor frequency, L , as recorded by the Rubidium vapor magnetometer at the magnetometer base, can be converted to gammas of total field strength, R , by applying:

$$R = \frac{L}{4.667 \times 10^{-3}},$$

where 4.667 is the calibration constant of the instrument.

A base datum of 53,000 gammas was chosen to reduce each Rubidium vapor magnetometer reading to a positive fluctuation of the geomagnetic field. This diurnal correction, B , corresponding to each reading

of L, is given by:

$$B = 5300 - R.$$

Values of diurnal correction, B, as calculated from the geomagnetic variation as measured at the magnetometer base are presented in Figure A.1.

The Rubidium vapor magnetometer was inoperative during the surveys conducted on July 13 and July 14, 1969. From a composite of all other diurnal variation curves (field versus time) a rate of daily geomagnetic fluctuation was assumed. Commonly, the field decreased at the rate of 9.8 gammas per hour in the mornings until 1300 local time; then it increased at the rate of 10.9 gammas per hour until evening. Since the base station was occupied with the Elsec magnetometer at the start and conclusion of these survey days, it was a simple task to impose these common fluctuation rates to a datum dictated by the Elsec base station data. This was a procedure followed in applying a diurnal correction for magnetometer traverses A-A' and B-B'.

In reference to the above, it should be noted that for simultaneous readings at the magnetometer base, the Elsec magnetometer recorded a total field 771 gammas greater than that recorded by the Varian magnetometer (see Table A.1). This difference is assumed to result from the difference in the location of the proton-precession magnetometer over the wooden post and the Rubidium vapor magnetometer sensing head buried a few feet away and an uncalibrated crystal oscillator in the Rubidium magnetometer. In practice, this discrepancy is of little consequence as it is the variation which is of interest,

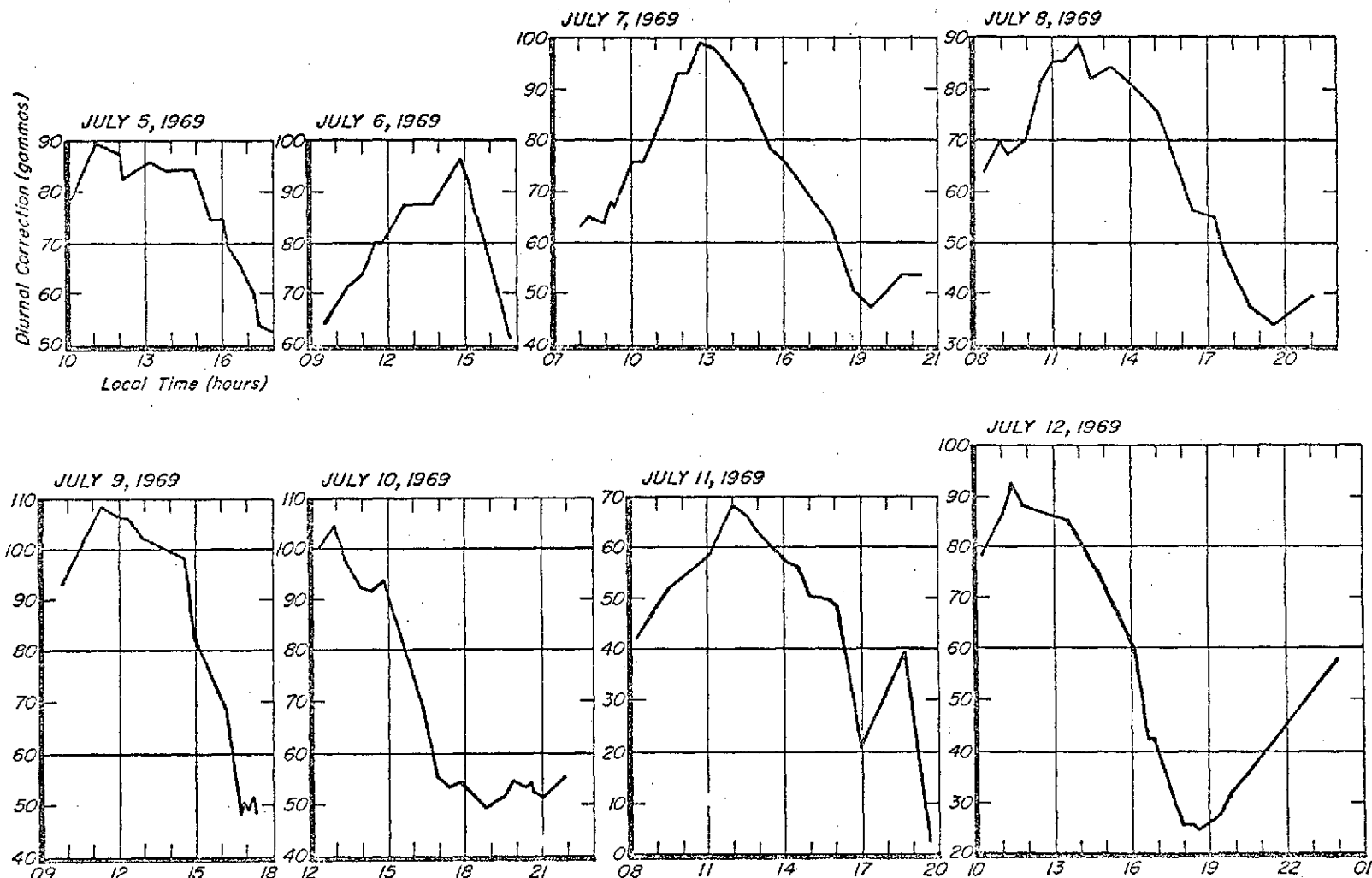


Figure A.1. The diurnal correction 'B' as a function of local time. Refer to text for details.

Table A.1

Simultaneous Magnetometer Readings at the
Magnetometer Base Station

Date	Time	Elsec Reading (gammas)	Varian Reading (gammas)	Difference of columns 3&4
7-7-69	9:30	53701	52930	771
7-7-69	15:20	53690	52919	771
7-9-69	16:42	53726	52949	774
7-9-69	17:26	53728	52908	771
7-10-69	19:35	53731	52952	782
7-11-69	11:30	53678	52957	770

(the average deviation of the difference from 771 gammas is 2.5 gammas)

and the 771 gamma difference was constant over the whole survey period. It does, however, require that a base datum of 53,771 gammas be used for July 13 and 14, so that the survey readings on these days will be corrected to the same reference as the other traverses; i.e., in these cases, the diurnal correction is found by:

$$B = F + 53771 - E$$

where 'F' is the amount of fluctuation incurred at the "common" rate
 1) since the time of the initial Elsec base reading before 1300, or
 2) leading to the final Elsec base reading after 1300. The time and value of the Elsec base readings determined the locus of the F values by specifying a point on each rate line. To effect the same datum for all surveys, i.e., to cause all survey data to be corrected relative to a singular magnitude for the geomagnetic field at the magnetometer base station, a constant must be added to the survey data which have no corresponding Rubidium vapor base data. This constant is determined by the difference between the Elsec base reading, E, and 53771 gammas.

The regional geomagnetic field in the Valley as interpolated from maps of the earth's field in Alaska (Deel, 1944) is approximately 53,800 gammas with inclination 71.2 degrees and declination 22.5 degrees. This mean field for the general area was used to reduce survey values to anomalies in the total field.

The proton precession (Elsec) magnetometer was commonly read more than once at each station to eliminate electronic errors and short term fluctuations in the earth's field. The method used to select the single value used in further computations was (in order of preference):

- a) a repeated reading;
- b) the nearest even integer to the arithmetic mean of clustered values; and
- c) the nearest even integer to the arithmetic mean of those multiple measurements differing by less than ten instrumental units. (Statistically, using only even integers reduces the chance of biasing the overall data.)

Proton precession, P as displayed on the Elsec instrument, can be converted to gammas of magnetic field strength, S , using the instrument calibration constant, so that:

$$S = \frac{2.4051 \times 10^9}{P} .$$

The diurnal geomagnetic variations were removed from each of the base magnetometer readings with respect to time of survey station occupation. If B' represents the diurnal correction interpolated to the time of occupation of a station of Elsec reading, S , then the value S' of the magnetic field at that station (with diurnal effects removed) is given by:

$$S' = S + B' .$$

The value of the total anomaly (with respect to a regional field of 53,800 gammas) at this station would then be found by:

$$TA = S' - 53800 .$$

Or in a complete form, the reduction of survey data to total anomalies could be accomplished by:

$$TA = R' - S + 800 ,$$

where R' represents the total field at base as recorded by the Rubidium

vapor magnetometer, interpolated to the time of occupation of a survey station with field reading S.

A sample of the computer program designed to reduce total-field magnetometer survey data is given in Appendix A2.

b) Reduction of Vertical Field Data

As discussed in Chapter 1, the fluxgate magnetometer displays differences in the vertical field directly in gammas. Obviously no conversion factor is required.

Removal of diurnal effects from vertical magnetometer survey data is treated differently from that for the Elsec field data. Repeated base readings with the fluxgate instrument often showed a change in the vertical field opposite in sign to the total diurnal variation, presumably due to instrument drift. Field stations were not systematically reoccupied because the object of the fluxgate surveys was to obtain a rapid, general view of the magnetic situation. It is therefore impossible to determine a detailed correction for the combined effects of instrumental and diurnal geomagnetic variations.

The vertical field traverse data have been adjusted for diurnal drift (instrumental and geomagnetic) by linear interpolation of the difference in base readings with respect to times of station occupation. The vertical survey readings were further adjusted to give a unique value per location in the case of a station common to two or more traverses.

Using 53,771 gammas as the total field at the base station, with an inclination of 71.2 degrees, the absolute vertical field at the

base would be 50899 gammas. However, to obtain the vertical anomaly, VA, one must remove the regional vertical field of 50927 gammas ($= 53800 \times \sin 71.2$).

One must also remember that the fluxgate instrument was set to +150 gammas at the magnetometer base station at the onset of each survey day. Thus, the vertical survey reading, V, which has been corrected for diurnal variations, can be reduced to the vertical anomaly by:

$$VA = V - 177 .$$

APPENDIX A.2

```

C SAMPLE PROGRAM FOR THE REDUCTION OF GROUND MAGNETOMETER DATA
C TO RESIDUAL ANOMALIES IN TOTAL FIELD
C PREPARED IN 1970 BY MARLA CAVE TRIBLE
C DIMENSION T(200),U(200),E(200),XX(200),YY(200),VG(200),
C ISH(200),SL(200),R(50),RH(50),RM(50),EX(10),TX(10)
C STATE TOTAL DATA POINTS- N=TOTAL STATIONS ALONG TRAVERSE
C M=TOTAL DIURNAL FIELD MEASUREMENTS
C NM=TOTAL BASE ALTIMETER READINGS
C 1 READ(1,2,END=90) N,M,NM
C 2 FORMAT(3(I4,2X))
C INPUT FIELD DATA- STATION=I SEPARATED FROM PREVIOUS STATION
C BY D=CABLE LENGTHS & YY= ESTIMATED
C FEET, AT TIME- T=HOURS & XX=MINUTES,
C ALTIMETER READING- E=FEET, MAGNETOMETER
C READINGS SH=AT HIGH PROBE POSITION
C AND SL=AT LOW POSITION.
C 3 DO 4 I=1,N
C 4 FORMAT (2(F2.0,2X),F4.0,2X,F4.0,2X,F2.0,2X,2(F6.1,2X))
C 4 READ (1,3) T(I),XX(I),E(I),R(I),YY(I),SH(I),SL(I)
C INPUT BASE MAGNETOMETER READINGS=R, AT TIME RH=HOURS,& RM=
C MINUTES
C 5 DO 6 I=1,M
C 6 FORMAT (F6.1,2(2X,F2.0))
C 6 READ (1,5) R,RH,RM
C INPUT BASE ALTIMETER READINGS=EX FEET AT TX=HOURS &
C VG=MINUTES
C 7 DO 8 I=1,NM
C 8 FORMAT (F4.0,2(2X,F2.0))
C 8 READ (1,7) EX,TX,VG
C TO CONVERT DATA TO METERS, DECIMAL HOURS, GAMMAS
C 9 DO 10 I=1,N
C 10 D(I)=(25.04*D(I))+(YY(I)*0.304801)
C 10 T(I)=T(I)+(XX(I)/60.)
C 10 E(I)=E(I)*0.304801
C 10 SH(I)=2.4051E9/SH(I)
C 10 SL(I)=2.4051E9/SL(I)
C 10 DO 12 I=1,M
C 10 RH(I)=RH(I)+(RM(I)/60.)
C 10 R(I)=R(I)/4.667E-3
C 10 DO 14 I=1,NM
C 10 TX(I)=TX(I)+(VG(I)/60.)
C 10 EX(I)=EX(I)*0.304801
C TO INTERPOLATE TIME FOR EACH STATION
C 20 DO 20 I=1,N
C 20 XX(I)=0.

```

```

20 YY(I)=0.
DO 25 I=1,N
IF (T(I).EQ.0.) GO TO 26
YY(I)=D(I)
XX(I)=T(I)
25 CONTINUE
CALL YLNTPL (YY,XX,D,T,N)
C SUBROUTINE YLNTPL DOES LINEAR INTERPOLATION BETWEEN KNOWN VALUES
C TO REDUCE ALTIMETER DATA TO BASE DATUM=2550 FEET
DO 30 I=1,NM
30 EX(I)=771.21-EX(I)
DO 32 I=1,N
32 VG(I)=0.
CALL YLNTPL (TX,EX,T,VG,N)
DO 35 I=1,N
35 E(I)=E(I)+VG(I)
C TO INTERPOLATE ELEVATION FOR EACH STATION
DO 40 I=1,N
40 XX(I)=0.
40 YY(I)=0.
DO 45 I=1,N
IF (E(I).EQ.VG(I)) GO TO 45
YY(I)=E(I)
XX(I)=T(I)
45 CONTINUE
C TO CONVERT SURFACE SPACING INTO HORIZONTAL DISTANCE FROM
C THE INITIAL STATION
XX(I)=0.
D(I)=0.
DO 50 I=2,N
XX(I)=SORT(ABS((D(I)**2)-((E(I)-E(I-1))**2)))
50 D(I)=D(I-1)+XX(I)
C TO CORRECT MAGNETOMETER DATA FOR DIURNAL VARIATIONS
DO 60 I=1,M
60 R(I)=53000.-R(I)
DO 62 I=1,N
62 VG(I)=0.
CALL YLNTPL (RH,R,T,VG,N)
DO 65 I=1,N
SH(I)=SH(I)+VG(I)
65 SL(I)=SL(I)+VG(I)
C TO REDUCE DATA TO ANOMALIES IN REGIONAL FIELD=53800 GAMMAS
DO 80 I=1,N
SH(I)=SH(I)-53800.
80 SL(I)=SL(I)-53800.

```

```

C TO CALCULATE THE VERTICAL GRADIENT FOR PROBE SEPARATION OF
C 1.524 METERS
C DO 90 I=1,N
C 90 VG(I)=(SL(I)-SH(I))/1.524
C THE DATA REDUCTION IS NOW COMPLETE
C FOR STATION=I, THE ANOMALY IN THE TOTAL FIELD = SH(I) GAMMAS
C THE VERTICAL GRADIENT OF THIS = VG(I) G/METER
C THE STATION IS DI(I)METERS FROM STATION
C THE STATION ELEVATION IS E(I)METERS
C THE TIME OF OCCUPATION IS T(I) HOURS
C THE OUTPUT CAN CONSIST OF PRINTED DATA, PUNCHED CARDS, OR
C PLOTTED PROFILES.
C AN APPROPRIATE FORMAT SHOULD BE CHOSEN BY THE INTERPRETER.
C DO CALL EXIT
C END

```

```

SUBROUTINE YLNTPL (X,Y,XE,YE,L)
DIMENSION XI(1),Y(1),XE(1),YE(1)
98 I=1
99 J=2
100 IF (XE(I)-X(J))105,101,104
101 YE(I)=Y(J)
GO TO 106
104 J=J+1
GO TO 100
105 DO 115 K=1,L
IF (X(J-K)) 110,114,112
110 WRITE(3,111) K,J,I
111 FORMAT(' ', 'ILLEGAL VALUE ',I3,' BEFORE ',I3,' FOR ',I3)
GO TO 115
112 IF (XE(I).EQ.X(J-K)) GO TO 113
YE(I)=Y(J-K)+((Y(J)-Y(J-K))/(X(J)-X(J-K)))*(XE(I)-X(J-K))
GO TO 106
113 YE(I)=Y(J-K)
GO TO 106
114 IF ((J-K)-1) 110,112,115
115 CONTINUE
106 I=I+1
107 IF (I.GT.L) GO TO 109
GO TO 99
109 RETURN
END

```

APPENDIX B.1a

Survey Information for Magnetometer Traverses
in the Valley of Ten Thousand Smokes

Traverse	Type*	Date July '69	Duration	Bearing (degrees E of N)	Valley	Survey Party**
A-A'	TG	14	13:40-18:46	36	Lower	TSB
B-B' (1)	TG	13	10:15-13:25	22	Broken & Knife	TSB
B-B' (2)	TG	14	9:55-12:30	22	Knife	TSB
B-B''	T	7	13:48-15:12	57	Broken	TSB
B-b	V	10	18:17-19:05	57	Broken	F
B''-b''	T	7	12:50-13:27	116	Broken	TSB
b'-b''	V	10	17:50-18:01	116	Broken	F
b-b'	V	10	18:02-18:16	114	Broken	F
B-B'''	T	7	9:35-11:26	79	Broken	TSB
B-B'''	V	10	16:27-17:41	79	Broken	F
b'''-B'''	T	7	13:31-13:45	188	Broken	TSB
C-C' (3)	V	5	14:12-17:10	93	Upper	TF
C-C' (4)	V	6	11:20-15:25	93	Upper	TF
D-D'	TG	10	13:00-17:50	94	Upper	TSB
E-E'	TG	8	10:48-14:44	182	Novarupta	TSB
F-F'	V	14	afternoon	128	Novarupta	F
F'-F''	V	14	afternoon	84	Novarupta	F
F''-F'''	V	14	afternoon	175	Novarupta	F
G'-G	V	23	17:00-17:30	76	Novarupta	SB
G'-G''	V	23	17:30-17:36	151	Novarupta	SB
G'''-g	V	23	17:40-18:10	65	Novarupta	SB
H-H'	V	23	16:30-16:48	131	Trident	SB
I-I'	V	23	15:27-16:09	127	Trident	SB
I'-I''	V	23	16:09-16:14	37	Trident	SB
I'''-I'''	V	23	16:14-16:19	127	Trident	SB
I-J	V	23	14:44-15:27	66	Trident	SB
J'-J	V	19	18:56-19:15	195	Fenner Ridge	TB
J''-J'	V	19	19:15-19:20	154	Fenner Ridge	TB
J-K'''	V	19	18:49-18:56	49	Fenner Ridge	TB
K'''-K''	V	19	17:27-18:49	57	Knife	TB
K'-K''	V	19	15:29-17:27	152	Knife	TB
K-K'	V	19	12:21-15:29	112	Knife	TB
L-L'	V	17	afternoon	191	Novarupta (5)	F
Fumarole Grid	T	12	10:22-13:48	22	Broken	TSL
Fumarole Grid	T	16	afternoon	22	Broken	TGM

- (1) From Baked Mtn. to Knife Creek
- (2) From Knife Creek to Mt. Griggs
- (3) From Baked Mtn. to mid-valley
- (4) From mid-valley to the Buttress Range
- (5) From Stumbling Mtn. to Broken Mtn.

** T = Tribble
 S = Stone
 B = Bingham
 F = Forbes
 L = Lofgren
 G = Gedney
 M = Matheson

* V = vertical field
 T = total field
 G = vertical gradient of total

Table B.1b

Survey Information for Spot Readings of the Vertical Field
 in the Vicinity of Novarupta Volcano (measured by Forbes)

Station	Date July '69	Time	Location
1	23	16:52	rim of Novarupta Crater
2	23	16:54	crater rim
3	23	16:56	crater rim
4	13	?	summit of Novarupta
5	17	afternoon	crater rim
6	17	afternoon	crater rim
7	13	?	west slope of Stumbling Mtn.
8	17	afternoon	crater rim
9	?	?	crater rim
10	17	afternoon	summit of Stumbling Mtn.
11	13	?	crater rim
12	14	afternoon	west slope of Broken Mtn.
13	17	afternoon	west slope of Broken Mtn.
14	17	afternoon	south slope of Greasy Pass
15	13	?	Greasy Pass
15	17	afternoon	Greasy Pass

APPENDIX B.2
Magnetometer Survey Data

MAGNETOMETER TRAVERSE A -A'

STATION NUMBER	STATION DISTANCE (METERS)	STATION ELEVATION (METERS)	TOTAL ANOMALY (GAMMAS)	VERT DER OF TOTAL (G/METER)
1	0.0	407.5	-106.	-4.6
2	54.5	394.3	-133.	-17.4
3	109.0	380.6	-239.	-22.7
4	164.0	369.9	400.	5.4
5	220.1	369.8	132.	62.2
6	275.0	372.4	781.	68.4
7	359.6	381.4	437.	1.6
8	414.7	381.2	299.	-3.1
9	470.5	374.9	405.	8.5
10	526.5	377.9	519.	22.5
11	582.5	377.8	375.	34.8
12	638.7	377.8	292.	-49.2
13	694.7	380.8	474.	7.0
14	750.5	386.8	-173.	-45.4
15	806.6	386.8	-485.	-84.4
16	862.6	383.7	32.	-70.0
17	918.7	383.7	191.	-9.2
18	974.7	380.5	-47.	40.4
19	1030.4	380.5	666.	172.0
20	1086.9	380.4	301.	0.0
21	1143.0	380.3	343.	-2.3
22	1199.0	383.3	148.	16.9
23	1255.1	383.2	157.	-55.1
24	1311.2	383.1	359.	0.0
25	1367.3	383.0	183.	-19.2
26	1423.4	382.9	194.	-19.9
27	1479.5	382.9	127.	-18.4
28	1535.6	384.3	244.	28.5
29	1591.7	385.7	218.	-13.8
30	1647.8	385.7	-109.	-117.9
31	1703.8	382.6	74.	64.3
32	1759.9	382.5	236.	48.5
33	1815.7	376.3	56.	29.0
34	1871.7	379.3	232.	-10.0
35	1927.5	385.3	153.	2.3
36	1983.5	382.2	-22.	-43.3
37	2039.3	388.3	-92.	-50.8
38	2095.0	382.1	177.	-7.7
39	2150.8	388.1	138.	-8.4

MAGNETOMETER TRAVERSE A -A' (CONT.)

STATION NUMBER	STATION DISTANCE (METERS)	STATION ELEVATION (METERS)	TOTAL ANOMALY (GAMMAS)	VERT DER OF TOTAL (G/METER)
40	2206.1	378.9	-189.	-0.8
41	2262.1	381.9	219.	-17.6
42	2317.9	387.9	235.	-9.2
43	2374.0	387.8	47.	-16.8
44	2430.0	384.7	177.	-10.7
45	2486.1	387.8	145.	-17.6
46	2542.1	389.2	118.	-3.8
47	2598.2	392.2	201.	-36.8
48	2654.2	390.7	-37.	-35.7
49	2710.0	396.7	-541.	-43.2
50	2766.1	398.2	30.	11.4
51	2822.2	399.7	-215.	0.0
52	2877.9	405.8	-218.	-19.6
53	2934.0	408.8	-647.	-13.4
54	2989.7	420.9	847.	-785.1
55	3044.7	423.8	-420.	36.2

MAGNETOMETER TRAVERSE B -B'

MAGNETOMETER TRAVERSE B -B' (CONT.)

STATION NUMBER	STATION DISTANCE (METERS)	STATION ELEVATION (METERS)	TOTAL ANOMALY (GAMMAS)	VERT DER OF TOTAL (G/METER)
1	0.0	740.3	32.	-6.3
2	27.6	745.1	-98.	-14.9
3	55.4	741.0	-228.	-53.0
4	83.1	737.0	-249.	-61.6
5	110.2	729.4	-539.	-80.1
6	134.7	715.8	-375.	-21.7
7	160.2	704.2	-215.	-10.9
8	182.3	686.9	83.	-30.8
9	209.5	680.3	317.	-16.7
10	243.7	665.8	261.	-21.5
11	319.5	659.8	468.	-18.4
12	375.2	653.2	489.	-32.1
13	431.3	653.9	381.	-52.7
14	487.4	654.0	120.	-54.5
15	543.4	651.0	177.	-7.9
16	599.5	648.9	190.	-33.3
17	655.6	646.6	433.	-53.6
18	711.6	645.2	528.	-27.3
19	767.6	641.7	642.	13.7
20	823.6	638.1	96.	-52.9
21	879.6	640.9	-210.	-57.8
22	935.7	640.1	-0.	-45.7
23	991.8	638.3	-304.	-17.9
24	1047.8	641.4	-255.	-17.2
25	1103.8	644.3	-350.	-34.2
26	1158.9	655.2	-379.	-44.3
27	1214.4	663.3	-521.	0.0
28	1270.5	664.7	-512.	-10.8
29	1326.4	669.4	-461.	-27.9
30	1382.4	666.9	-355.	-29.5
31	1440.0	672.1	-559.	-338.7
32	1431.0	657.6	-402.	28.0
33	1457.5	642.5	-257.	-31.2
34	1431.1	627.3	50.	4.7
35	1508.1	619.7	362.	-6.4
36	1534.9	611.3	477.	-41.7
37	1562.0	604.0	507.	-3.2
38	1590.0	603.1	455.	-24.0
39	1645.1	592.6	246.	-35.8

STATION NUMBER	STATION DISTANCE (METERS)	STATION ELEVATION (METERS)	TOTAL ANOMALY (GAMMAS)	VERT DER OF TOTAL (G/METER)
40	1700.9	587.1	222.	-34.9
41	1728.6	582.6	154.	-41.2
42	1756.7	582.3	215.	-32.6
43	1812.8	582.7	-6.	-55.1
44	1868.7	579.1	165.	1.6
45	1924.8	577.7	24.	-41.8
46	1980.8	573.8	-4.	-55.1
47	2036.5	567.1	309.	-26.3
48	2064.5	566.6	298.	31.1
49	2120.6	551.2	345.	83.9
50	2176.1	559.7	417.	14.7
51	2232.0	555.2	495.	-3.1
52	2287.9	560.2	443.	1.6
53	2344.0	560.0	458.	17.1
54	2400.1	560.0	422.	20.9
55	2456.1	561.6	646.	10.9
56	2512.2	563.2	675.	10.2
57	2568.3	563.3	792.	26.7
58	2623.9	571.0	722.	16.0
59	2680.0	569.5	687.	18.0
60	2736.1	569.6	511.	3.9
61	2792.2	569.6	379.	-10.8
62	2848.2	568.1	350.	-3.1
63	2904.3	570.6	355.	-70.1
64	2960.4	571.3	439.	34.1
65	3016.5	571.4	333.	4.6
66	3072.6	569.9	365.	6.2
67	3128.6	571.4	327.	1.5
68	3184.7	571.5	311.	-0.8
69	3240.8	568.5	333.	9.3
70	3296.8	570.0	219.	12.3
71	3352.9	570.1	74.	-23.7
72	3409.0	570.1	67.	-9.9
73	3465.1	568.6	98.	-8.4
74	3521.2	570.2	178.	13.0
75	3577.2	567.2	199.	-3.8
76	3633.3	565.7	100.	-2.3
77	3689.4	567.4	-22.	11.4
78	3745.5	567.3	-105.	8.3

MAGNETOMETER TRAVERSE B -B' (CONT.)

STATION NUMBER	STATION DISTANCE (METERS)	STATION ELEVATION (METERS)	TOTAL ANOMALY (GAMMAS)	VERT DER OF TOTAL (G/METER)
79	3801.6	567.4	-420.	-9.7
80	3857.7	567.4	-253.	1.5
81	3913.8	567.5	-91.	-1.5
82	3969.9	567.5	-138.	-1.5
83	4026.0	567.6	-125.	-1.5
84	4081.7	573.7	343.	-4.6
85	4136.1	587.5	397.	-49.4
86	4190.9	599.7	39.	-23.6
87	4244.8	615.0	323.	-29.3

MAGNETOMETER TRAVERSE B'' -b'''

STATION NUMBER	STATION DISTANCE (METERS)	STATION ELEVATION (METERS)	TOTAL ANOMALY (GAMMAS)
1	0.0	733.1	474.
2	0.4	733.0	491.
3	1.2	732.9	464.
4	1.8	732.8	462.
5	2.4	732.7	457.
6	3.0	732.6	462.
7	3.6	732.5	362.
8	4.2	732.4	484.
9	4.8	732.3	463.
10	5.4	732.2	423.
11	6.0	732.1	389.
12	6.6	732.0	348.
13	7.2	731.9	305.
14	7.8	731.8	304.
15	8.4	731.7	246.

MAGNETOMETER TRAVERSE b - b'

STATION NUMBER	STATION DISTANCE (METERS)	STATION ELEVATION (METERS)	VERTICAL ANOMALY (GAMMAS)
1	0.0	680.7	98.
2	28.0	680.8	-47.
3	56.1	681.0	33.
4	84.1	682.5	-167.
5	112.1	684.0	-152.
6	140.2	685.5	-257.
7	168.2	687.0	-197.
8	196.2	688.5	-427.
9	224.2	691.5	-77.
10	252.3	694.5	13.
11	280.3	697.5	73.
12	308.3	700.7	63.

MAGNETOMETER TRAVERSE B -B''

STATION NUMBER	STATION DISTANCE (METERS)	STATION ELEVATION (METERS)	VERTICAL ANOMALY (GAMMAS)	TOTAL ANOMALY (GAMMAS)
1	0.0	765.2	-32.0	-95.0
2	5.7	764.0	58.0	*****
3	32.1	758.6	-57.0	*****
4	55.1	754.6	*****	-87.0
5	58.7	753.2	-97.0	*****
6	85.1	747.8	-47.0	*****
7	110.7	747.0	*****	-167.0
8	111.7	742.3	-57.0	*****
9	134.1	736.9	-102.0	*****
10	144.6	731.5	-287.0	-276.0
11	173.5	729.9	-102.0	*****
12	197.5	728.3	-107.0	*****
13	220.3	725.2	-317.0	-319.0
14	242.8	708.3	-267.0	*****
15	255.1	691.4	213.0	267.0
16	272.6	686.8	233.0	*****
17	320.1	680.2	198.0	206.0
18	348.0	677.1	223.0	*****
19	375.9	674.1	303.0	265.0
20	411.9	672.4	323.0	*****
21	431.9	670.8	153.0	140.0
22	450.0	670.5	203.0	*****
23	488.0	670.3	183.0	165.0
24	516.0	671.3	243.0	*****
25	544.0	672.2	173.0	136.0
26	572.1	670.7	343.0	*****
27	600.0	669.2	273.0	90.0
28	628.1	670.3	73.0	*****
29	656.1	671.4	283.0	100.0
30	684.1	673.0	283.0	*****
31	712.1	674.5	243.0	107.0
32	740.2	674.5	133.0	*****
33	768.2	674.5	133.0	-32.0
34	796.2	676.4	-77.0	*****
35	824.2	678.2	13.0	-115.0
36	852.3	679.5	13.0	*****
37	880.2	680.7	98.0	-24.0
38	916.3	680.8	*****	-177.0
39	992.4	682.3	*****	-254.0

MAGNETOMETER TRAVERSE B -B'' (CONT.)

STATION NUMBER	STATION DISTANCE (METERS)	STATION ELEVATION (METERS)	VERTICAL ANOMALY (GAMMAS)	TOTAL ANOMALY (GAMMAS)
40	1048.0	690.0	*****	-332.0
41	1102.7	702.3	*****	-594.0
42	1156.7	717.5	*****	-304.0
43	1210.6	733.1	*****	232.0

MAGNETOMETER TRAVERSE B'' -b''

STATION NUMBER	STATION DISTANCE (METERS)	STATION ELEVATION (METERS)	VERTICAL ANOMALY (GAMMAS)	TOTAL ANOMALY (GAMMAS)
1	0.0	733.1	*****	230.0
2	27.7	728.6	*****	220.0
3	80.9	710.9	*****	-380.0
4	136.5	703.0	*****	-173.0
5	192.2	696.1	*****	-104.0
6	248.1	700.7	63.0	-41.0
7	276.1	699.8	73.0	*****
8	304.1	698.9	-47.0	-152.0
9	332.1	698.6	-47.0	*****
10	360.2	698.4	-62.0	-184.0
11	388.2	700.0	-97.0	*****
12	416.2	701.5	-107.0	-229.0
13	444.2	701.4	*****	-117.0
14	472.3	701.4	-17.0	-151.0

MAGNETOMETER TRAVERSE B -B'''

STATION NUMBER	STATION DISTANCE (METERS)	STATION ELEVATION (METERS)	VERTICAL ANOMALY (GAMMAS)	TOTAL ANOMALY (GAMMAS)
1	0.0	766.6	-32.0	-77.0
2	26.8	763.0	-82.0	*****
3	53.6	759.4	-87.0	*****
4	56.0	763.5	*****	-103.0
5	80.4	755.7	-77.0	*****
6	107.2	752.1	-107.0	*****
7	111.1	752.7	*****	-112.0
8	134.0	748.5	-107.0	*****
9	160.8	744.9	3.0	*****
10	166.5	744.1	-2.0	-53.0
11	193.2	735.6	-297.0	*****
12	218.0	727.6	-347.0	*****
13	220.3	728.2	*****	-347.0
14	242.8	719.7	-417.0	*****
15	246.6	719.5	-477.0	*****
16	273.3	709.9	-197.0	6.0
17	300.9	704.8	243.0	*****
18	322.5	699.7	198.0	228.0
19	356.5	697.5	183.0	*****
20	383.7	689.9	*****	164.0
21	384.8	695.3	143.0	*****
22	414.2	693.0	223.0	*****
23	439.3	682.2	*****	265.0
24	441.5	690.9	293.0	*****
25	469.8	688.7	523.0	*****
26	495.2	686.7	413.0	333.0
27	530.5	687.0	198.0	*****
28	551.3	697.6	*****	313.0
29	585.9	687.3	373.0	*****
30	601.2	687.6	263.0	*****
31	607.4	688.7	*****	349.0
32	636.7	687.9	383.0	*****
33	663.5	688.1	323.0	326.0
34	686.6	687.7	433.0	*****
35	710.5	687.2	273.0	*****
36	719.5	685.0	*****	93.0
37	737.9	685.8	323.0	*****
38	747.5	686.5	283.0	214.0
39	778.0	688.0	303.0	*****

MAGNETOMETER TRAVERSE B -B''' (CONT.)

STATION NUMBER	STATION DISTANCE (METERS)	STATION ELEVATION (METERS)	VERTICAL ANOMALY (GAMMAS)	TOTAL ANOMALY (GAMMAS)
40	803.5	689.4	*****	371.0
41	809.2	689.4	343.0	*****
42	831.6	689.4	*****	257.0
43	838.7	690.9	*****	363.0
44	869.0	692.4	323.0	*****
45	887.5	693.9	*****	183.0
46	899.4	693.9	463.0	*****
47	929.9	695.3	363.0	*****
48	943.6	696.0	323.0	150.0
49	974.6	697.0	263.0	*****
50	999.7	695.4	*****	54.0
51	1005.7	698.0	223.0	*****
52	1036.9	699.0	223.0	*****
53	1059.7	697.5	253.0	109.0
54	1083.7	700.5	153.0	*****
55	1111.7	701.4	3.0	-151.0
56	1139.5	705.6	-92.0	*****
57	1167.2	709.8	-72.0	-274.0
58	1184.9	714.2	-237.0	*****
59	1202.5	718.6	-397.0	*****
60	1220.0	723.0	-527.0	*****
61	1230.3	725.6	*****	-550.0
62	1237.6	727.4	-437.0	*****
63	1255.3	731.8	-352.0	*****
64	1269.9	735.5	-347.0	*****
65	1284.7	739.2	-347.0	-385.0

MAGNETOMETER TRAVERSE C - C'

STATION NUMBER	STATION DISTANCE (METERS)	STATION ELEVATION (METERS)	VERTICAL ANOMALY (GAMMAS)
1	0.0	605.9	123.
2	30.5	596.2	173.
3	38.4	593.8	43.
4	61.0	591.9	-197.
5	91.4	589.5	-37.
6	107.0	587.4	-207.
7	122.2	585.2	313.
8	136.2	581.1	413.
9	153.0	580.5	243.
10	183.5	576.1	353.
11	213.7	569.7	33.
12	228.9	566.6	33.
13	244.1	563.6	238.
14	272.2	558.4	213.
15	274.6	557.8	213.
16	305.1	552.9	233.
17	324.3	549.9	243.
18	336.8	548.0	423.
19	352.3	545.6	123.
20	363.6	544.1	243.
21	367.9	543.8	233.
22	398.7	542.2	183.
23	429.2	540.4	233.
24	451.7	539.2	233.
25	459.6	538.9	313.
26	490.4	538.0	313.
27	504.1	537.7	333.
28	521.2	537.4	313.
29	542.3	536.4	223.
30	564.8	536.1	103.
31	583.1	535.8	3.
32	614.2	535.5	473.
33	615.0	535.2	523.
34	645.0	534.9	413.
35	676.0	534.3	-67.
36	707.1	534.0	323.
37	709.6	533.4	383.
38	740.1	533.1	323.
39	761.7	532.8	273.

MAGNETOMETER TRAVERSE C - C' (CONT.)

STATION NUMBER	STATION DISTANCE (METERS)	STATION ELEVATION (METERS)	VERTICAL ANOMALY (GAMMAS)
40	770.5	532.8	298.
41	801.0	532.5	238.
42	816.9	532.2	-47.
43	831.8	531.9	78.
44	862.3	531.3	323.
45	871.1	531.3	343.
46	893.1	530.4	223.
47	920.8	529.1	53.
48	923.9	529.1	173.
49	954.6	530.0	338.
50	964.1	530.4	228.
51	985.7	530.4	233.
52	1016.5	530.4	133.
53	1022.9	530.4	173.
54	1047.6	529.4	223.
55	1078.4	530.4	363.
56	1080.8	530.4	423.
57	1109.8	530.4	198.
58	1116.8	530.4	223.
59	1140.6	529.4	103.
60	1159.8	528.2	223.
61	1171.7	528.2	273.
62	1200.3	527.6	303.
63	1220.4	527.3	243.
64	1230.8	527.0	248.
65	1261.6	526.4	423.
66	1273.3	526.1	583.
67	1289.9	525.5	483.
68	1320.7	524.3	323.
69	1336.2	524.0	623.
70	1346.9	523.0	483.
71	1377.7	520.3	423.
72	1392.6	525.5	733.
73	1405.1	527.0	623.
74	1420.7	527.0	83.
75	1451.5	527.0	223.
76	1482.2	527.0	173.
77	1485.3	527.6	173.
78	1514.3	527.3	-7.

MAGNETOMETER TRAVERSE C - C' (CONT.)

STATION NUMBER	STATION DISTANCE (METERS)	STATION ELEVATION (METERS)	VERTICAL ANOMALY (GAMMAS)
79	1544.1	527.0	323.
80	1562.7	527.0	253.
81	1575.2	527.3	-87.
82	1606.0	527.9	-437.
83	1621.5	528.2	123.
84	1634.0	528.8	-437.
85	1665.1	529.7	28.
86	1695.9	530.7	173.
87	1726.4	530.7	153.
88	1735.5	530.7	163.
89	1769.5	530.7	198.
90	1776.8	530.7	203.
91	1798.9	530.7	203.
92	1829.7	530.7	303.
93	1855.2	530.7	243.
94	1860.5	530.7	233.
95	1891.6	530.7	323.
96	1915.7	530.7	223.
97	1922.4	530.7	238.
98	1953.2	530.7	123.
99	1970.2	530.7	303.
100	1982.7	530.7	373.
101	2013.8	530.7	443.
102	2029.1	530.7	383.
103	2047.7	530.7	463.
104	2078.7	530.7	443.
105	2109.5	530.7	213.
106	2119.6	531.0	203.
107	2137.9	531.3	128.
108	2163.7	531.9	28.
109	2199.4	532.8	53.
110	2232.4	533.4	53.
111	2261.3	534.0	153.
112	2292.4	534.9	3.
113	2323.2	535.5	3.
114	2354.0	535.8	-17.
115	2384.8	535.8	-62.
116	2415.2	536.1	283.
117	2456.1	536.8	243.

MAGNETOMETER TRAVERSE C - C' (CONT.)

STATION NUMBER	STATION DISTANCE (METERS)	STATION ELEVATION (METERS)	VERTICAL ANOMALY (GAMMAS)
118	2484.6	537.7	113.
119	2517.0	538.6	133.
120	2547.5	539.5	263.
121	2578.0	540.4	223.
122	2608.5	541.3	193.
123	2639.0	542.2	323.
124	2669.4	543.2	353.
125	2700.5	545.6	233.
126	2731.3	548.0	273.
127	2745.3	548.9	283.
128	2762.1	550.5	273.
129	2793.2	552.6	323.
130	2802.6	552.9	243.
131	2824.3	553.8	273.
132	2855.1	558.1	223.
133	2886.2	560.2	103.
134	2895.9	561.1	3.
135	2914.2	563.6	-27.
136	2943.8	566.6	-147.
137	2958.7	568.5	-287.
138	2973.3	570.0	-477.
139	3004.4	573.9	-117.
140	3032.2	577.9	-312.
141	3035.2	578.2	-367.
142	3062.6	583.1	-47.
143	3093.1	588.5	-142.
144	3108.4	589.8	-7.
145	3126.6	592.5	-47.
146	3144.9	595.0	-217.
147	3157.4	596.8	-272.
148	3188.2	600.8	-52.
149	3205.0	602.9	-227.
150	3219.0	604.4	73.
151	3250.7	608.7	-32.
152	3252.5	608.1	-57.
153	3279.4	613.6	-72.
154	3281.2	614.8	-77.
155	3312.0	618.7	-117.
156	3327.2	621.2	-87.

MAGNETOMETER TRAVERSE C - C' (CONT.)

STATION NUMBER	STATION DISTANCE (METERS)	STATION ELEVATION (METERS)	VERTICAL ANOMALY (GAMMAS)
157	3342.4	623.6	-137.
158	3372.9	628.5	-297.
159	3397.0	634.6	-447.
160	3403.1	636.1	-447.
161	3433.0	643.7	-447.
162	3455.5	650.1	-417.
163	3462.8	651.7	-452.
164	3483.3	659.9	-377.
165	3492.1	662.3	-347.
166	3524.7	676.4	-347.

MAGNETOMETER TRAVERSE D -D'

STATION NUMBER	STATION DISTANCE (METERS)	STATION ELEVATION (METERS)	TOTAL ANOMALY (GAMMAS)	VERT DER OF TOTAL (G/METER)
1	0.0	625.5	-32.	-0.8
2	55.6	617.9	313.	103.2
3	110.3	605.8	334.	16.8
4	165.8	597.6	172.	4.0
5	221.1	588.1	364.	-42.3
6	276.1	576.9	270.	-10.3
7	331.6	568.4	463.	35.3
8	387.6	546.0	470.	1.6
9	443.5	561.7	247.	3.8
10	499.6	560.2	302.	-8.8
11	554.7	549.5	139.	-13.5
12	610.5	555.6	91.	-11.9
13	666.6	555.0	-59.	-25.1
14	722.6	552.6	118.	1.6
15	778.7	552.3	-74.	-29.8
16	834.8	552.0	-152.	-29.7
17	890.9	551.1	-79.	-48.6
18	947.0	549.6	110.	-4.0
19	1003.0	552.4	168.	18.2
20	1059.1	551.8	132.	19.9
21	1115.2	551.2	272.	-177.4
22	1171.3	550.6	433.	0.0
23	1227.5	545.1	573.	-32.9
24	1283.6	546.0	191.	44.5
25	1339.6	547.0	-99.	18.8
26	1451.7	547.7	214.	60.4
27	1507.8	548.5	-191.	-35.1
28	1535.6	552.7	-88.	7.1
29	1563.6	552.1	-371.	-92.9
30	1619.7	551.9	-90.	-1.6
31	1675.8	551.6	-66.	13.4
32	1731.9	553.2	-218.	3.9
33	1788.0	551.7	-225.	-70.1
34	1844.1	550.8	131.	36.4
35	1900.2	552.6	-342.	-89.4
36	1956.2	553.8	-291.	10.9
37	2012.3	554.5	-11.	12.6
38	2068.4	555.7	207.	17.5
39	2124.5	555.7	39.	-18.9

MAGNETOMETER TRAVERSE D -D' (CONT.)

STATION NUMBER	STATION DISTANCE (METERS)	STATION ELEVATION (METERS)	TOTAL ANOMALY (GAMMAS)	VERT DER OF TOTAL (G/METER)
40	2180.6	556.4	355.	21.5
41	2236.7	557.9	-2.	-4.7
42	2232.8	557.9	-224.	-39.0
43	2320.8	558.0	-12.	1.6
44	2348.9	558.0	-124.	-7.8
45	2405.0	555.8	16.	-0.8
46	2451.1	556.2	-257.	-119.6
47	2517.2	556.2	-113.	13.3
48	2573.2	557.1	-48.	5.5
49	2629.2	561.1	-4.	-18.1
50	2685.3	562.1	-18.	12.6
51	2741.4	562.4	98.	11.1
52	2797.5	562.4	66.	-26.0
53	2853.6	562.4	262.	-28.6
54	2909.7	562.7	281.	-17.5
55	2965.5	568.2	93.	-7.9
56	3021.5	571.9	-46.	-12.6
57	3077.5	574.9	-101.	-5.5
58	3133.5	578.0	46.	38.7
59	3189.4	582.9	-206.	9.4
60	3245.4	587.2	-313.	10.9
61	3301.3	591.8	-375.	-38.0
62	3357.0	598.2	-63.	11.8
63	3412.9	602.5	-11.	32.3
64	3469.0	604.0	-166.	-0.8
65	3468.9	606.1	-218.	-98.1
66	3496.9	607.1	-153.	29.0
67	3524.8	610.1	-186.	7.8
68	3552.6	614.1	-201.	-6.2
69	3580.4	617.8	-124.	-16.4
70	3608.1	622.1	-11.	2.4
71	3636.0	625.4	-26.	-35.3
72	3663.3	631.8	-75.	-25.9
73	3691.2	634.6	-51.	-42.4
74	3717.4	644.7	91.	12.7
75	3745.3	647.1	134.	-41.1
76	3772.9	652.0	58.	-20.5
77	3799.1	662.1	-47.	18.8
78	3827.1	663.0	-370.	4.7

MAGNETOMETER TRAVERSE D -D' (CONT.)

STATION NUMBER	STATION DISTANCE (METERS)	STATION ELEVATION (METERS)	TOTAL ANOMALY (GAMMAS)	VERT DER OF TOTAL (G/METER)
79	3854.9	667.3	-451.	-49.4
80	3910.4	675.3	-484.	-3.1
81	3966.2	681.1	-621.	-4.6
82	4018.9	700.3	-498.	802.5
83	4069.4	724.7	785.	-34.0

MAGNETOMETER TRAVERSE E -E'

STATION NUMBER	STATION DISTANCE (METERS)	STATION ELEVATION (METERS)	TOTAL ANOMALY (GAMMAS)	VERT DER OF TOTAL (G/METER)
1	0.0	747.1	-997.	10.7
2	23.5	731.8	-1323.	-26.9
3	50.6	724.5	-1398.	-20.1
4	77.1	715.4	-1283.	-18.7
5	104.7	710.2	-1016.	-0.8
6	132.1	704.1	-896.	8.4
7	160.1	702.0	-664.	24.6
8	187.9	698.3	-929.	-26.6
9	215.8	696.2	-865.	-26.6
10	243.7	692.8	-951.	-137.7
11	271.5	689.2	-556.	-70.0
12	299.5	687.3	-729.	-65.7
13	327.5	686.1	-612.	-18.5
14	355.5	684.3	-532.	-11.6
15	383.4	681.2	-263.	28.9
16	411.4	680.3	-504.	-1.5
17	439.5	679.7	-618.	-11.5
18	467.5	678.8	-891.	-88.8
19	495.4	676.4	-724.	-155.6
20	523.5	675.1	-188.	3556.9
21	551.4	672.1	-28.	19.7
22	579.4	673.0	136.	-9.5
23	607.2	669.0	-449.	-6.2
24	635.2	669.0	-75.	59.8
25	665.9	669.0	-1106.	-253.4
26	719.3	670.6	808.	322.4
27	747.3	669.0	96.	-372.1
28	775.3	668.1	-545.	-91.5
29	803.3	670.6	429.	263.5
30	831.3	670.6	-464.	-1.5
31	859.4	670.6	-428.	21.7
32	887.4	670.3	-253.	18.7
33	915.5	670.6	-182.	10.2
34	943.5	670.6	-283.	-24.9
35	971.5	672.1	-400.	-59.6
36	999.6	673.6	989.	204.5
37	1027.4	678.2	-432.	15.5
38	1083.5	679.7	-389.	28.0
39	1111.4	681.8	-802.	-71.7

MAGNETOMETER TRAVERSE E -E' (CONT.)

STATION NUMBER	STATION DISTANCE (METERS)	STATION ELEVATION (METERS)	TOTAL ANOMALY (GAMMAS)	VERT DER OF TOTAL (G/METER)
40	1139.5	682.8	-2867.	501.2
41	1167.5	683.7	784.	175.1
42	1195.5	685.8	220.	-65.0
43	1223.5	686.4	-776.	-30.6
44	1251.5	688.9	-306.	-171.2
45	1279.4	691.0	-745.	-163.1
46	1307.4	691.5	-640.	-151.5
47	1335.4	691.9	-75.	14.9
48	1363.4	693.4	-374.	3.1
49	1391.4	693.4	-596.	-40.0
50	1419.3	696.5	-601.	4.6
51	1447.2	696.5	-744.	-74.9
52	1475.2	696.5	-674.	0.0
53	1503.3	696.5	-557.	7.7
54	1531.4	696.5	-501.	-2.3
55	1557.3	707.1	-496.	-18.5
56	1585.3	707.1	-437.	-6.2
57	1597.4	708.1	-421.	-5.4
58	1625.3	710.2	-462.	-4.6
59	1653.4	711.1	-320.	16.3
60	1680.9	716.3	-387.	9.5
61	1708.7	720.1	-578.	-2.3
62	1736.5	723.9	-855.	-11.4
63	1764.1	728.5	-826.	-16.0
64	1792.0	731.5	-294.	21.8
65	1847.8	737.6	-33.	-0.8

MAGNETOMETER TRAVERSE F' - F

STATION NUMBER	STATION DISTANCE (METERS)	STATION ELEVATION (METERS)	VERTICAL ANOMALY (GAMMAS)
1	0.0	725.4	-542.
2	30.4	725.7	-592.
3	61.0	726.0	-531.
4	91.4	724.3	-521.
5	121.9	727.0	-701.
6	152.4	727.3	-800.
7	182.9	727.6	380.
8	213.4	727.9	-30.
9	243.8	728.5	-69.
10	274.3	728.8	-309.
11	304.8	729.1	341.
12	335.3	729.4	341.
13	365.8	730.0	502.
14	396.2	730.3	262.
15	426.7	730.6	232.
16	457.2	730.9	273.
17	487.7	731.5	643.
18	518.2	734.0	473.
19	548.3	735.7	1244.
20	578.8	739.1	794.
21	609.3	741.9	1244.
22	639.5	744.3	1444.
23	670.0	747.1	945.
24	700.4	749.5	995.
25	730.6	752.2	645.
26	761.1	754.7	746.
27	791.6	757.1	846.
28	821.7	759.6	746.
29	852.2	762.0	747.
30	882.4	765.7	947.
31	912.9	769.3	1047.
32	943.1	773.0	1097.
33	973.2	776.6	1048.
34	1003.7	780.3	1248.

MAGNETOMETER TRAVERSE F' - F

STATION NUMBER	STATION DISTANCE (METERS)	STATION ELEVATION (METERS)	VERTICAL ANOMALY (GAMMAS)
1	0.0	713.2	980.
2	30.4	713.5	980.
3	61.0	713.8	530.
4	91.4	714.1	879.
5	121.9	714.5	1329.
6	152.4	715.1	929.
7	182.9	715.7	1728.
8	213.4	716.3	568.
9	243.8	717.8	1428.
10	274.3	719.3	1603.
11	304.8	720.9	1727.
12	335.3	722.4	1627.
13	365.8	723.9	1627.
14	396.0	725.4	1176.
15	426.4	727.0	926.
16	456.9	728.5	901.
17	487.4	731.5	1025.
18	517.2	737.6	875.
19	547.1	743.7	850.
20	577.0	749.8	665.
21	606.9	755.9	904.
22	636.7	762.0	724.
23	666.6	768.1	924.
24	696.5	774.2	1073.
25	726.3	780.3	1248.

MAGNETOMETER TRAVERSE F' - F''

STATION NUMBER	STATION DISTANCE (METERS)	STATION ELEVATION (METERS)	VERTICAL ANOMALY (GAMMAS)
1	0.0	725.4	-542.
2	30.4	725.1	-663.
3	61.0	724.5	-603.
4	91.4	723.9	-44.
5	121.9	723.6	-394.
6	152.4	723.0	-684.
7	182.9	722.4	-745.
8	213.4	721.8	-605.
9	243.8	721.5	-645.
10	274.3	720.9	-846.
11	304.8	720.2	534.
12	335.3	719.6	414.
13	365.8	719.3	584.
14	396.2	718.7	-117.
15	426.7	718.1	63.
16	457.2	717.5	103.
17	487.7	717.2	272.
18	518.2	716.6	-48.
19	548.6	716.0	632.
20	579.1	715.4	1331.
21	609.6	715.1	471.
22	640.1	714.5	471.
23	670.6	713.8	981.
24	701.0	713.2	980.

MAGNETOMETER TRAVERSE G' - G

STATION NUMBER	STATION DISTANCE (METERS)	STATION ELEVATION (METERS)	VERTICAL ANOMALY (GAMMAS)
1	0.0	716.3	450.
2	30.4	717.5	440.
3	61.0	719.0	379.
4	91.4	720.2	499.
5	121.9	721.8	759.
6	152.4	723.0	818.
7	182.9	724.5	1078.
8	213.4	725.7	1158.
9	243.8	727.3	1228.
10	274.3	728.5	1107.
11	304.8	729.4	1027.
12	320.1	730.3	1117.
13	335.3	731.5	1197.
14	365.5	736.4	1477.
15	395.6	741.6	1536.
16	425.8	745.5	1366.
17	456.0	751.6	1016.
18	486.2	756.5	566.
19	516.3	761.7	936.
20	546.5	766.6	1355.
21	576.7	771.8	1155.
22	606.9	776.6	1155.
23	637.0	781.8	935.
24	667.2	786.4	1615.

MAGNETOMETER TRAVERSE G*** - G

STATION NUMBER	STATION DISTANCE (METERS)	STATION ELEVATION (METERS)	VERTICAL ANOMALY (GAMMAS)
1	0.0	716.3	623.
2	30.4	717.2	612.
3	61.0	717.8	732.
4	91.4	718.7	822.
5	121.9	719.6	862.
6	152.4	720.5	942.
7	182.9	721.5	921.
8	213.4	722.4	1061.
9	228.6	722.7	1363.
10	243.8	723.3	1413.
11	274.3	724.2	1293.
12	304.8	725.1	1384.
13	335.3	726.0	1364.
14	365.8	727.0	1284.
15	396.2	727.9	1324.
16	426.7	728.8	1365.
17	457.2	729.7	1365.
18	487.7	730.6	1365.
19	518.2	731.5	1365.

MAGNETOMETER TRAVERSE H - H'

STATION NUMBER	STATION DISTANCE (METERS)	STATION ELEVATION (METERS)	VERTICAL ANOMALY (GAMMAS)
1	0.0	847.3	1903.
2	15.2	848.3	1893.
3	30.4	849.2	1733.
4	45.7	850.4	1553.
5	60.7	847.0	1883.
6	90.8	843.7	1702.
7	121.0	840.3	1472.
8	151.2	837.0	1412.
9	181.4	833.6	1272.
10	211.8	830.6	1232.
11	242.3	827.5	1021.
12	272.5	831.2	801.
13	302.7	834.5	731.
14	332.8	837.9	711.
15	363.0	841.3	521.

MAGNETOMETER TRAVERSE G' - G''

STATION NUMBER	STATION DISTANCE (METERS)	STATION ELEVATION (METERS)	VERTICAL ANOMALY (GAMMAS)
1	0.0	716.3	450.
2	45.7	718.4	440.
3	91.4	720.2	600.
4	137.2	722.4	1061.

MAGNETOMETER TRAVERSE I - I'

STATION NUMBER	STATION DISTANCE (METERS)	STATION ELEVATION (METERS)	VERTICAL ANOMALY (GAMMAS)
1	0.0	881.1	1601.
2	30.4	859.5	1551.
3	61.0	857.4	1401.
4	91.4	855.3	1262.
5	121.9	853.1	1322.
6	152.4	851.0	1352.
7	192.9	849.9	1222.
8	213.4	846.7	1173.
9	228.6	844.6	1143.
10	275.9	842.5	1043.
11	239.9	840.3	873.
12	242.0	838.2	744.
13	257.3	836.7	644.
14	272.5	835.2	774.
15	303.0	833.6	754.
16	333.5	832.1	724.
17	363.9	830.6	684.
18	394.4	832.1	675.
19	424.9	833.6	685.
20	455.4	835.2	605.
21	465.9	836.7	435.
22	516.3	838.2	505.
23	546.5	841.9	295.
24	576.7	845.8	216.
25	606.9	849.8	26.
26	637.0	853.4	-144.
27	665.7	857.8	-234.
28	694.3	873.9	-344.
29	723.0	883.9	-234.
30	752.9	890.0	-203.
31	782.7	896.1	-273.
32	810.8	908.3	-713.
33	840.6	914.4	-593.

MAGNETOMETER TRAVERSE I' - I''

STATION NUMBER	STATION DISTANCE (METERS)	STATION ELEVATION (METERS)	VERTICAL ANOMALY (GAMMAS)
1	0.0	914.4	-593.
2	45.7	914.4	407.
3	91.4	914.4	508.
4	137.2	914.4	298.

MAGNETOMETER TRAVERSE I'' - I'''

STATION NUMBER	STATION DISTANCE (METERS)	STATION ELEVATION (METERS)	VERTICAL ANOMALY (GAMMAS)
1	0.0	883.9	321.
2	29.6	891.5	149.
3	59.2	899.2	348.
4	88.7	906.8	528.
5	118.3	914.4	298.

MAGNETOMETER TRAVERSE J' - J

STATION NUMBER	STATION DISTANCE (METERS)	STATION ELEVATION (METERS)	VERTICAL ANOMALY (GAMMAS)
1	0.0	899.8	761.
2	61.0	899.2	851.
3	91.5	899.2	661.
4	121.9	898.9	1571.
5	213.4	898.6	1233.
6	305.9	886.7	714.

MAGNETOMETER TRAVERSE I - J

STATION NUMBER	STATION DISTANCE (METERS)	STATION ELEVATION (METERS)	VERTICAL ANOMALY (GAMMAS)
1	0.0	861.0	1601.
2	30.4	858.9	1701.
3	60.9	857.1	1540.
4	91.4	855.3	1400.
5	121.9	853.4	1310.
6	152.4	852.5	1400.
7	182.8	851.9	1330.
8	213.3	851.0	1349.
9	243.8	850.1	1279.
10	274.3	849.2	1199.
11	304.8	848.6	1179.
12	335.2	847.7	1179.
13	365.7	846.7	1039.
14	396.2	845.8	1018.
15	426.7	844.7	948.
16	441.9	847.3	938.
17	457.2	848.3	888.
18	472.4	848.9	838.
19	487.6	849.8	858.
20	518.1	850.4	827.
21	533.4	851.3	817.
22	548.6	851.9	577.
23	579.1	852.8	517.
24	609.6	853.4	557.
25	640.0	856.2	717.
26	670.5	858.9	676.
27	701.0	861.2	476.
28	731.5	864.4	626.
29	762.0	867.2	626.
30	792.4	869.9	511.
31	822.9	872.6	515.
32	853.4	875.4	255.
33	883.9	878.1	415.
34	914.4	880.9	45.
35	944.8	883.6	150.
36	1005.8	886.7	714.

MAGNETOMETER TRAVERSE J - K

STATION NUMBER	STATION DISTANCE (METERS)	STATION ELEVATION (METERS)	VERTICAL ANOMALY (GAMMAS)
1	0.0	886.7	714.
2	49.0	903.7	934.
3	118.5	894.6	924.
4	179.5	897.6	809.

MAGNETOMETER TRAVERSE K - K'

STATION NUMBER	STATION DISTANCE (METERS)	STATION ELEVATION (METERS)	VERTICAL ANOMALY (GAMMAS)
1	0.0	593.5	334.
2	304.8	593.5	448.
3	609.6	584.3	357.
4	914.1	594.7	517.
5	1218.9	591.6	399.
6	1523.4	616.0	765.
7	1675.5	623.3	615.
8	1910.3	623.3	1014.
9	1995.5	626.4	714.
10	2071.7	629.4	594.
11	2254.0	612.3	683.
12	2264.5	613.9	733.
13	2285.1	639.8	937.
14	2770.9	642.9	771.
15	3075.4	631.6	629.
16	3380.2	630.0	574.
17	3685.0	623.3	283.
18	3989.9	647.1	462.

MAGNETOMETER TRAVERSE K* - K**

STATION NUMBER	STATION DISTANCE (METERS)	STATION ELEVATION (METERS)	VERTICAL ANOMALY (GAMMAS)
1	0.0	647.1	462.
2	304.5	660.8	211.
3	609.3	666.9	320.
4	914.1	676.7	200.
5	1218.3	692.5	274.
6	1339.9	702.6	81.
7	1355.1	699.8	59.
8	1370.4	699.8	32.
9	1385.6	699.8	12.
10	1400.9	699.8	-23.
11	1415.1	699.8	-191.
12	1431.3	699.8	-93.
13	1446.6	699.8	-187.
14	1461.8	701.3	-312.
15	1477.1	702.9	-382.
16	1492.3	704.4	-227.
17	1508.4	709.6	-202.
18	1520.7	715.4	-106.
19	1570.9	716.9	-27.
20	1587.2	716.3	-120.
21	1607.5	717.8	-170.
22	1625.8	719.3	-84.
23	1680.7	720.9	-184.
24	1703.2	713.2	-170.
25	1762.7	726.6	-96.
26	1808.4	726.6	-182.
27	1823.6	726.6	-256.
28	1841.6	722.7	-180.
29	1882.8	719.0	-228.
30	1897.7	715.4	-368.
31	1944.9	711.7	-303.
32	1975.1	709.1	-186.
33	2126.6	724.8	36.

MAGNETOMETER TRAVERSE K***- K**

STATION NUMBER	STATION DISTANCE (METERS)	STATION ELEVATION (METERS)	VERTICAL ANOMALY (GAMMAS)
1	0.0	877.6	809.
2	42.4	903.7	724.
3	60.4	906.8	724.
4	121.0	901.9	595.
5	136.3	900.9	415.
6	151.5	899.8	525.
7	211.2	887.3	435.
8	272.2	887.0	415.
9	332.2	897.6	346.
10	393.2	901.9	316.
11	453.9	897.0	216.
12	514.5	891.5	206.
13	575.2	885.8	146.
14	634.9	876.3	166.
15	694.3	859.2	26.
16	755.3	862.0	207.
17	816.0	856.6	117.
18	876.6	861.4	-38.
19	896.4	858.9	-88.
20	914.4	856.2	-138.
21	937.0	853.1	-152.
22	997.9	850.4	48.
23	1042.7	841.9	128.
24	1103.7	838.5	23.
25	1164.3	833.6	-87.
26	1225.0	828.8	8.
27	1285.7	822.4	158.
28	1345.7	811.4	358.
29	1405.1	797.4	3.
30	1462.4	787.9	279.
31	1523.4	792.2	209.
32	1583.8	784.6	209.
33	1643.8	773.6	299.
34	1704.1	764.1	120.
35	1763.9	751.6	-40.
36	1824.8	748.3	-70.
37	1885.8	744.9	-146.
38	1946.2	737.0	-80.
39	2005.9	724.8	36.

MAGNETOMETER TRAVERSE L' - L

STATION NUMBER	STATION DISTANCE (METERS)	STATION ELEVATION (METERS)	VERTICAL ANOMALY (GAMMAS)
1	0.0	1005.8	-247.
2	50.1	995.5	-197.
3	119.9	983.9	-247.
4	179.8	972.3	-67.
5	239.7	960.7	-87.
6	299.5	949.2	13.
7	359.4	937.6	73.
8	419.3	926.0	63.
9	479.1	914.4	243.
10	538.9	926.6	263.
11	599.5	932.7	273.
12	659.8	941.8	423.
13	719.8	957.1	473.
14	778.5	969.3	723.

ISOLATED STATIONS

STATION NUMBER	STATION ELEVATION (METERS)	VERTICAL ANOMALY (GAMMAS)
1	789.4	1934.
2	807.7	2164.
3	789.4	1755.
4	841.3	1473.
5	861.1	1948.
6	908.3	1823.
7	855.6	1293.
8	972.3	1648.
9	983.0	1623.
10	1008.9	1198.
11	865.6	1573.
12	865.6	253.
13	820.9	243.
14	838.2	403.
15	868.7	-497.

APPENDIX C

Accumulated Density Determinations for Rocks from the Katmai Area

Classification	Reference	Rock Type	Location	Identity	Density (gm/cc)
Naknek sediments	Kienle, 1969, p. 63	Naknek sandstone	Grosvenor Lake	KG-71	2.60
Naknek sediments	Kienle, 1969, p. 63	Naknek marly shale	Grosvenor Lake	KG-38	2.60
Naknek sediments	Kienle, 1969, p. 63	Naknek shale	Grosvenor Lake	KG-39	2.48
Naknek sediments	Kienle, 1969, p. 63	Chisik conglomerate	Grosvenor Lake	KG-69	2.75
Naknek sediments	Kienle, 1969, p. 63	Naknek sandstone	Grosvenor Lake	KG-72	2.75
rhyolitic glass	Curtis, 1968, p. 192	rhyolite glass	Novarupta dome		2.25 to 2.30
mixed lava	Kienle, 1971, pers.com.	porous banded lava	Novarupta central dome	KN-3-1-65	2.22
mixed lava	Kienle, 1971, pers.com.	porous banded lava	Novarupta east margin	KN-4-1-65	1.70
mixed lava	Kienle, 1971, pers.com.	porous banded lava	Novarupta east margin	KN-4-2-65	1.81
andesitic lava	Kienle, 1971, pers.com.	andesite	Falling Mtn.	KFM-1-70	2.51
andesitic lava	Kienle, 1971, pers.com.	andesite	Falling Mtn.	KFM-1a-70	2.47
andesitic lava	Kienle, 1971, pers.com.	andesite	Fissure Dome	KFD-1-70	2.49
andesitic lava	Kienle, 1971, pers.com.	andesite	Fissure Dome	KFD-1a-70	2.55
andesitic lava	Kienle, 1969, p. 63	porous andesite	Mt. Trident	KT-28	2.44
andesitic lava	Kienle, 1969, p. 63	basaltic andesite	Knife Peak	KKP2-1	2.47
tephra	Griggs, 1922, p. 293	ash			1.03
tephra	Lovering, 1957, p. 1593	fumarolic altered ash	Lower Valley, Fumarole #1, zone 1	1TL53	0.75
tephra	Lovering, 1957, p. 1593	fumarolic altered ash	Lower Valley, Fumarole #1, zone 2	2TL53	1.10
tephra	Lovering, 1957, p. 1593	fumarolic altered ash	Lower Valley, Fumarole #1, zone 3	3TL53	1.18
tephra	Lovering, 1957, p. 1593	fumarolic altered ash	Lower Valley, Fumarole #1, zone 4	4TL53	1.09
tephra	Lovering, 1957, p. 1593	fumarolic altered ash	Lower Valley, Fumarole #1, zone 5	5TL53	0.84
tephra	Lovering, 1957, p. 1593	fumarolic altered ash	Lower Valley, Fumarole #1, zone 6	6TL53	1.00
tephra	Lovering, 1957, p. 1593	normal ash	Lower Valley, Fumarole #1, zone 7	7TL53	0.98
tephra	Curtis, 1968, p. 207	tephra Layer D	upper southeast branch		1.09
tuff	Curtis, 1968, p. 183	tuff	Middle Valley, Knife Creek Gorge		1.15
tuff	Curtis, 1968, p. 183	upper tuff unit	Middle Valley		1.35
tuff	Curtis, 1968, p. 183	tuff	southern branch, Fissure Lake		1.50
tuff	Curtis, 1968, p. 184	dense tuff	southeast branch, Explosion pit		1.78 to 1.85
tuff	Curtis, 1968, p. 183	dark gray tuff	upper southeast branch		1.60 to 1.72
tuff	Curtis, 1968, p. 194	center of dike-like body of tuff	upper southeast branch		1.75

Classification	Reference	Rock Type	Location	Identity	Density (gm/cc)
tuff	Kienle, 1971, pers.com.	tuff	Middle Valley, Knife Creek Canyon	KPFG-1-70	1.62
tuff	Kienle, 1971, pers.com.	tuff	Middle Valley, Knife Creek Canyon	KPFG-1a-70	1.55
tuff	Kienle, 1971, pers.com.	tuff	Middle Valley, Knife Creek Canyon	KPFG-1b-70	1.53
tuff	Kienle, 1971, pers.com.	tuff	upper south branch, Corner Lake	KPFC-1-70	1.52
tuff	Kienle, 1971, pers.com.	tuff	upper south branch, Fissure Lake	KPFL1-1-70	1.61
tuff	Kienle, 1971, pers.com.	tuff	upper south branch, Fissure Lake	KPFL1-2-70	1.63
tuff	Kienle, 1971, pers.com.	tuff	upper south branch, Fissure Lake	KPFL1-3-70	1.61
tuff	Kienle, 1971, pers.com.	tuff	upper south branch, Fissure Lake	KPFL1-4-70	1.66
tuff	Kienle, 1971, pers.com.	tuff	upper south branch, Fissure Lake	KPFL1-5-70	1.67
tuff	Kienle, 1971, pers.com.	tuff	upper southeast branch, Peckish Springs	KPPF-1-70	1.57
tuff	Kienle, 1971, pers.com.	tuff	upper southeast branch, Peckish Springs	KPPF-2-70	1.62
tuff	Kienle, 1971, pers.com.	tuff	upper southeast branch, Peckish Springs	KPPF-4-70	1.73
tuff	Kienle, 1971, pers.com.	tuff	upper southeast branch, Peckish Springs	KPPF-5-70	1.85
tuff	Kienle, 1971, pers.com.	tuff	upper southeast branch, base of Knife Creek Glacier	KPFK3-1a-70	1.78
tuff	Kienle, 1971, pers.com.	tuff	upper southeast branch, base of Knife Creek Glacier	KPFK3-1b-70	1.84
tuff	Kienle, 1971, pers.com.	tuff	Novarupta Basin	KPFN-2-70	1.93
tuff	Kienle, 1971, pers.com.	tuff	Novarupta Basin	KPFN-3-70	1.94
tuff	Kienle, 1971, pers.com.	tuff	Novarupta Basin	KPFN-4-70	1.96
tuff	Kienle, 1970, p. 6645	ash	Lower Valley	5 samples throughout section	1.03 average

APPENDIX D
Accumulated Seismic Refraction Data
Parameters of Seismic Layers thickness (meters)
velocity (km/sec)

Investigator	Profile	Location	Layer 1	Layer 2	Layer 3	Layer 4	Layer 5	Layer 6	Layer 7	Total Thickness (m)
Matumoto and Ward(1967)		Lower Valley		2.4 0.3	7.3 0.6	36. 1.00			1 3.8	45.7
Kienle (1971) E-E'		Lower Valley		2.0 0.38		44.0 .99	?			46.0
Kienle (1971) H-H'		Middle Valley		1.0 ?	28.0 0.65		34.0 1.79	?	2.53	63.0
Kienle (1971) F-F'		Southeast Branch		1.0 0.30	18.0 0.67		?			19.0
Sbar and Matumoto(1971)	Profile 1 Section 7	Southeast Branch			22.0 0.61		?			22.0
Sbar and Matumoto "	Profile 1 Section 1	Broken Mtn. Valley			25.0 0.62		?			25.0
Sbar and Matumoto "	Profile 1 Section 2	Broken Mtn. Valley			22.0 0.56		?			22.0
Sbar and Matumoto "	Profile 1 Section 3	Broken Mtn. Valley			25.0 0.61		?			25.0
Sbar and Matumoto "	Profile 1 Section 4	Broken Mtn. Valley			22.0 0.52		?			22.0
Sbar and Matumoto "	Profile 1 Section 5	Broken Mtn. Valley	0.5 0.1	2.0 0.3	24.0 0.44		?			26.5
Gedney (1970)	B-B' Profile 5a	Broken Mtn. Valley		4.4 0.54	31.0 0.62		?			35.4
Gedney "	B-B' Profile 5b	Broken Mtn. Valley		4.7 0.38	22.0 0.65		?			26.7
Kienle (1970)	C-C' Profile 1a	Broken Mtn. Valley	2.5 0.28	5.0 0.50	25.0 0.71		58.0 2.10	?		90.5
Kienle "	C-C' Profile 1b	Broken Mtn. Valley	1.5 0.27	7.0 0.43	23.0 0.71		72.0 2.10	?	3.36	103.5
Kienle "	C-C' Profile 2a	Broken Mtn. Valley	2.0 0.17	7.0 0.34	22.0 0.62		73.0 2.09	?	3.71	104.0
Kienle "	C-C' Profile 2b	Broken Mtn. Valley	1.0 0.17	1.5 0.37	31.0 0.62		46.0 2.09	?	3.71	79.5
Kienle "	C-C' Profile 3a	Broken Mtn. Valley	1.0 0.13	2.0 0.37	32.0 0.62		42.0 2.44	?	3.68	77.0
Kienle "	C-C' Profile 3b	Broken Mtn. Valley	1.5 0.20	6.0 0.31	32.0 0.43		42.0 2.44	?	3.68	81.5
Sbar and Matumoto(1971)	Profile 2 Section 7	Southern Branch				35.0 0.87	?			35.0
Sbar and Matumoto "	Profile 2 Section 6	Southern Branch				50.0 1.1	?			50.0
Sbar and Matumoto "	Profile 2 Section 5b	Southern Branch	0.5 0.13	3.1 0.27	16.6 0.59		?			62.3
Sbar and Matumoto "	Profile 2 Section 5a	Southern Branch	0.7 0.13	4.7 0.40	45.8 0.74		40.8 1.8	?	3.8	92.0
Sbar and Matumoto "	Profile 2 Section 4b	Southern Branch	1.2 0.13	1.6 0.48	7.3 0.62	56.3 0.87		?		66.4
Sbar and Matumoto "	Profile 2 Section 4a	Southern Branch	0.6 0.14	8.3 0.35	25.9 0.65			?		34.8

Investigator	Profile	Location	Layer 1	Layer 2	Layer 3	Layer 4	Layer 5	Layer 6	Layer 7	Total Thickness (m)
Sbar and Matumoto(1971)	Profile 2	Southern Branch		30.0				?		30.0
	Section 3	Branch		0.30				3.2		
Sbar and Matumoto "	Profile 2	Southern Branch		25.0				?		25.0
	Section 2b	Branch		0.32				2.5		
Sbar and Matumoto "	Profile 2	Southern Branch		25.0		?				25.0
	Section 2a	Branch		?		1.0				
Gedney (1970)	A-A'	Southern Branch		1.4	47.0			?		48.4
	Profile 4a	Branch		0.25	0.60			3.0		
Gedney "	A-A'	Southern Branch		23.1			?			23.1
	Profile 4b	Branch		0.35			8.1			
Gedney "	A-A'	Southern Branch		3.7	43.1			?		46.8
	Profile 3a	Branch		0.33	0.70			2.87		
Gedney "	A-A'	Southern Branch		1.6	13.8	24.1	?			39.5
	Profile 3b	Branch		0.38	0.43	0.87	2.15			
Gedney "	A-A'	Southern Branch		1.9	24.3		45.6	?		71.8
	Profile 2a	Branch		0.54	0.65		1.42	2.9		
Gedney "	A-A'	Southern Branch		4.5	30.6		32.7	?		67.8
	Profile 2b	Branch		0.50	0.60		1.87	2.98		
Gedney "	A-A'	Southern Branch		2.1		35.6		?		37.7
	Profile 1a	Branch		0.25		0.80		2.62		
Gedney "	A-A'	Southern Branch		5.3		59.7		?		65.0
	Profile 1b	Branch		0.33		0.95		2.75		
Sbar and Matumoto(1971)	Profile 3	Novarupta Basin			20.0		37.0	?		57.0
	Section 2	Basin			?		1.8	3.1		
Sbar and Matumoto "	Profile 3	Novarupta Basin					42.0		?	42.0
	Section 3a	Basin					?		4.6	
Sbar and Matumoto "	Profile 3	Novarupta Basin			17.0	62.0	?			79.0
	Section 3b	Basin			?	1.2	2.3			
Sbar and Matumoto "	Profile 3	Novarupta Basin	0.9	1.2	4.9	?				7.0
	Section 4a	Basin	0.11	0.42	0.61	0.80				
Sbar and Matumoto "	Profile 3	Novarupta Basin	1.1	1.4	73.3				?	75.8
	Section 4b	Basin	0.12	0.59	0.65				4.4	
Sbar and Matumoto "	Profile 3	Novarupta Basin			12.0		?			12.0
	Section 5a	Basin			?		1.5			
Sbar and Matumoto "	Profile 3	Novarupta Basin			10.0	?				10.0
	Section 5b	Basin			?	1.1				
Sbar and Matumoto "	Profile 3	Novarupta Basin			15.0	?				15.0
	Section 6a	Basin			?	0.98				
Sbar and Matumoto "	Profile 3	Novarupta Basin			15.0	35.0	?			50.0
	Section 6b	Basin			?	1.1	2.3			
Sbar and Matumoto "	Profile 3	Novarupta Basin			15.0	?				15.0
	Section 7	Basin			?	1.1				
Kienle (1970)	D-D'	Novarupta Basin		5.0		16.0	73.0	?		94.0
	Section a	Basin		0.36		0.87	1.55	2.84		
Kienle (1970)	D-D'	Novarupta Basin		2.5		43.0	33.0	?		78.5
	Section b	Basin		0.49		0.87	1.55	2.84		

APPENDIX E.1

DEVELOPMENT OF FUNDAMENTAL EQUATIONS

This mathematical derivation is based on the methods presented by Hintler et al., (1962) and Sharma (1966).

Consider a right-handed coordinate system: x, y, z , such that z is positive downwards. Let the unit vectors in the x, y, z , directions be $\hat{i}, \hat{j}, \hat{k}$, respectively.

If $V = \Delta x \Delta y \Delta z$ represents a volume element at (x, y, z) with magnetic moment $\vec{\mu}$, then its magnetization, M , is given by:

$$\vec{M} = \frac{\vec{\mu}}{V} = \frac{1}{\Delta x \Delta y \Delta z} \vec{\mu},$$

where:

$$\vec{M} = M_x \hat{i} + M_y \hat{j} + M_z \hat{k}.$$

The vector, \vec{r} , from position (A, B, C) to the element V at (x, y, z) is given by

$$\vec{r} = (x-A)\hat{i} + (y-B)\hat{j} + (z-C)\hat{k},$$

or letting:

$$(x-A) = X,$$

$$(y-B) = Y, \text{ and}$$

$$(z-C) = Z,$$

$$\vec{r} = X\hat{i} + Y\hat{j} + Z\hat{k},$$

which yields:

$$r = \sqrt{X^2 + Y^2 + Z^2}.$$

The magnetic potential P at (A, B, C) due to V is

$$P = \frac{\vec{\mu} \cdot \vec{r}}{r^3}$$

which, upon substitution and solving, becomes

$$P = \left(\frac{XM_x + YM_y + ZM_z}{(X^2 + Y^2 + Z^2)^{3/2}} \right) \Delta x \Delta y \Delta z$$

Consider a body of cross section $\Delta x \Delta z$ which is infinite in the y -direction. The potential at (A, B, C) is given by

$$P = \Delta x \Delta z \int_{-\infty}^{\infty} \left\{ \frac{M_x X + M_z Z}{(X^2 + Y^2 + Z^2)^{3/2}} + \frac{M_y Y}{(X^2 + Y^2 + Z^2)^{3/2}} \right\} \Delta y$$

solving:

$$P = \partial \Delta x \Delta z \left(\frac{M_x X + M_z Z}{X^2 + Z^2} \right)$$

The negative gradient of the potential in any direction gives a corresponding component of magnetic field strength. Thus the vertical field strength, V is found by

$$V = - \frac{\partial P}{\partial Z},$$

$$V = \partial \Delta x \Delta z \frac{\partial X Z M_x - M_z (X^2 - Z^2)}{(X^2 + Z^2)^2}$$

Likewise, the horizontal field strength in the x -direction is given by

$$H = \frac{-\partial P}{\partial X},$$

$$H = \partial \Delta x \Delta z \frac{\partial X Z M_z + M_x (X^2 - Z^2)}{(X^2 + Z^2)^2}$$

Clearly, $\frac{-\partial P}{\partial y} = 0$ and there is no component of field strength in the y -direction. This result follows intuitively from symmetry considerations. Similarly, one sees that locations (A, B, C) and (x, y, z) are fully represented by (A, C) and (x, z) , respectively. Also, the magnetization

in the y-direction is inconsequential.

Assuming that the body causing the anomaly extends from c_1 to c_2 in the z-direction, V can be expressed as

$$V = \partial \Delta x \int_{c_1}^{c_2} \left[\partial X M_x \left(\frac{z}{(x^2+z^2)^2} \right) - M_z x^2 \left(\frac{1}{(x^2+z^2)^2} \right) + M_z \left(\frac{z^2}{(x^2+z^2)^2} \right) \right] dz;$$

which reduces to

$$V = \partial \Delta x \left[\frac{-x M_x - z M_z}{z^2 + x^2} \right]_{c_1}^{c_2}$$

Similarly for H:

$$H = \partial \Delta x \left[\frac{z M_x - x M_z}{z^2 + x^2} \right]_{c_1}^{c_2}$$

If the magnetization \vec{M} , has only a component induced by the earth's field, then

$$\vec{M} = k \vec{F},$$

where k is the magnetic susceptibility of the causative body. Clearly, the components of the magnetization are given by

$$M_x = kF \cos I \sin S; \text{ and}$$

$$M_z = kF \sin I,$$

where, I is the regional inclination of the earth's field, F is the magnitude of the regional total field, and S is the clockwise angle from magnetic north to the positive direction of the strike, $+y$, which is determined by correspondence with x being positive with increasing

station distance along the traverse. Refer to Figure E.2.

If it is assumed that the anomalous total field ($\bar{T} = V\hat{i} + H\hat{k}$) is in essentially the same direction as the earth's field ($F = F_x\hat{i} + F_y\hat{j} + F_z\hat{k}$) ie, that V and H are small relative to F , then the magnitude of the anomalous field is approximately equal to its projection onto \bar{F} :

$$|\bar{T}| = \frac{\bar{F} \cdot \bar{T}}{|\bar{F}|} = \frac{F_x H + F_z V}{\sqrt{F_x^2 + F_y^2 + F_z^2}} ;$$

or referring to the geometrical relationships illustrated in Figures E.3 and E.4.

$$T = H \cos I \sin S + V \sin I .$$

Ultimately, V , H , and T can be expressed in terms of their fundamental components:

$$V = -\partial k F \Delta x \left[\frac{(x-A) \cos I \sin S + (z-C) \sin I}{(x-A)^2 + (z-C)^2} \right]_{c_1}^{c_2} ;$$

$$H = \partial k F \Delta x \left[\frac{(z-C) \cos I \sin S - (x-A) \sin I}{(x-A)^2 + (z-C)^2} \right]_{c_1}^{c_2} ;$$

$$T = \partial k F \Delta x \left[\frac{(z-C) (\cos^2 I \sin^2 S - \sin^2 I) - \partial (x-A) \sin I \cos I \sin S}{(x-A)^2 + (z-C)^2} \right]_{c_1}^{c_2} .$$

Where x is the midpoint of increment x and z varies from c_1 to c_2 ;

(A, C) is the station location.

The vertical gradient of the total field anomaly, G , can be found by:

$$G = \partial T / \partial z ;$$

which reduces to:

$$G = \partial k F \Delta x \frac{(\cos^2 I \sin^2 S - \sin^2 I) [(x-A)^2 - (z-C)^2]}{[(x-A)^2 + (z-C)^2]^2} - \frac{\partial (x-A) (z-C) \sin I \cos I \sin S}{[(x-A)^2 + (z-C)^2]^2} \bigg|_{c_1}^{c_2}$$

These expressions for the various anomalies can be greatly simplified by letting:

$$L = \partial k F \Delta x$$

$$R_1 = \sqrt{(x-A)^2 + (c_1 - C)^2}$$

$$R_2 = \sqrt{(x-A)^2 + (c_2 - C)^2}$$

$$M1 = (x-A)$$

$$M2 = (x-A)$$

$$N1 = (c_1 - C)$$

$$N2 = (c_2 - C)$$

$$M = M2 - M1$$

$$N = N2 - N1$$

$$P = \cos I \sin S$$

$$Q = \sin I$$

With the above relationships one obtains:

$$H = L (NP - MQ)$$

$$V = -L (MP + NQ)$$

$$T = L [N(P^2 - Q^2) - 2MPQ]$$

$$G = L [(M2^2 - M1^2) - (N2^2 - N1^2)] (P^2 - Q^2) + 4(M2N2 - M1N1)PQ$$

In practice, the anomalies at position (A,C) are determined by solving the previous equations for the contribution from each elemental strip, $Dx \times (c2-c1)$, and summing. This technique can be extended to cover cases of several bodies with varying magnetic properties, dimension, shape, position and strike, and any number and location of station (provided they are exterior to the magnetic bodies).

A program has been written for the IBM 360/40 to determine V,T, and G in this manner; i.e., at evenly spaced stations along straight line traverses over level bodies of parallel orientation and specified depth, width and thickness and susceptibility, uniformly magnetized in the present regional field. A sample of the program utilized in determining the model anomalies is presented in Appendix E.2.

There are a few limitations of this program which deserve attention, although most are clear from its derivation.

It was found that altering the number of elemental strips within a body of arbitrary width does not markedly effect the resultant computed anomaly. But, as a rule of thumb, the width of the elemental strips should be at least half the station spacing.

The relative position of each station above the anomalous body can be very important, especially if the body is narrow, and more particularly if it is also shallow. Obviously, as the body narrows, so does its anomaly; and as it nears the surface, its effect is more pronounced. So, station location and spacing become critical for realistic representation of a shallow and/or narrow body. Carelessness in this detail of the modeling can cause the profile of the anomaly to be misshaped and incorrect; or, the anomaly missed entirely. Thus, the minimum model width

should dictate the maximum station spacing. Also, since the elemental strips are in effect narrow bodies, it is wise to have the stations positioned directly over the center of any elemental strip, and definitely not alternately at the center and then the edge of elemental strips.

Station spacing is also critical in computing the anomaly due to a thin body in order to avoid producing erroneous profiles. Basically, the station spacing should be less than the thickness of the anomalous body to be modeled.

Computation of this type of two-dimensional model is common in analysis of ocean-floor magnetic anomalies. Of course, such analysis is much simplified since essentially all parameters are defined except the magnetization. The modeling program presented here could be used for such analysis without modification.

3

APPENDIX E.2

Sample Computer Program of Two Dimensional Magnetic Analysis

```

C PREPARED IN 1970 BY MARLA CAVE TRIBLE
C *****
C
C JY=MODEL IDENTITY
C X=INITIAL PT OF BODY ALONG TRAVERSE, METERS
C D=DEPTH TO TOP OF BODY,M
C DD=VERTICAL EXTENT OF BODY,M
C W=HORIZONTAL EXTENT, M
C DX=INCREMENTAL WIDTH, M
C JH=TOTAL DX IN BODY
C SV=STRIKE OF BODY, CW FROM TRUENORTH, DEGREES.
C XK=SUSCEPTIBILITY, (10)-6 EMU/CC
C
C V(I)= VERTICAL ANOMALY, GAMMAS
C T(I)= TOTAL ANOMALY IN GAMMAS
C G(I)= VERT. GRAD. OF TOTAL ANOMALY,GAMMAS
C
C SS=STRIKE OF TRAVERSE, DEG CW OF TN
C SP=STATION SPACING, M
C A(I)=STATION DISTANCE
C C=STATION ELEVATION (DATUM,M)
C I=TOTAL STATIONS
C XX=X STRIPS /SP ALONG X-AXIS
C F=ORIGINAL TOTAL FIELD, GAMMAS
C FI=INCLINATION OF F, DEG
C FD=DECLINATION OF F
C
C S = CW ANGLE FROM FD TO SM, RADIANS
C R = ACUTE ANGLE BETWEEN SS AND X
C L= INCREMENT INDEX
C *****
C
C DIMENSION V(101),T(101),G(101),A(101)
C READ (1,2,F5D=105) JY,XK,D,DD,W,SS,SM,FI,FD,F,I,XN,DX,C
C FORMAT (13,2X,F5.0,3(2X,F4.0),4(2X,F4.1),2X,F5.0,2X,I3,2X,
C 1F4.0,2X,F3.0,1X,F4.0)
C WRITE (3,3) JY,XK,D,DD,W,SS,SM,FI,FD,F,I,XN,DX,C
C FORMAT (11',13,2X,F6.0,3(2X,F5.0),4(2X,F5.1),2X,F6.0,2X,I4,
C 12X,F5.0,2X,F4.0,2X,F5.0)
C FI=FI/57.2958
C DX=DX*100.
C C=100.
C L=7*100.

```

```

C2=(D+DD)*100.
R=ABS((SM-90.)-SS)
R=R/57.2958
S=SM-FD
IF (SM.LT.FD) S=360.-S
S=S/57.2958
P=COS(FI)*SIN(S)
Q=SIN(FI)
SP=(DX/COS(R))*XN
A(1)=0.
DO 17 I=2,11
17 A(I)=A(I-1)+SP
W= W*100.
X=A(11/2)-(W/(COS(R)*2.))-(DX/(COS(R)*2.))
IJ=11*IFIX(XN)
DO 19 I=1,IJ
XI=FLOAT(I)
XP=XI*DX
IF (X.NE.XP) GO TO 19
X=X+DX/(COS(R)*2.))
GO TO 20
19 CONTINUE
20 XL=2.*XK*QX*F/(10.**11)
JU=IFIX(W)/IFIX(DX)
DO 32 I=1,11
V(I)=0.
T(I)=0.
32 G(I)=0.
DO 47 I=1,11
DO 47 L=1,JU
XX=((X-A(I))*COS(R))+(L*DX)-(DX/2.)
Z1=C1-C
Z2=C2-C
36 X91=(XX**2)+(Z1**2)
37 X92=(XX**2)+(Z2**2)
38 XM1=XX/XR1
39 XM2=XX/XR2
40 XM=XM2-XM1
41 XN1=71/XR1
42 XN2=Z2/XR2
43 XN=XN2-XN1
44 V(I)=V(I)+((-X1)*((XM**2)+(XN**2)))
T(I)=T(I)+(XL*((XN**2)-(10**2)))-(2.*XN**2*Q))
G(I)=G(I)+(XL*((((XM2**2)-(XM1**2))-((XN2**2)-(XN1**2)))*
I*((P**2)-(Q**2)))+(4.*((XM2*XN2)-(XN1*XN1))*P*Q)))

```

```

47 CONTINUE
  DD 51 I=1,II
48 V(I)=V(I)*(10.**5)
49 T(I)=T(I)*(10.**5)
50 G(I)=G(I)*(10.**7)
51 A(I)=(A(I)/100.)
  C=C/100.
  DX=DX/100.
  SP=SP/100.
  W=W/100.
  X=X/100.
  F1=F1*57.2958
  WRITE(3,80) JM,W,D0,X
80 FORMAT('1','MODEL ',I3,' CONSISTS OF A MAGNETIC BODY ',F5.0
  1,' X ',F5.0,' METERS AT (',F5.0,',')
  WRITE(3,81) D,XX,SM
81 FORMAT('1',F5.0,' METERS, OF SUSCEPTIBILITY ',F6.0,' X 10
  1-6 EMU/CG, STRIKING ',F5.1)
  WRITE(3,82) DX
82 FORMAT('1',DEGREES EAST OF NORTH. INCREMENT BODY WIDTH
  1FOR COMPUTATION IS ',F4.0)
  WRITE(3,83) F,F1
83 FORMAT('1','THE TOTAL FIELD IS TAKEN AS ',F6.0,' GAMMAS,
  1HAVING A DIP OF ',F5.1,' AND')
  WRITE(3,84) D0,SS
84 FORMAT('1','DECLINATION OF ',F5.1,'. THE POSITION IS TAKEN
  1ALONG ',F5.1,' DEGREES EAST')
  WRITE(3,85) SP,C
85 FORMAT('1','OF NORTH AT ',F4.0,' METER INTERVALS AT AN
  1ELEVATION OF ',F5.0,' METERS.')
  NN=1
90 WRITE(3,91) JM
91 FORMAT('1',I4,'POSITION ON TRAVERSE',T29,'MAGNETIC
  1ANOMALIES FOR MODEL ',I3)
92 WRITE(3,93)
93 FORMAT('1',I4,'STATION',T14,'DISTANCE',T27,'VERTICAL',T39,
  1'TOTAL',T44,'VERT. GRAD.')
94 WRITE(3,95)
95 FORMAT('1',T48,'OF TOTAL')
96 WRITE(3,97)
97 FORMAT('1',T14,'(METERS)',T27,'(GAMMAS)',T38,'(GAMMAS)',
  1T49,'(G/METER)')
  MM=NN+25
  DD 99 I=NN,MM
  IF (I.GT.1) GO TO 100

```

```

98 FORMAT('0',T6,I3,T15,F6.1,T28,F6.0,T39,F6.0,T50,F7.1)
99 WRITE(3,98) I,A(I),V(I),T(I),G(I)
  NN=NN+26
  GO TO 90
100 DD 104 I=1,II
102 FORMAT (I3,I4,2X,F6.1,2X,F6.0,2X,F6.0,2X,F7.1)
103 WRITE (2,102) JM,I,A(I),V(I),T(I),G(I)
104 CONTINUE
105 CALL EXIT
  END

```

APPENDIX E.3

Total Magnetic Anomalies (in Gammas) at 20 Meter Intervals over Wedges of
 1250×10^{-6} emu/cc Material (from Computerized Two-Dimensional Models)

Width of Body* (m) →	250	250	250	250	250	250	250	500	500	500	500	500	500	500	500	750	750	750	750	750
Depth to Top (m) →	2	5	30	55	65	105	205	2	5	30	55	65	105	205	300	2	5	30	55	65
Depth to Base (m) →	5	30	55	65	105	205	300	5	30	55	65	105	205	300	5	30	55	65	105	
Station Number ↓																				
1	0	-1	-1	-1	-2	-3	-2	0	-3	-3	-1	-4	-7	-4	-1	-5	-5	-2	-6	
2	0	-1	-1	-1	-2	-4	-2	0	-3	-3	-1	-4	-7	-3	-1	-5	-5	-2	-7	
3	0	-2	-1	-1	-2	-4	-2	-1	-3	-3	-1	-4	-8	-3	-1	-6	-5	-2	-7	
4	0	-2	-2	-1	-2	-4	-2	-1	-4	-3	-1	-5	-8	-3	-1	-6	-6	-2	-8	
5	0	-2	-2	-1	-2	-4	-2	-1	-4	-4	-1	-5	-8	-3	-1	-7	-6	-2	-8	
6	0	-2	-2	-1	-2	-4	-2	-1	-4	-4	-1	-5	-8	-3	-1	-7	-7	-3	-8	
7	0	-2	-2	-1	-2	-4	-2	-1	-4	-4	-2	-5	-8	-2	-1	-8	-7	-3	-9	
8	0	-2	-2	-1	-3	-4	-2	-1	-5	-4	-2	-6	-9	-2	-1	-9	-8	-3	-9	
9	0	-2	-2	-1	-3	-5	-2	-1	-5	-5	-2	-6	-9	-2	-1	-10	-9	-3	-10	
10	0	-2	-2	-1	-3	-5	-2	-1	-6	-5	-2	-6	-9	-1	-2	-11	-10	-3	-11	
11	0	-3	-2	-1	-3	-5	-1	-1	-6	-5	-2	-7	-9	0	-2	-13	-10	-4	-12	
12	0	-3	-3	-1	-3	-5	-1	-1	-7	-6	-2	-7	-9	1	-2	-15	-11	-4	-12	
13	0	-3	-3	-1	-3	-5	-1	-1	-7	-6	-2	-8	-8	2	-2	-17	-13	-4	-11	
14	-1	-3	-3	-1	-4	-5	-1	-1	-8	-7	-3	-8	-8	3	-3	-20	-14	-4	-9	
15	-1	-3	-3	-1	-4	-5	0	-1	-9	-8	-3	-8	-7	5	-4	-24	-16	-4	-6	
16	-1	-4	-3	-1	-4	-5	1	-1	-10	-9	-3	-9	-5	6	-4	-30	-16	-3	-2	
17	-1	-4	-4	-1	-4	-5		-2	-12	-10	-3	-9	-4	9	-9	-38	-12	-1	7	
18	-1	-5	-4	-2	-5	-5	2	-2	-13	-11	-3	-9	-1	11	-12	-45	2	4	19	
19	-1	-5	-5	-2	-5	-4	3	-2	-16	-12	-4	-9	3	14	-31	20	34	11	33	
20	-1	-6	-5	-2	-5	-4	4	-3	-19	-13	-4	-7	9	17	271	172	60	16	46	
21	-1	-7	-6	-2	-6	-3	5	-3	-23	-14	-4	-5	15	21	258	116	59	18	52	
22	-1	-7	-6	-2	-6	-2	7	-5	-29	-14	-3	1	24	24	254	89	50	17	52	
23	-1	-9	-7	-2	-6	0	9	-7	-37	-11	0	9	34	28	253	75	42	15	50	
24	-1	-10	-8	-3	-6	3	11	-11	-43	3	5	21	46	32	252	67	35	13	46	
25	-2	-12	-9	-3	-6	6	14	-30	22	36	11	36	58	36	251	62	30	12	43	
26	-2	-14	-10	-3	-5	11	16	272	174	62	17	48	68	39	251	58	27	11	39	
27	-3	-18	-11	-3	-2	17	19	258	118	61	19	54	76	42	250	55	24	10	36	
28	4	-22	-11	-2	2	25	22	255	92	52	18	55	81	45	250	53	22	9	33	
29	5	-26	-10	0	8	34	26	253	78	44	16	53	83	47	250	52	20	8	31	
30	8	38	-2	3	19	45	29	252	70	37	14	49	83	48	250	50	19	8	30	
31	17	31	22	9	33	56	32	252	65	33	13	46	82	49	250	49	18	7	28	
32	306	214	58	16	48	67	34	251	61	29	12	42	80	49	250	49	17	7	27	
33	263	147	69	20	57	75	36	251	59	27	11	40	78	49	250	48	16	7	26	
34	257	109	63	20	61	81	38	251	57	25	10	37	75	48	250	47	16	6	25	
35	255	92	54	19	60	83	38	251	56	24	9	36	72	47	250	47	15	6	24	

36	254	83	47	17	57	82	38	250	55	23	9	34	69	45	250	47	15	6	24
37	253	78	43	16	53	78	36	250	54	22	9	33	67	44	250	47	15	6	23
38	253	76	40	15	49	73	34	250	54	22	9	32	64	42	250	47	15	6	23
39	253	75	38	14	45	65	31	250	54	22	8	31	61	40	250	47	15	6	23
40	254	77	37	13	39	56	28	250	54	22	8	31	59	37	250	47	15	6	22
41	255	81	35	11	32	44	24	251	55	22	8	30	56	35	250	47	15	6	22
42	256	88	30	8	22	31	19	251	56	22	8	29	52	32	250	47	15	6	22
43	261	93	15	3	8	17	14	251	58	23	8	29	48	28	250	47	15	6	22
44	280	27	-19	-4	-8	4	10	251	60	34	9	28	43	25	250	48	16	6	22
45	-22	-126	-46	-10	-22	-9	6	252	62	25	8	26	36	21	250	49	16	6	23
46	-9	-70	-45	-12	-29	-16	2	252	66	26	8	23	29	16	250	49	17	6	23
47	-5	-44	-36	-11	-30	-25	-2	253	72	26	7	18	19	12	250	50	17	7	23
48	-4	-31	-28	-10	-29	-29	-5	256	80	22	5	9	8	7	250	52	18	7	23
49	-3	-23	-22	-8	-26	-30	-7	260	86	8	0	-4	-5	3	250	53	19	7	23
50	-2	-18	-18	-7	-23	-30	-9	279	21	-25	-7	-18	-17	-2	251	55	20	7	23
51	-2	-15	-15	-6	-20	-29	-10	-23	-131	-51	-13	-31	-23	-6	251	58	23	7	22
52	-1	-12	-12	-5	-17	-28	-11	-9	-75	-50	-14	-37	-36	-10	252	61	24	7	20
53	-1	-10	-10	-4	-15	-26	-12	-6	-49	-41	-13	-38	-41	-13	252	66	21	7	17
54	-1	-9	-9	-4	-14	-25	-12	-4	-35	-32	-11	-35	-44	-15	254	73	14	5	10
55	-1	-7	-8	-3	-12	-23	-12	-3	-27	-26	-10	-32	-44	-17	257	82	-8	2	-1
56	-1	-7	-7	-3	-11	-21	-12	-3	-21	-21	-8	-28	-43	-18	16	76	-44	-4	-14
57	-1	-6	-6	-3	-9	-19	-12	-2	-17	-18	-7	-25	-41	-19	-57	-55	-11	-28	
58	-1	-5	-5	-2	-9	-18	-11	-2	-15	-15	-6	-22	-39	-20	-14	-99	-48	-15	-38
59	-1	-5	-5	-2	-8	-17	-11	-2	-13	-13	-5	-20	-37	-20	-7	-61	-48	-15	-41
60	-1	-4	-4	-2	-7	-15	-11	-1	-11	-11	-5	-17	-34	-20	-5	-42	-38	-13	-40
61	-1	-4	-4	-2	-6	-14	-10	-1	-10	-10	-4	-16	-32	-19	-4	-32	-30	-11	-36
62	-1	-4	-4	-2	-6	-13	-9	-1	-9	-9	-4	-14	-20	-19	-3	-25	-25	-9	-33
63	0	-3	-3	-1	-5	-12	-9	-1	-8	-8	-3	-13	-27	-18	-2	-20	-21	-8	-34
64	0	-3	-3	-1	-5	-11	-9	-1	-7	-7	-3	-12	-25	-18	-2	-17	-18	-7	-26
65	0	-3	-3	-1	-5	-11	-8	-1	-6	-7	-3	-11	-24	-17	-2	-15	-15	-6	-23
66	0	-3	-3	-1	-4	-10	-8	-1	-6	-6	-3	-10	-22	-16	-2	-13	-13	-5	-20
67	0	-2	-2	-1	-4	-9	-8	-1	-5	-5	-2	-9	-21	-15	-1	-11	-12	-5	-18
68	0	-2	-2	-1	-4	-9	-7	-1	-5	-5	-2	-8	-19	-15	-1	-10	-10	-4	-16
69	0	-2	-2	-1	-3	-8	-7	-1	-5	-5	-2	-8	-18	-14	-1	-9	-9	-4	-15
70	0	-2	-2	-1	-3	-8	-7	-1	-4	-4	-2	-7	-17	-13	-1	-8	-9	-4	-14
71	0	-2	-2	-1	-3	-7	-6	-1	-4	-4	-2	-7	-16	-13	-1	-7	-8	-3	-13
72	0	-2	-2	-1	-3	-7	-6	-1	-4	-4	-2	-6	-15	-12	-1	-7	-7	-3	-12
73	0	-2	-2	-1	-3	-6	-6	-1	-3	-4	-2	-6	-14	-12	-1	-6	-7	-3	-11
74	0	-2	-2	-1	-3	-6	-5	0	-3	-3	-1	-5	-13	-11	-1	-6	-6	-3	-10
75	0	-1	-2	-1	-2	-6	-5	0	-3	-3	-1	-5	-12	-11	-1	-5	-6	-2	-9

* 250 meter wide body extends from 615 to 865 meters from the beginning of the traverse;
500 meter wide body extends from 485 to 985 meters from the beginning of the traverse;
750 meter wide body extends from 365 to 1115 meters from the beginning of the traverse;
1000 meter wide body extends from 235 to 1235 meters from the beginning of the traverse.

APPENDIX E.3 (continued)

Width of Body* (m) →	750	750	750	750	750	750	750	750	750	750	750	1000	1000	1000	1000	1000	1000	1000
Depth to Top (m) →	105	150	205	250	300	350	400	500	600	700	800	2	5	30	55	65	105	205
Depth to Base (m) →	150	205	250	300	350	400	500	600	700	800	900	5	30	55	65	105	205	300
Station Number	1	2	3	4	5	6	7	8	9	10	11	12	13	14	15	16	17	18
	-7	-4	-3	-1	-1	1	3	5	5	5	5	-1	-9	-8	-3	-10	-13	-1
	-6	-5	-2	-2	1	0	4	5	6	6	5	-1	-10	-9	-3	-10	-12	1
	-7	-4	-3	0	1	1	4	6	6	6	6	-2	-11	-10	-4	-11	-11	2
	-7	-4	-3	0	0	2	5	6	7	6	6	-2	-13	-11	-4	-11	-10	4
	-7	-5	-1	-1	2	1	6	7	7	7	6	-2	-14	-12	-4	-12	-7	6
	-7	-4	-2	1	1	3	7	7	7	7	7	-2	-16	-13	-4	-11	-4	9
	-7	-4	-1	1	2	3	8	8	8	7	7	-3	-19	-14	-4	-11	0	12
	-7	-4	0	1	3	4	8	9	8	7	7	-3	-23	-16	-4	-9	6	15
	-8	-2	-1	2	4	4	9	10	9	8	7	-4	-28	-17	-4	-6	14	19
	-7	-1	0	5	3	5	11	10	10	9	8	-6	-35	-15	-3	1	23	23
	-6	-1	2	5	5	6	12	11	10	9	8	-9	-44	-8	1	11	34	27
	-4	0	4	5	7	6	13	12	11	9	8	-18	-38	15	7	25	45	31
	-3	3	5	7	7	8	14	13	11	10	8	305	205	50	14	39	56	34
	0	5	7	8	9	8	15	13	12	10	9	262	138	61	17	48	65	38
	3	9	9	10	10	9	17	14	12	10	9	256	99	54	17	51	71	40
	8	12	12	11	11	10	18	15	13	11	9	253	81	44	16	50	74	43
	15	16	14	12	13	10	19	16	13	11	9	252	70	37	14	46	75	44
	22	20	17	13	15	10	20	17	14	11	10	251	63	31	12	43	74	46
	30	24	19	15	16	11	21	17	14	12	10	251	59	27	11	39	73	46
	36	28	21	17	17	12	22	18	15	12	10	250	55	24	10	36	70	46
	42	29	25	16	20	11	23	19	15	12	10	250	53	22	9	33	67	46
	44	32	26	17	21	11	24	19	15	13	10	250	51	20	8	30	65	46
	45	33	28	17	23	11	25	20	16	13	10	250	49	18	7	28	62	45
	44	34	28	19	22	13	26	20	16	13	11	250	48	17	7	27	59	45
	43	34	28	20	22	14	27	20	16	13	11	250	47	16	6	25	57	44
	41	34	28	20	23	13	27	21	16	13	11	249	46	15	6	24	55	43
	40	32	29	19	24	13	27	21	17	13	11	249	45	14	6	23	53	42
	38	32	28	20	23	14	28	21	17	13	11	249	45	13	5	21	49	40
	36	31	28	20	23	14	28	21	17	13	11	249	45	13	5	20	48	40
	34	31	26	21	22	15	28	21	17	13	11	249	44	13	5	20	48	40
	33	29	27	19	23	14	28	21	17	13	11	249	44	12	5	20	47	39
	32	28	26	19	23	13	28	21	17	13	11	249	44	12	5	19	45	38
	30	28	25	19	22	14	27	21	16	13	11	249	43	12	5	19	44	37
	29	27	24	19	21	14	27	21	16	13	10	249	43	12	5	18	43	36
	28	27	23	19	20	15	26	20	16	13	10	249	43	11	5	18	43	36

36	28	25	24	17	21	13	26	20	16	12	10	249	43	11	5	18	42	35
37	28	24	24	16	21	12	25	19	15	12	10	249	43	11	5	18	41	34
38	27	24	22	17	19	13	25	19	15	12	10	249	43	11	5	17	41	34
39	26	24	21	17	18	13	24	18	15	12	9	249	43	11	5	17	40	33
40	26	23	21	16	18	12	23	18	14	11	9	249	43	11	5	17	40	33
41	26	22	21	15	18	11	22	17	14	11	9	249	43	11	5	17	39	32
42	25	22	20	14	17	10	21	16	13	11	9	249	43	11	5	17	39	31
43	25	21	19	14	16	10	20	16	12	10	8	249	43	11	5	17	39	31
44	24	21	18	13	15	9	19	15	12	10	8	249	44	12	5	18	39	30
45	24	20	17	13	14	9	17	14	11	9	8	249	44	12	5	18	39	29
46	24	19	16	12	13	8	16	13	11	9	7	249	44	12	5	18	38	29
47	22	19	14	11	11	8	15	12	10	8	7	249	45	12	5	18	38	28
48	22	17	14	9	11	6	13	11	9	8	7	249	45	13	5	18	38	27
49	21	15	13	7	11	4	12	10	8	7	6	249	45	13	5	19	38	26
50	19	14	10	7	8	5	10	9	8	7	6	249	46	14	5	19	37	24
51	17	11	8	6	6	5	9	8	7	6	5	250	47	14	5	20	36	23
52	14	8	6	4	5	3	7	7	6	6	5	250	48	15	6	20	36	21
53	10	6	2	4	2	4	6	6	5	5	5	250	49	16	6	20	34	19
54	3	1	1	1	2	1	4	5	5	5	4	250	50	17	6	21	33	17
55	-5	-2	-3	0	-1	2	3	4	4	4	4	250	52	18	6	21	30	15
56	-11	-8	-4	-3	-1	0	1	3	3	3	3	251	54	19	7	21	27	12
57	-19	-11	-8	-3	-4	0	0	2	3	3	3	251	57	20	7	20	23	9
58	-25	-15	-9	-5	-5	-1	-1	1	2	2	3	252	60	21	7	18	17	5
59	-29	-17	-12	-5	-7	-1	-3	0	1	2	2	252	65	22	6	15	9	2
60	-31	-18	-14	-6	-8	-1	-4	-1	1	1	2	254	72	21	5	8	-1	-3
61	-30	-20	-14	-8	-8	-3	-5	-2	0	1	2	257	81	14	1	-2	-12	-7
62	-30	-20	-15	-8	-9	-3	-6	-3	-1	1	1	266	75	-10	-5	-16	-23	-11
63	-27	-21	-14	-10	-8	-5	-7	-3	-1	0	1	-57	-168	-45	-11	-30	-34	-14
64	-26	-20	-15	-9	-10	-4	-8	-4	-2	0	1	-14	-101	-56	-15	-39	-43	-18
65	-25	-18	-16	-8	-12	-3	-8	-4	-2	-1	0	-8	-62	-48	-15	-42	-49	-21
66	-23	-17	-16	-8	-12	-3	-9	-5	-3	-1	0	-5	-43	-39	-13	-41	-53	-23
67	-20	-18	-13	-11	-9	-6	-9	-5	-3	-1	0	-4	-33	-31	-11	-38	-54	-25
68	-17	-18	-12	-11	-9	-7	-10	-6	-3	-2	-1	-3	-26	-26	-10	-34	-53	-26
69	-17	-16	-12	-10	-9	-7	-10	-6	-4	-2	-1	-3	-21	-22	-8	-30	-51	-27
70	-17	-13	-14	-8	-11	-4	-10	-6	-4	-2	-1	-2	-18	-18	-7	-27	-49	-27
71	-14	-14	-11	-10	-8	-7	-10	-7	-4	-2	-1	-2	-15	-16	-6	-24	-46	-27
72	-14	-12	-12	-8	-10	-5	-10	-7	-4	-3	-2	-2	-14	-14	-6	-21	-43	-27
73	-13	-12	-11	-8	-9	-6	-10	-7	-5	-3	-2	-1	-12	-12	-5	-19	-40	-26
74	-12	-11	-10	-8	-9	-5	-10	-7	-5	-3	-2	-1	-11	-11	-5	-18	-38	-25
75	-11	-11	-9	-8	-8	-6	-10	-7	-5	-3	-2	-1	-10	-10	-4	-16	-35	-25

* 250 meter wide body extends from 615 to 865 meters from the beginning of the traverse;
500 meter wide body extends from 485 to 985 meters from the beginning of the traverse;
750 meter wide body extends from 365 to 1115 meters from the beginning of the traverse;
1000 meter wide body extends from 235 to 1235 meters from the beginning of the traverse.

BIBLIOGRAPHY

BIBLIOGRAPHY

- Abbot, C. G., Do Volcanic Eruptions Affect Our Climate, Natl. Geog. Soc., vol. 24, no. 2, pp. 181-198, 1913.
- Allen, E. T. and E. J. Zies, A Chemical Study of the Fumaroles of the Katmai Region, Natl. Geog. Soc. Contributed Tech. Papers, Katmai Ser., vol. 1, no. 2, pp. 75-155, 1923.
- Anma, K., An Aeromagnetic Survey in the Valley of Ten Thousand Smokes, Alaska, Univ. of Alaska, unpublished thesis, 1972.
- Bordet, P., G. Marinelli, M. Mittempergher, and H. Tazieff, Contributions à l'Etude Volcanologique du Katmai et de la Vallée des Dix Mille Fumées (Alaska), Mémoires de la Société Belge de Géologie, de Paléontologie et d'Hydrologie (Bruxelles), Série IN-8°-No. 7, pp. 1-114, 1963.
- Chantry-Price, R. E., A Palaeomagnetic Investigation of Some Post-Carboniferous Rocks from Alaska, Univ. of Newcastle Upon Tyne, unpublished dissertation, 1967.
- Collinson, D. W., L. Molyneux, and D. B. Stone, A Total and Anisotropic Magnetic Susceptibility Meter, Journal of Scientific Instruments, vol. 40, pp. 3010-3312, 1963.
- Curtis, G. H., The Stratigraphy of the Ejecta from the 1912 Eruption of Mount Katmai and Novarupta, Alaska, Geol. Soc. Amer. Mem., No. 116, pp. 153-210, 1968.
- Deel, S. A., Alaska Magnetic Tables and Magnetic Charts for 1940, U. S. Dept. of Commerce, Coast and Geodetic Survey, Washington, D. C., 1944.
- Dobrin, M. B., Introduction to Geophysical Prospecting, McGraw-Hill Book Co., Inc., New York, 446 pp., 1960.
- Fenner, C. N., The Katmai Region, Alaska, and the Great Eruption of 1912, J. of Geol., vol. 28, no. 7, pp. 569-606, 1920.
- _____, Evidence of Assimilation During the Katmai Eruption of 1912, (abstr.), Geophys. J., vol. 33, p. 129, 1922.
- _____, The Origin and Mode of Emplacement of the Great Tuff Flow Deposit in the Valley of Ten Thousand Smokes, Natl. Geog. Soc. Contributed Tech. Papers, Katmai Ser., no. 1, 74 pp., 1923.

Fenner, C. N., Earth Movements Accompanying the Katmai Eruption, pt. 1, J. of Geol., vol. 33, pp. 116-139, 1925a; pt. 11, pp. 193-233, 1925b.

_____, The Katmai Magmatic Province, J. of Geol., vol. 34, no. 7, pt. 2, pp. 673-772, 1926.

_____, Tuffs and Other Volcanic Deposits of Katmai and Yellowstone Park, Trans. Am. Geophys. Union, 18th Ann. Mtg., pt. 1, pp. 236-239, 1937.

_____, Incandescent Tuff Flows in Southern Peru, Geol. Soc. Amer. Bull., vol. 59, pp. 879-893, 1948.

_____, The Chemical Kinetics of the Katmai Eruption, pt. 1, Am. Jour. Sci., vol. 248, pp. 593-627, 1950a; pt. 11, pp. 697-725, 1950b.

Forbes, R. B., D. K. Ray, T. Katsura, H. Matsumoto, H. Haramura, and M. J. Furst, The Comparative Chemical Composition of Continental vs. Island Arc Andesites in Alaska, Proc. of the Andesite Conf., Internatl. Upper Mantle Comm., pp. 111-120, 1969.

Gedney, L., C. Matteson, and R. B. Forbes, Seismic Refraction Profiles of the Ash-Flow in the Valley of Ten Thousand Smokes, Katmai National Monument, Alaska, J. Geophys. Res., vol. 75, no. 14, pp. 2619-2624, 1970.

Gilbert, C. M., Welded Tuff in Eastern California, Geol. Soc. America Bull., vol. 49, pp. 1829-1862, 1938.

Grant, F. S. and G. F. West, Interpretation Theory in Applied Geophysics, McGraw-Hill Book Co., inc., New York, 583 pp., 1965.

Griggs, R. F., The Valley of Ten Thousand Smokes, Natl. Geog. Soc., vol. 31, 341 pp., 1922.

Handbook of Chemistry and Physics, Chemical Rubber Pub. Co., Cleveland, pp. E-95 - E-100, 1965-1966.

Heirtzler, J. R., G. Peter, M. Talwani, and E. G. Zurflueh, Magnetic Anomalies Caused by Two-Dimensional Structures: Their Computation by Digital Computers and Their Interpretation, Tech. Rep. No. 6, Lamont Geological Observatory, 1962.

Hood, P. and D. J. McClure, Gradient Measurements in Ground Magnetic Prospecting, Geophysics, vol. 30, no. 3, pp. 403-410, 1965.

Jakosky, Exploration Geophysics, Trija Pub. Co., Los Angeles, 1195 pp., 1950.

Keller, A. S. and H. N. Reiser, Geology of the Mount Katmai Area, Alaska, U. S. Geological Survey Bull. 1058-G, pp. 261-282, 1959.

Kienle, J., Gravity Survey in the General Area of the Katmai National Monument, Alaska, Univ. of Alaska, unpublished dissertation, 1969.

_____, Gravity Traverses in the Valley of Ten Thousand Smokes, Katmai National Monument, Alaska, J. Geophys. Res., vol. 75, pp. 6641-6649, 1970.

Kuboto, S. and E. Berg, Evidence for Magma in the Katmai Volcanic Range, Bull. Volcanologique, Tome 31, pp. 175-214, 1967.

Lovering, T. S., Halogen-acid Alteration of Ash at Fumarole No. 1, Valley of Ten Thousand Smokes, Alaska, Geol. Soc. America Bull., vol. 68, pp. 1585-1604, 1957.

Mackin, J. H., Hematite Veinlets in an Ignimbrite in Iron Springs District, southwestern Utah, (abstr.), Geol. Soc. America Bull., vol. 63, pp. 1337-1338, 1952.

Martin, G. C., The Recent Eruption of Katmai Volcano in Alaska, Natl. Geog. Soc., vol. 24, no. 2, pp. 131-181, 1913.

Matumoto, T. and P. L. Ward, Microearthquake Study of Mount Katmai and Vicinity, Alaska, J. Geophys. Res., vol. 72, no. 10, pp. 2557-2568, 1967.

Müller, G., Methods in Sedimentary Petrology, Hafner Publishing Co., New York, 283 pp., 1967.

Nagata, T., Rock Magnetism, Maruzen Co., Ltd., Tokyo, 350 pp., 1961.

Noltimier, H. C., Impregnation of Weak Sediments for Paleomagnetic Measurements, Earth and Planetary Sci. Letters, vol. 2, pp. 177-178, 1967.

Ray, D. K., Geochemistry and Petrology of the Mt. Trident Andesites, Katmai National Monument, Alaska, Univ. of Alaska, unpublished dissertation, 1967.

Sayre, J. D. and P. R. Hagelbarger, A Study of Temperatures in the Valley of Ten Thousand Smokes, Ohio Jour. Sci., vol. 19, no. 5, pp. 249-278, 1919.

Sbar, M. L. and T. Matumoto, Refraction Profiles in the Valley of Ten Thousand Smokes, Katmai National Monument, Alaska, Trans. Am. Geophys. Union, vol. 50, no. 40, p. 340, 1969.

- Sbar, M. L. and T. Matumoto, Refraction Profiles in the Valley of Ten Thousand Smokes, Katmai, Alaska, *Bull. Volcanologique*, in press 1971.
- Sharma, P. V., Digital Computation of Gravitational and Magnetic Anomalies and Their Derivatives for Two-dimensional Bodies of Arbitrary Shape, *Pure and Applied Geophys.*, vol. 64, pt. 11, pp. 14-18, 1966.
- Sheridan, M. F., Fumarolic Mounds and Ridges of the Bishop Tuff, California, *Geol. Soc. America Bull.*, vol. 81, pp. 851-868, 1970.
- Shipley, J. W., Some Chemical Observations on the Volcanic Emanations and Incrustations in the Valley of Ten Thousand Smokes, *Am. Jour. Sci.*, vol. 50, pp. 141-153, 1920.
- Smith, R. L., Ash Flows, *Geol. Soc. America Bull.*, vol. 71, pp. 795-842, 1960.
- Spurr, J. E., A Reconnaissance in Southwestern Alaska in 1898, U. S. Geol. Survey, 20th Ann. Rep., No. 7, pp. 43-263, 1900.
- Ward, P. L. and T. Matumoto, A Summary of Volcanic and Seismic Activity in Katmai National Monument, Alaska, *Bull. Volcanologique*, Tome 31, pp. 107-129, 1967.
- Williams, H., Preliminary Notes on Geological Work Done on Mount Katmai and in the Valley of Ten Thousand Smokes, U. S. Natl. Park Service Interim Rept. on Katmai Project, pp. 55-61, 1954.
- Zies, E. G., The Fumarolic Incrustations in the Valley of Ten Thousand Smokes, *Natl. Geog. Soc. Contributed Tech. Papers, Katmai Ser.*, vol. 1, no. 3, pp. 159-179, 1924a.
- _____, Hot Springs of the Valley of Ten Thousand Smokes, *J. of Geol.*, vol. 32, pp. 303-310, 1924b.
- _____, The Valley of Ten Thousand Smokes; I, The Fumarolic Incrustations and Their Bearing on Ore Deposition; II, The Acid Gasses Contributed to the Sea During Volcanic Activity, *Natl. Geog. Soc. Contributed Tech. Papers, Katmai Ser.*, vol. 1, no. 4, 79 pp., 1929.